DETERMINATION OF AGGLOMERATION CHARACTERISTICS OF OLTU-STONE (JET STONE) WASTES

A THESIS SUBMITTED TO
THE GRADUATE SCHOOL OF NATURAL AND APPLIED SCIENCES
OF
MIDDLE EAST TECHNICAL UNIVERSITY

BY

MUHAMMAD RAHEEL BAWANI

IN PARTIAL FULFILLMENT OF THE REQUIREMENTS
FOR
THE DEGREE OF DOCTOR OF PHILOSOPHY
IN
MINING ENGINEERING

DECEMBER 2021

Approval of the thesis:

DETERMINATION OF AGGLOMERATION CHARACTERISTICS OF OLTU-STONE (JET STONE) WASTES

submitted by **MUHAMMAD RAHEEL BAWANI** in partial fulfillment of the requirements for the degree of **Doctor of Philosophy** i**n Mining Engineering, Middle East Technical University** by,

Prof. Dr. Halil Kalıpçılar
Dean, Graduate School of **Natural and Applied Sciences** _____

Prof. Dr. Naci Emre Altun
Head of the Department, **Mining Engineering** _____

Prof. Dr. Ali İhsan Arol
Supervisor, **Mining Engineering** _____

Assoc. Prof. Gülşen Tozsin
Co-Supervisor, **Metallurgical and Materials Engineering, Ataturk University** _____

Examining Committee Members:

Prof. Dr. Naci Emre Altun
Mining Engineering, METU _____

Prof. Dr. Ali İhsan Arol
Mining Engineering, METU _____

Assoc. Prof. Dr. Erhan Bat
Chemical Engineering, METU _____

Assoc. Prof. Özlem Bıçak
Mining Engineering, Hacettepe University. _____

Assistant Prof. Dr. Meral Büyükyazıcı
Jewelry and Jewelry Design Department, Ankara Hacı Bayram Veli University. _____

Date: 17.12.2021

I hereby declare that all information in this document has been obtained and presented in accordance with academic rules and ethical conduct. I also declare that, as required by these rules and conduct, I have fully cited and referenced all material and results that are not original to this work.

Name, surname: Muhammad Raheel Bawani

Signature:

ABSTRACT

DETERMINATION OF AGGLOMERATION CHARACTERISTICS OF OLTU-STONE (JET STONE) WASTES

Bawani, Muhammad Raheel
Doctor of Philosophy, Mining Engineering
Supervisor: Prof. Dr. Ali Ihsan Arol
Co-Supervisor: Assoc. Prof. Dr. Gülşen Tozsin

December 2021, 109 pages

Oltu-stone (Jet Stone), also known as black amber, is a fossilized, organic, and natural material formed by the transformation of certain trees under high pressure. It is called Oltu-stone because its occurrences are primarily located in the Oltu district of Erzurum. Generally, it is mined by small miners from nearby villages using rather primitive methods. After a rough sorting at the mine site, Oltu-stone is mainly used in manufacturing worry beads, tespih, and to a lesser extent, certain ornamental goods. It has been reported that only 2% of Oltu-stone mined is converted to sellable end products. The rest, the waste, is either burnt or disposed of, causing economic losses. On the other hand, a much cheaper product known as Russian Stone produced in Georgia replaced Oltu-stone. To protect the brand, Oltu-stone, and produce higher economic values from this stone, the wastes of Oltu-stone should be converted into products.

First, the cleaned Oltu-stone wastes obtained from dense medium separation were characterized in this study. Cleaned Oltu-stone had nearly similar petrographical, physical and chemical properties coMPared to standard Oltu-stone. It was found that the cleaned Oltu-stone is liptinite-rich (including suberinite, resinite, and sporinite) coal with a small amount of huminite. Due to liptinite content, cleaned Oltu-stone has high volatile matters and aliphatic hydrocarbons. It is a well-known fact that this

type of waste, especially amber, has been converted to sellable products by agglomeration under heat and pressure treatment. To produce such agglomerates from the Oltu-stone wastes by this method, first, the agglomeration parameters such as pre-heating time, pressure, and temperature were optimized. The cleaned Oltu-stone was successfully pressed without a binder at 450 MPa pressure with two-stage heating until 200 ˚C temperature. Compared to standard Oltu-stone, pressed Oltu-stones were nearly similar in bulk density (1.22-1.25 g.cm-3), indirect tensile strength (8-9 MPa), and nano-indentation hardness (Hv=464.6 MPa, E=5.2 GPa). But chemically, it was degraded, such as reducing volatile matters and losing conjugated carbonyl groups. The pressed Oltu-stone obtained from the binderless agglomeration of cleaned Oltu-stone waste was tested by ateliers in Oltu, the quality of the pressed Oltu-stone was found to be satisfactory.

Keywords: Agglomeration, cleaned Oltu-stone waste, pressed Oltu-stone, liptinite, resinite.

ÖZ

OLTU-TAŞI ATIKLARININ TOPAKLANMA ÖZELLİKLERİNİN BELİRLENMESİ

Bawani, Muhammad Raheel
Doktora, Maden Mühendisliği
Tez Yöneticisi: Prof. Dr. Ali Ihsan Arol
Ortak Tez Yöneticisi: Assoc. Prof. Dr. Gülşen Tozsin

Aralık 2021, 109 sayfa

Siyah kehribar olarak da bilinen Oltu Taşı, bazı ağaçların basınç altında başkalaşıma uğrması sonucu oluşan fosilleşmiş organik ve doğal bir maddedir. Erzurum'un Oltu bölgesinde bulunduğu için Oltu Taşı olarak adlandırılmıştır. Genellikle, yakın köylerden gelen küçük madenciler tarafından oldukça ilkel yöntemler ile çıkarılmaktadır. Kaba bir ayıklamadan sonra, Oltu Taşı daha çok tespih olmak üzere farklı süs eşyalarının üretiminde kullanılmaktadır. Araştırmalar, çıkarılan Oltu Taşının yalnızca %2'sinin satılabilir son ürüne dönüştürülebildiğini göstermiştir. Geri kalan kısım ya yakılmakta ya da atılmaktadır. Bu da ekonomik kayıplara neden olmaktadır. Diğer taraftan, Gürcistan'da üretilmekte olan Rus Taşı olarak da bilinen çok daha ucuz bir ürün, Oltu Taşı'nın yerine geçmeye başlamıştır. Oltu Taşı markasını korumak ve yüksek ekonomik değerde ürün üretmek için, Oltu Taşı atıklarının da ürüne dönüştürülmesi gerekmektedir.

Bu çalışmada, önce ağır ortam yöntemiyle temizlenmiş Oltu Taşı atıkları karakterize edilmiştir. Temizlenmiş Oltu Taşı'nın standard Oltu Taşı'na benzer petrografik, fiziksel ve kimyasal özelliklere sahip olduğu anlaşılmıştır. Temizlenmiş Oltu Taşı atıklarının liptinitce (suberinit, resinit ve sporinit) zengin olduğu ve az miktarda huminit içerdiği belirlenmiştir. Liptinit içeriğinden dolayı, temizlenmiş Oltu Taşı atıkları yüksek oranda uçucu madde ve alifatik hidrokarbona sahip olmaktadır. Bu

tür atık toz malzemelerin, kehribarda olduğu gibi, yüksek ısı ve basınç altında sıkıştırılarak topaklandığı (aglomerasyon) ve satılabilir ürünlere dönüştürüldüğü bilinmektedir. Bu yöntem ile Oltu Taşı atıklarından ürün elde edebilmek için önce ön-ısıtma, basınç ve ısı gibi topaklanmaya etki eden faktörlerden en uygun değerler bulunmuştur. Temizlenmiş Oltu Taşı atıklarının 450 MPa basınç ve 200^{o}C sıcaklığa kadar iki aşamalı ısıtıldığında, herhangi bir bağlayıcı kullanmadan etkili bir biçimde topaklanabildiği belirlenmiştir. Standart Oltu Taşı ile karşılaştırıldığında, sıkıştırılmış Oltu Taşının görünür yoğunluğunun (1.22-1.25 g.cm^{-3}), dolaylı çekme kuvvetinin (8-9 MPa) ve nano-indentasyon sertliğinin (Hv=464.6 MPa, E=5.2 GPa) standart Oltu Taşı'na benzer olduğu görülmüştür. Ancak, kimyasal yapının, uçucu maddenin azalması ve karbonil grupların kaybolması ile, bozulduğu tespit edilmiştir. Bağlayıcı kullanılmadan sıkıştırılmış Oltu Taşı, Oltu İlçesinde bulunan atölyelerde test edilerek, sıkıştırılmış ürünlerin kalitesinin tatminkar olduğu bulunmuştur.

Anahtar Kelimeler: Topaklama, temizlenmiş Oltu Taşı, sıkıştırılmış Oltu Taşı, liptinit, resinit.

This work is dedicated to my family

ACKNOWLEDGMENTS

I would like to convey my sincere gratitude to my supervisor, Prof. Dr. Ali Ihsan Arol, for guiding me during my Ph.D. studies with his extensive knowledge and inspiring criticism.

I would like to thank my co-supervisor, Assoc. Prof. Dr. Gülşen Tozsun, for her dedicated support and guidance in the project.

I specially thankful to Assoc. Prof. Dr. Selami Toprak for supporting me in analyzing the petrography at MTA.

I would like to thank the Thesis monitoring committee members, Prof. Dr. Naci Emre Altun and Assoc. Prof. Dr. Erhan Bat, for their suggestions during committee meetings.

This Ph.D. research was supported by the BAP (Office of Scientific Projects Coordination) of Middle East Technical University, Ankara, Turkey (Project No: TEZ-D-305-2021-10761). The hydraulic press of Atatürk University (Erzurum, Turkey) was used in the experiments under the supervision of the co-supervisor, Assoc. Prof. Dr. Gülşen Tozsin.

TABLE OF CONTENTS

APPENDICES

LIST OF TABLES

TABLES

LIST OF FIGURES

FIGURES

LIST OF ABBREVIATIONS

ABBREVIATIONS

OW = Oltu-stone wastes

CO = Cleaned Oltu-stone wastes

CO1 = Cleaned Oltu-stone wastes (density fraction = -1.25+1.20 $g.cm^{-3}$)

CO2 = Cleaned Oltu-stone wastes (density fraction = -1.20+1.15 $g.cm^{-3}$)

CO3 = Cleaned Oltu-stone wastes (density fraction = -1.15 $g.cm^{-3}$)

SO = Standard Oltu-stone

PO = Pressed Oltu-stone

MA = Method-A

MB = Method-B

MC = Method-C

CHAPTER 1

INTRODUCTION

1.1 Background

Oltu-stone is a semi-precious stone found in the Oltu region, Erzurum, Turkey. In the literature, it is referred to as Erzurum Stone, black amber, gagat, Jayet, and Jet (Ethem, 1990; Kalkan et al., 2012; Kara-Gülbay et al., 2018). In Turkish, it is also known as Oltu-stone, Erzurum taşı, Kara Kehribar, and Sengi Musa. The Oltu-stone is a geological material that is not a true mineral but rather a mineraloid formed by wood-decaying under extreme pressure (Hatipoğlu et al., 2012; Karayigit, 2007). It lacks crystallinity and has a density nearly to coal. It is usually black, but it can also be velvet-black, blackish, gray, or greenish. The most exciting feature of Oltu-stone when excavated is its softness. When exposed to air, it begins to harden. As a result, it is easy to carve (Hatipoğlu et al., 2012; Kara-Gülbay et al., 2018; Toprak, 2013).

Based on the study of Lahn (1939), only particular deposits in the Oltu district were known as Oltu-stone formation due to resin-rich content, while others were classified as coal formation due to resin-poor content. Oltu-stone colors were similar to jet (Ethem, 1990; Parlak, 2001). Jet has organic fossil-origin characteristics similar to Oltu-stone but differs in chemical properties (Hunter et al., 1993; Smith, 2005). Oltu-stone was found to be impregnated with clay and resin components and macroscopically generated from the fossilization of tree trunks (Kara-Gülbay et al., 2018). After the latest research on the genesis of Oltu-stone, it was determined to be liptinite-rich coal (Toprak, 2013).

The Oltu-stone and its evidence can be found in most Oltu regions, such as the Dutlu mountains. It was found in the Liassic lower Malm formation with a few meters of

lateral continuity and a maximum thickness of 50 cm (Kara-Gülbay et al., 2018; Ozen et al., 2013). Oltu-stone is extracted in the underground galleries using primitive methods and processed into valuable products such as ornamentals and jewelry by local ateliers. From mining to final processing, a huge amount of wastes is generated containing Oltu-stone. As a result, about 2% of extracted Oltu-stone is used as ornamental objects.

Oltu-stone's economic impact on the region is significant. The scope and relevance of this value for the area become apparent by considering the families of individuals who produce, process, and sell the Oltu-stone. However, the Russian stone (from Georgia), similar in appearance, gained popularity and badly damaged the local's business. As a reason, a preliminary methodology should be designed for Oltu-stone waste utilization as an alternative source.

1.2 Problem Statement

Oltu-stone is extracted with the conventional mining method. After extraction, large pieces of Oltu-stone are transported to the surface and hammered to remove impurities from the cleats. The quality Oltu-stone is separated by hand sorting. After hand sorting, the Oltu-stone chips less than 3mm thick or containing mineral impurities are discarded. Based on the atelier's data, this Oltu-stone wastes comprises 90-95% of extracted material from mines, and another 2-3% is thrown out during workshop processing, such as grinding and polishing. As a result, only 2% of extracted Oltu-stone is used in the final ornaments product. Given these issues, Oltu-stone wastes produced from mines can be used as an alternative product. Processing techniques are required in this regard to make it worthwhile. As used in the processing of amber powder, high-pressure agglomeration is the best suitable technique. It usually requires high pressure and softening temperatures, with or without the addition of a binder.

1.3 Aims &Objectives:

This study aims to develop a way for obtaining new products from Oltu-stone wastes, as simplified in Figure 1.1. Oltu-stone containing wastes is divided into waste generated during hand sorting and generated during final processing. This study primarily looked at wastes generated during hand sorting, referred to as "Oltu-stone waste (OW)." Following are the objectives.

1. Cleaning characteristics of Oltu-stone wastes.
2. High-pressure agglomeration of cleaned Oltu-stone wastes.
3. Characterization of pressed stone obtained from cleaned Oltu-stone wastes.

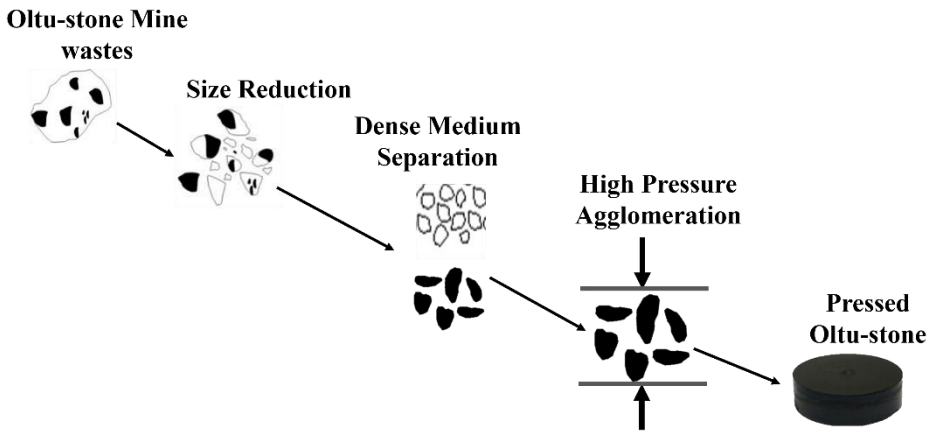

Figure 1.1 The layout to produce pressed Oltu-stone

1.4 Thesis Layout

The dissertation was structured into five chapters. Chapter 1 provides information on Oltu-stone and its problems, which led to this study. The second chapter is the literature on previous studies related to the problem. It provides insight into the characterization studies of Oltu-stone. Since no agglomeration studies on Oltu-stone wastes have been reported yet, the work documented on coal agglomeration and amber pressing is included. The method for sample preparation, impurity removal, and characterization of cleaned Oltu-stone wastes before and after pressing are

described in Chapter 3. The results of Oltu-stone waste characteristics after cleaning, optimized parameters for pressing cleaned Oltu-stone wastes, and, finally, various properties of pressed product obtained from cleaned Oltu-stone wastes are presented in Chapter 4. Chapter 5 summarizes the findings and suggests a method for producing pressed stone from Oltu-stone wastes.

CHAPTER 2

LITERATURE REVIEW

2.1 Site Location

Oltu-stone is located on the southern side of Dultu mountain in Oltu town, 124km NE of Erzurum, eastern Turkey (Toprak, 2013). Several studies (Kalkan et al., 2012; Kara-Gülbay et al., 2018; Kocaman, 2011; Parlak, 1989, 2018) presumed that Oltu-stone mining started by the end of the 18th century.

Figure 2.1 Site Location and of Oltu-stone mines (Toprak, 2013).

The search for the Oltu-stone extraction was based on field observations and expertise. The primary parameter for gallery site selection is circumstantial evidence of Oltu-stone and lignite levels on outcrops of Oltu-stone-bearing strata (Figure 2.2a). The lens form of Oltu-stone can be found in the Oltu-stone-bearing sediments (Figure 2.2b). Locals extract it in underground galleries with widths ranging from 50 to 70 cm (Figure 2.2d). Limited laborers from Dutlu Village were employed at these galleries, ranging from two to five people. Non-technological methods are used to develop the Oltu-stone extraction galleries. (Bilgin et al., 2011).

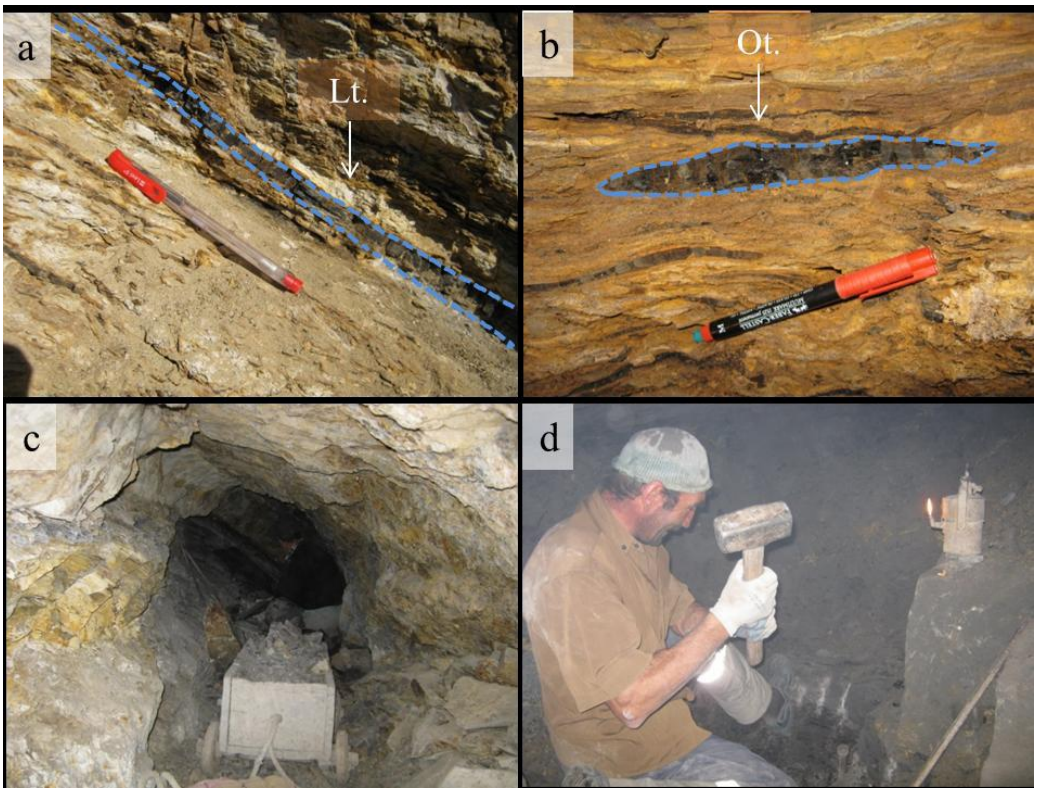

Figure 2.2 Oltu-stone-bearing deposits mine (a) lignite (Lt) outcrop, (b) Oltu-stone(ot) lens, (c) gallery extracted Oltu-stone and transport tool in the gallery for waste material disposal, and (d) local worker extracting the Oltu-stone in the gallery (Kalkan et al., 2012).

The excavation was done with simple tools like a shovel with a short handle, a hammer, and chisels (Figure 2.2d). As the galleries proceed, the created waste material is transported out of the galleries using four-wheeled wooden transport equipment that can be pulled by a rope (Figure 2.2c). Local artisans process the raw Oltu-stone utilizing key instruments such as an electric lathe, polishing wheel, drill, and hand tools such as steel knife, file, and sandpaper, to make it appropriate for working (Kalkan et al., 2012).

2.2 Geological Setting

The basement of the Oltu region contains Permo-Carboniferous dacite and rhyodacite, and granite porphyry stocks and dykes (Figure 2.3) cut these volcanic rocks.

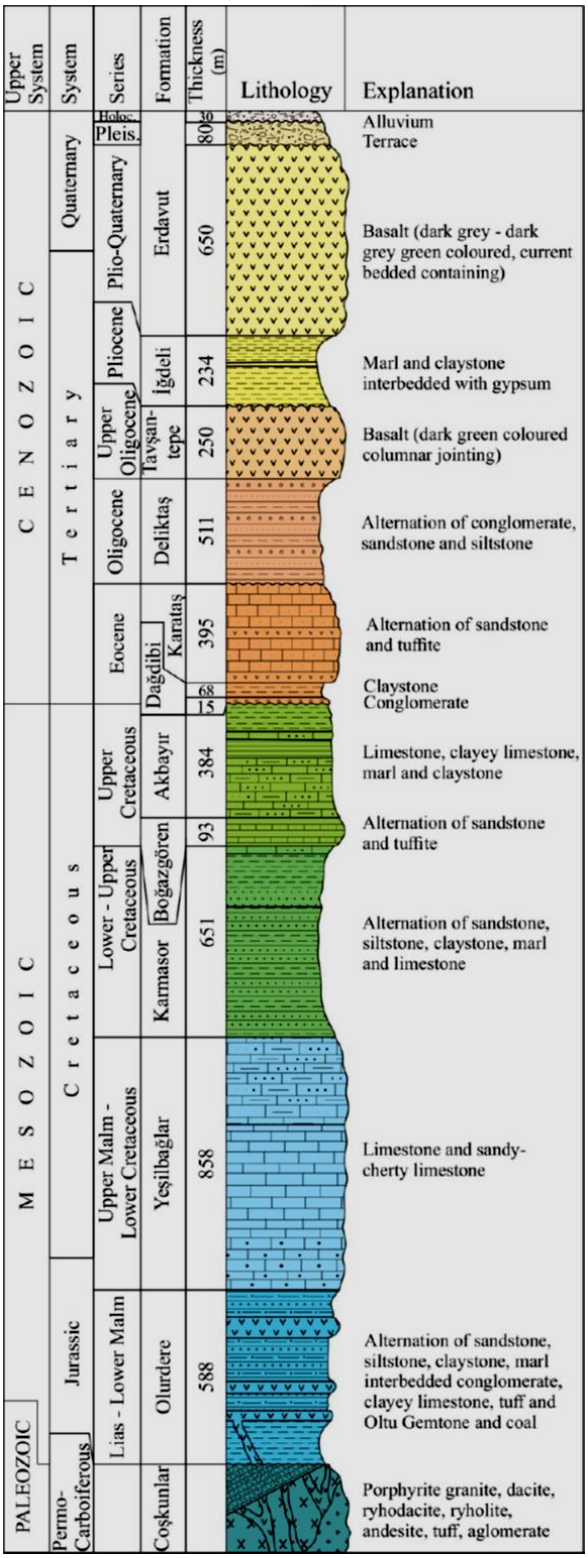

Figure 2.3 Comprehensive columnar section of the study area (Kara-Gülbay et al., 2018)

Unconformable Liassic lower Malm formation claystone, sandstone, and volcanic stuff are interbedded with thin coal bands and Oltu-stone. Upper Malm Lower Cretaceous limestone and sandy cherty limestone make up the final arrangement. During the Early Late Cretaceous period, sandstone, siltstone, limestone, and marl series were deposited. The underlying unit was covered by a sequence of sandstone, tuffite, limestone, clayey limestone, marl, and claystone in the Late Cretaceous. Eocene aged claystone, conglomerate, sandstone, and tuffite cover Cretaceous parts, which are also unconformably enclosed by an Oligocene aged conglomerate, sandstone, and siltstone order. Upper Oligocene basalt, Pliocene gypsum interbedded marl, and claystone make up the Tertiary arrangement, ending with Plio-Quaternary basalts (Kara-Gülbay et al., 2018; Toprak, 2013).

The Oltu-stone occurrences under investigation were found in Liassic-Early Malm aged Olurdere Formation (Figure 2.3). Olurdere formation begins at the bottom with sandstone and clayey limestone interbedded claystone and continues upward with diabase, basalt, and pyroclastics and finishes up with limestone, marl, conglomerate, and claystone; interlayered thin medium and thick-bedded sandstone (Kara-Gülbay et al., 2018).

2.3 Uses of Oltu-stone

Oltu-stone is primarily utilized in the creation of decorations like as rings, earrings, necklaces, bracelets, tiepins, pipes, studs, cigarette holders, and prayer beads, and is frequently combined with a silver (Çiftçi et al., 2004, 2002; Hatipoğlu et al., 2012; Kalkan et al., 2012; Karayigit, 2007), as shown in Figure 2.4. However, the wastes generated from Oltu-stone mining and processing are used for burning purposes.

Figure 2.4 Different Ornaments made from Oltu-stone

2.4 Previous studies on Oltu-stone

2.4.1 Physical and Chemical Properties

The Oltu-stone and lignite coal are found chiefly in the form of lenses surrounded by sandstone and claystone deposits (Figure 2.5a). However, the physical properties of Oltu-stone and lignite coal differ from each other. The Oltu-stone has a matt

appearance, while lignite has deep black with a metallic look. The massive structure of Oltu-stone and compacted lignite also has distinctive features, as shown in Figure 2.5(a-b). Oltu-stone is renowned for its softness when first excavated and rigid in air contact; it helps to carve. On the other hand, lignite remains the same before and after excavation in terms of hardness (Figure 2.5c), as Kalkan et al. (2012) reported. Due to perfect cleavage during formation, Oltu-stone can be found as flattened pieces within the deposits. The top surface and cross-section part of such pieces are shown in Figure 2.6.

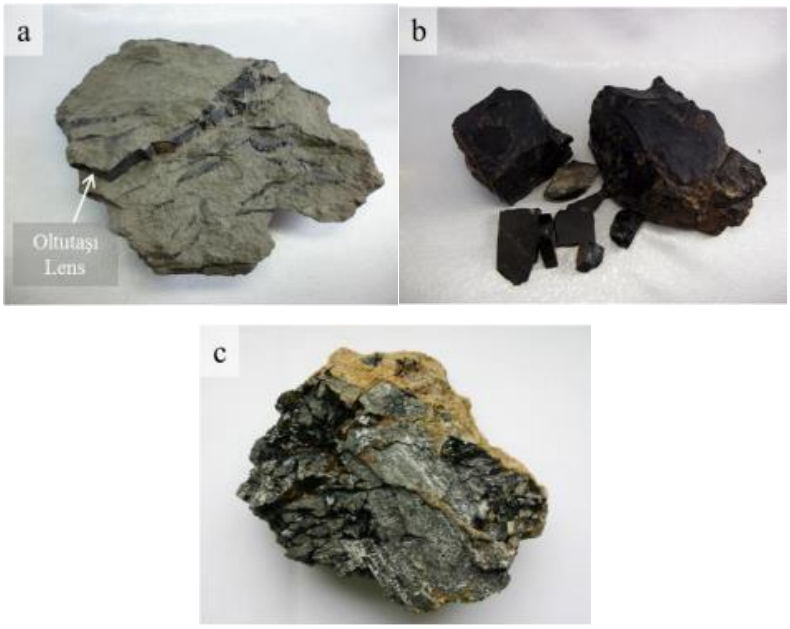

Figure 2.5 Oltu-stone and Lignite pieces; (a) Oltutaşi lens within the deposits, (b) Oltu-stone fragments, (c) Lignite piece. (Kalkan et al., 2012)

Figure 2.6 (a) Cross-section of Oltu-stone and (b) top surface of Oltu-stone (Kalkan et al., 2012)

Some chemical and physical properties of Oltu-stone are shown in Table 2.1. It gets a glossy appearance after surface grinding. It is found mainly in black color and rarely in brown color. Due to high elemental carbon and coaly characteristics, it gets burned during flame contact. Furthermore, Oltu-stone attracts static electricity-like substances such as dust when rubbed (Çiftçi et al., 2004; Ethem, 1990; Hatipoğlu et al., 2012; Karayigit, 2007; Parlak, 2001).

Table 2.1 Physical and chemical properties of Oltu-stone (Hatipoğlu et al., 2014; Kalkan et al., 2012; Kara-Gülbay et al., 2018)

Components	
Crystal System	Turbostratic or Amorphous
Hardness	3 (moh's scale)
Carbon	78%
Hydrogen	6.70%
Sulphur	0.90%
Ash	2.3%
Density	1.25-1.30 $g.cm^{-3}$
Volatile Matter	51- 65 %
Moisture	2.18%

Due to resin content, Oltu-stone was assumed as amber. Amber has an amorphous carbon structure with a 67-87% carbon ratio like Oltu-stone. Amber hardness varies 1.5-3 according to moh's scale and has a density of 1.023 to 1.125 $g.cm^{-3}$ (Pastorelli, 2009). Carbon content and hardness make Oltu-stone and amber identical but have variable densities. Amber has a complex chemical structure, primarily terpenoids and phenol, and small amounts of acids, alcohol, amino acids, and fat (Mills et al.,

1984). These components are variable and depend on different parameters, for instance, origin, geological background, diagenetic changes, paleobotanic, and palaeoclimate sources (Savkevich, 1981). Karayigit (2007) studied on the primary elements in Oltu-stone, which includes; Fe (0.32%) Ca (0.18%), Na (0.08%), Al (0.08%), Ti (0.07%), K (0.03%), P (0.01%), and Mg (0.01%). The concentration of these elements was deficient due to less ash content. Fe content was higher among all elements, indicating pyrite, consistent with mineralogical data. According to Kalkan et al. (2012), these trace elements were linked with organic matters or encapsulation of fine-size minerals or both.

2.4.2 Petrographic Investigation

Like coal, Oltu-stone contains two parts, organic and inorganic. Organic components are based on macerals distribution, and inorganics are on mineral content. For further understanding of macerals present in low and high ranks of coal, the detailed description of their origin is shown in Table 2.2. In general, brown coal is mainly composed of xylite, with a low coalification degree. Xylite makes a very distinct cellular structure due to the coalified lignin and cellulose. Based on previous petrographic investigations, Oltu-stone was made up of xylite, including corpohuminite and textinite, and a small amount of resinite and liptodetrinite (Kalkan et al., 2012; Karayigit, 2007). This Oltu-stone was marked as low-rank coal due to high volatile matters and low reflection values of corpohuminite and textinite. According to the thin-section examination by Karayigit (2007), Oltu-stone is mainly composed of amorphous carbon and different macerals, including resinite, fusinite, and semifusinite, as shown in Figure 2.7.

Table 2.2 Terminology of macerals and their suspected origin (Greb et al., 2017).

LOW RANK COAL		ORIGIN
GROUP	**MACERAL**	
Huminite	Texinite	Plant cell walls (visible structure)
	Ulminite	Plant cell walls (gelified, structureless)
	Attrinite	Small particles of attritus (huminitic)
	Densinite	Mottled groundmass (originally attritus)
	Corpohuminite	Primary and secondary cell infillings from humic gels
	Gelinite	Crack infillings of amorphous humic matter
Liptinite	Sporinite	Outer membranes of plant spores and pollen
	Cutinite	Outer coatings of leaves, roots, stems
	Suberinite	Suberinized cell walls of cork in bark and roots
	Resinite	Plant resins, balsams, latexes, fats & waxes
	Alginite	Algae (mostly planktonic)
	Bituminite	Amorphous degraded material of algal or bacterial origin
	Exsudatinite	Secondary crack-filling material after oil generation
	Liptodetrinite	Mechanically degraded particles, and residues of liptinite.
Inertinite	Fusinite	Fusinization of plant cell walls (fires, decarboxylation etc.)
	Semifusinnite	Weakly humified and dehydrated plant tissues Fungal spores,
	Funginite	Fungal spores, sclerotia,
	Secretinite	Oxidation of resin and possibly humic gels
	Macrinite	Dehydrated flocculated humic matrix substances
	Interto-detrinite	Fusinization of tiny varied inertinite precursors

Most of the researchers discuss resin-rich content and associate the Oltu-stone with amber. However, the genesis of Oltu-stone was not defined, which Toprak (2013)

explained. Fluorescent evidence makes his study unique compared to other reported work. This study marked Oltu-stone as liptinite coal rich in suberinite (Figure 2.8) and has a small amount of resinite, sporinite, and huminite content (Figure 2.8d) with 0.45-0.49% reflectance values (Toprak, 2013). During Oltu-stone formation, the huminite and inertinite constituents are decayed by the geo-chemical effect during formation and leave cavities behind, whereas the liptinite component remains in Oltu-stone more resistance (Sutcu and Toprak, 2013; White, 1933). Due to compaction, these cavities are destroyed and filled with silicates (Toprak, 2013). These amorphous and cryptocrystalline quartz-filled cellular structures contributed to Oltu-stone hardness (Göymen, 1976).

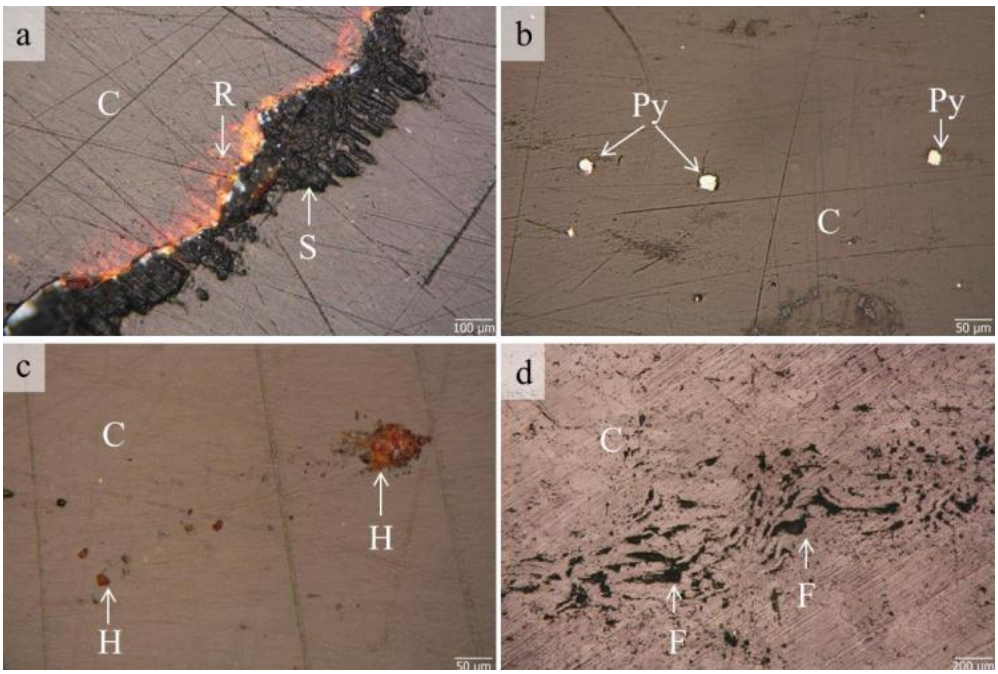

Figure 2.7 Polished section of Oltu-stone ; (a) resinite-R and semifusinite-S) (b) Pyrite-P mineral (euhedral), (c) hematite-H minerals with carbon-C based (d) fusinite-F showing curved structure (Kalkan et al., 2012).

Furthermore, the quality of the Oltu-stone is most likely due to liptinite macerals, particularly resinite content, which is originated from resin. Resinite is found by isolation of huminite or within the original cells huminite (Teichmüller, 1952; Tyson,

1995). Melted, dissolved, and rehardened or precipitated resins occur in fissures and cleats (Pickel et al., 2017). Based on the origin, two types of resinite exist; lipid resinite from fat and waxes and terpene resinite from resins (Taylor et al., 1998).

In terms of inorganic content, Oltu-stone contains quartz, hematite, and euhedral pyrite minerals (Bilgin et al., 2011; Karayigit, 2007). Inorganic content generally dilutes the semi-precious stone like Oltu-stone, but the deposition of precipitated silicate within the cellular structure of individual maceral suberinite gives more physical strength and resistance. It indicates the durability and toughness of this stone. This stone becomes soft when wet due to clay because clay absorbs water, but quartz does not (Toprak, 2013).

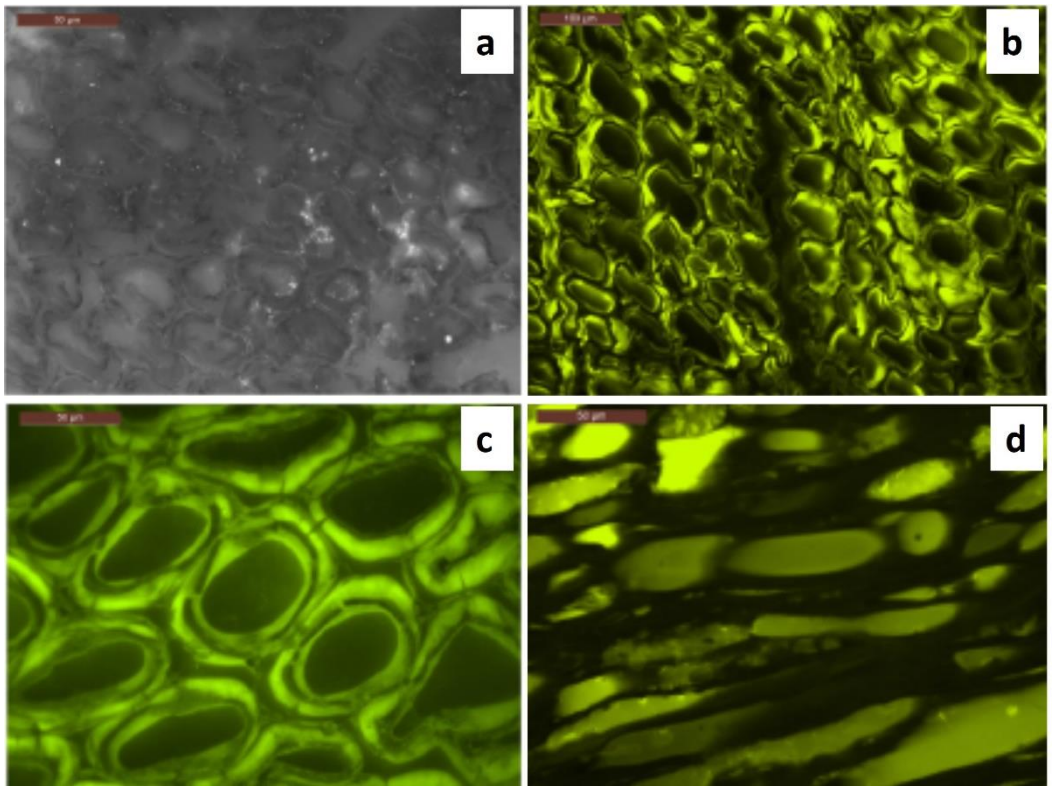

Figure 2.8 Oltu-stone polished section. (a) Suberinite cellular structure under white light. (b) Panel-a under blue light excitation (fluorescent image), (c) Panel-a under blue light excitation at high magnification. (d), Resinite and sporinite under blue light. (Toprak, 2013)

In combination with petrographic findings, the SEM-EDS analysis confirms the silicious inclusion as an inorganic impurity, more likely quartz in cell fillings (Figure 2.9c). The predominant cellular structure in Oltu-stone (Figure 2.9a) confirmed that the boundary contains carbon and oxygen (Figure 2.9b), whereas the inner core is filled with silicates (Figure 2.9c). In addition, some elements were found, such as Ca, Fe, Al, and Mg, as shown in Figure 2.9d (Toprak, 2013).

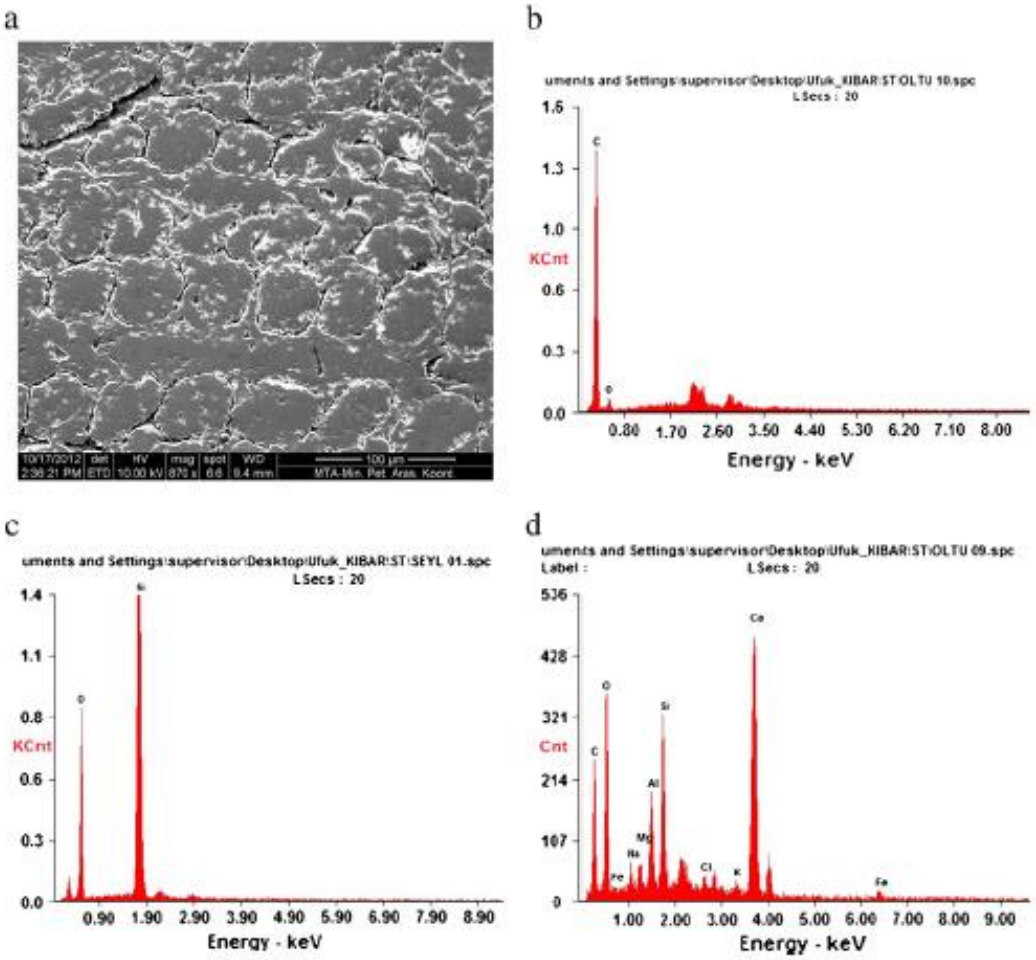

Figure 2.9 SEM-EDS examination of Oltu-stone (a). Oltu-stone cellular structure. (b) EDS results at the boundary of the cell. c)- EDS analysis of the inner cell core (d). EDS results of rarely found elements in Oltu-stone. (Toprak, 2013)

2.4.3 Mineralogical Investigation

Petrographic investigations give enough evidence to find the macerals content but not sufficient to find the exact mineral content. Therefore, mineralogical studies were needed. Based on the literature, the mineralogical investigation of Oltu-stone is mainly conducted by the XRD technique.

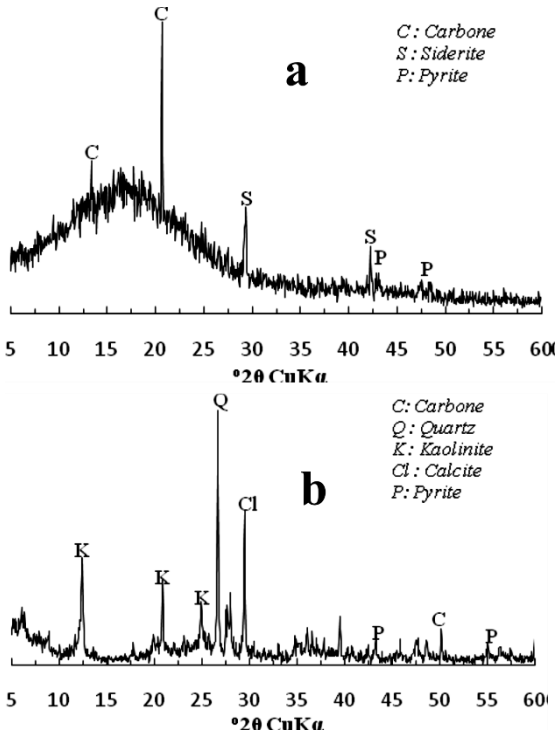

Figure 2.10 a)-The XRD pattern of Oltu-stone and b)- Oltu-stone bearing rock deposits (Kalkan et al., 2012)

Kalkan et al. (2012) reported that the Oltu-stone sample includes abundant amorphous carbon and crystalline phases and some trace matters, namely, siderite and pyrite minerals (Figure 2.10a). Oltu-stone bearing rock deposits represented are mainly composed of sandstone and siltstone. It includes minerals like pyrite, quartz, kaolinite, and calcite (Figure 2.10b). Hatipoğlu et al. (2014) found the turbostratic carbon in Oltu-stone, the intermediate stage between crystalline and amorphous

carbon, as shown in Figure 2.11. Some of the studies represent common findings, indicating the amorphous carbon and small amount of quartz and pyrite (Çiftçi et al., 2004; Hatipoğlu et al., 2012; Karayigit, 2007; King, 2006), but their petrographic findings were not sufficient. Kinaci (2013) conducted a comparative study of Oltu-stone with other carbonaceous material by using XRD to distinguish carbon phases. It revealed that the peaks with the following d-spacing, i.e., 14.79, 4.20, 3.78, 3.22, 3.05, and 1.95 Å, indicate carbonaceous material; the remaining represents the minerals contents such as silicates (2.51, 2.28, 2.25, and 2.12 Å) and pyrite (2.72 and 1.69 Å) respectively.

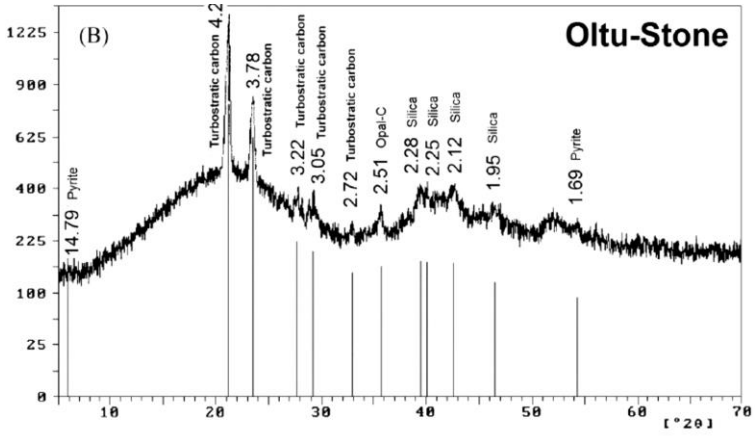

Figure 2.11 XRD pattern of Oltu-stone showing turbostratic carbon (Hatipoğlu et al., 2014)

2.4.4 Thermogravimetric Analysis

The physicochemical characterization of carbonaceous materials is obtained from thermogravimetric analysis (Feist et al., 2007; Rodgers and Currie, 1999). It helps to determine the amount of volatile content, softening temperature, Tmax values (the temperature at which maximum weight loss occurs), and decomposition point. It is not used for material classification, but it allows to distinguish the age of fossilized material among two materials, like resin and coal (Feist et al., 2007; Rodgers and Currie, 1999). According to Kinaci (2013), the pyrolysis study of Oltu-stone

indicates that most weight loss (around 58%) occurs due to low volatile carbonaceous material in between 315 ºC and 610 ºC, in a single-stage decomposition (Figure 2.12). Furthermore, the TGA pattern of Oltu-stone showed little difference from the pattern of carbon black. It's an indication that Oltu-stone has high resistance when overheated.

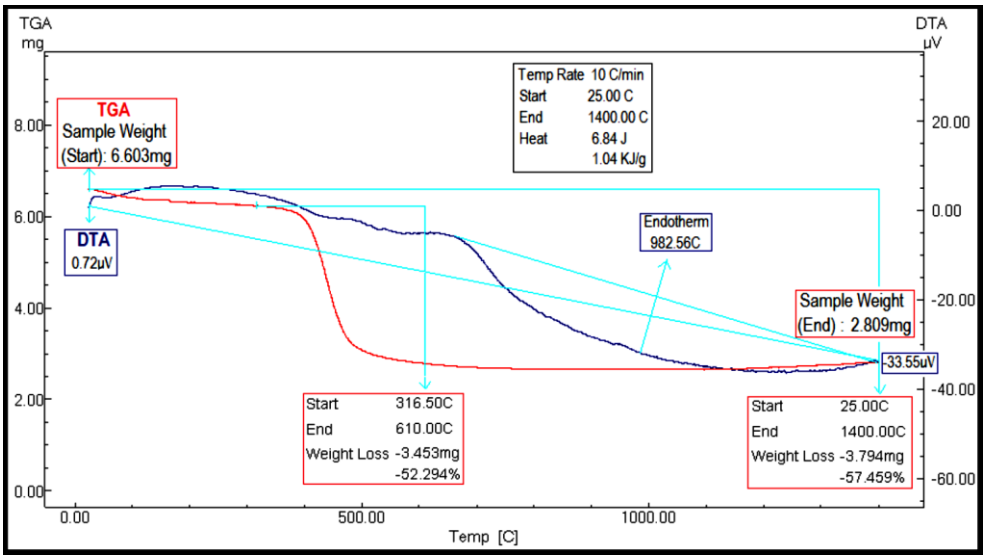

Figure 2.12 TGA analysis of Oltu-stone (Kinaci, 2013).

For Thermal treatment of coal, the starting point of decomposition and T_{max} values are considered. Based on Figure 2.12, the industrial processed temperature should not exceed 316˚C and be considered an accepted heat treatment value. T_{max} values of Oltu-stone were found to be 416-436˚C (Kara-Gülbay et al., 2018), which represents the point at which the hydrocarbon generated during pyrolysis. These values are extensively used to determine the thermal maturity of organic matter and marked material as immature if it is less than 435˚C (Cruz-Ceballos et al., 2020; El Nady et al., 2015; Labus and Matyasik, 2019). Therefore, Oltu-stone was marked as immature to early mature and ranked as lignite to sub-bituminous (Kara-Gülbay et al., 2018). In contrast, the T_{max} values for different ambers range 98-154˚C from younger to older resins (Pagacz et al., 2019), indicating that Oltu-stone has less resin content than amber.

Karayigit (2007) studied the thermal characteristics of Oltu-stone. The Proximate analysis shows the following findings, such as 1.70% moisture content, 2.30% ash, 64% volatile matter, and 32% fixed carbon. Other thermal parameters findings were 2% total sulfur (approximate) and 7703 kcal/kg calorific values on a dry basis. On a dry basis, a 2% increment in volatile matters was observed, which increased the non-agglomerating character of Oltu-stone. Based on previously documented work (Machnikowska et al., 2002), the carbon content increases for coal: vitrinite < liptinite < inertinite, opposite to the oxygen content. Volatile matter, hydrogen content, and the H/C atomic ratio rise in the following order: inertinite < vitrinite < liptinite.

2.4.5 Chemical Structural Analysis (FTIR)

Little research has been conducted on the chemical structural study of Oltu-stone using FTIR. The Oltu-stone genesis, on the other hand, is characterized as liptinite coal, and research on liptinite coal can be used as a reference. Hatipoğlu et al. (2014) studied the FTIR between Oltu-stone, graphite, and jet to distinguish their structure (Figure 2.13) with 7000-375 cm^{-1} wavenumber range found only the 5500-375 cm^{-1} helpful region. It revealed the presence of water content in Oltu-stone (3750 cm^{-1}), aliphatic carbon, C-O stretching (1000 cm^{-1} and 1026 cm^{-1}), and mineral content like Si-O stretching (880cm^{-1}).

The FTIR spectrum of various maceral groups of coal, shown in Figure 2.14. FTIR spectra are classified into four regions: O-H groups (3600-3100 cm^{-1}), C-H stretching bonds, especially aliphatic carbon (3100-2800 cm^{-1}), aromatic C=C and C=O (1800-1550 cm^{-1}), and aromatic C-H out of plane vibration (900-700 cm^{-1}) respectively (Machnikowska et al., 2002). The OH intensities in the liptinite groups are similar in vitrinite but are significantly lower in the lowest grade of liptinite. As the rank of liptinites increases, the absorbance intensity of OH groups diminishes, with the contribution of OH groups establishing hydrogen bonds of the OH-ether type rising in parallel. The contribution of OH groups to liptinites increased in the sequence:

(OH-free) < (OH-π) < (OH-ether) < (OH-cyclic +OH-N). This tendency is identical to low-grade cases (Machnikowska et al., 2002).

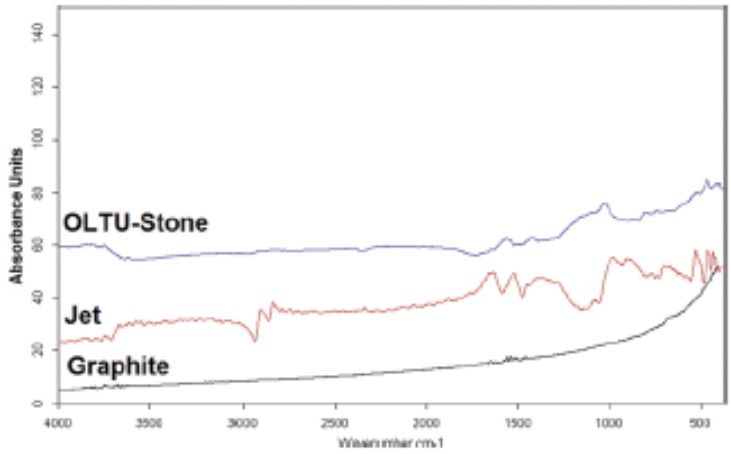

Figure 2.13 FTIR of Oltu-stone, Jet, and graphite

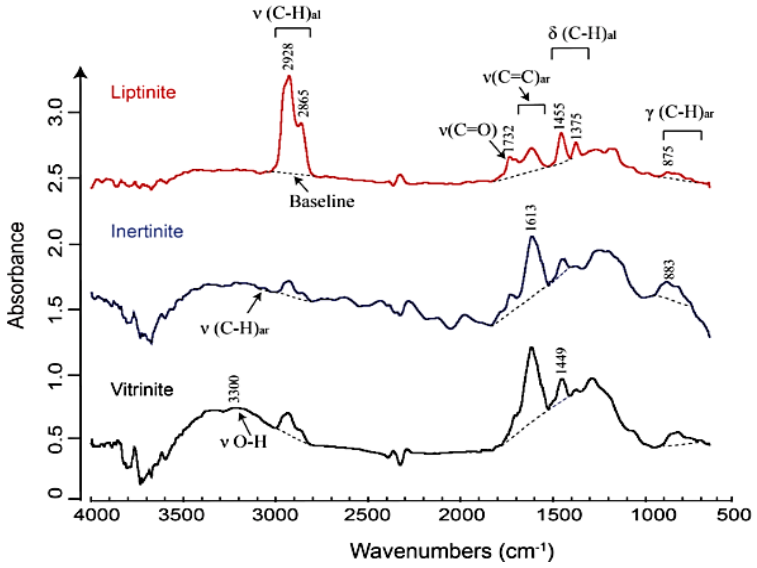

Figure 2.14 FTIR spectra of different coal maceral groups (Chen et al., 2015)

Liptinite coal differs from other characteristics in C-H stretched area by its greater aliphatic bands (3000-2800 cm^{-1}) than aromatic C-H bands (3100-3000 cm^{-1}). Liptinites only have two absorption bands ascribed between 2930 and 2860 cm^{-1} to aliphatic CH groups. Their intensity for all liptinites is distinctive. CH_2 modes have

a significantly more enormous contribution than in similar vitrinite. It is consistent with the known perspective on liptinite chemical composition, which involves the appearance of longer aliphatic chains and naphthenic rings. At 3050 cm^{-1}, the aromatic stretch band of liptinite is relatively weak, with the OH band significantly overlapping in the low-rank liptinite spectrum (Guo and Bustin, 1998). The peak at 1740–1700 cm^{-1} fluctuates in strength; it is inversely related to the strength of aliphatic CH stretching vibration at 3000–2800 cm^{-1}. At around 1740–1730 cm^{-1}, it is mostly a combination of aliphatic ester C=O groups and aromatic carbonyl/carboxyl C=O groups (Guo et al., 1996; Rochdi and Landais, 1991).

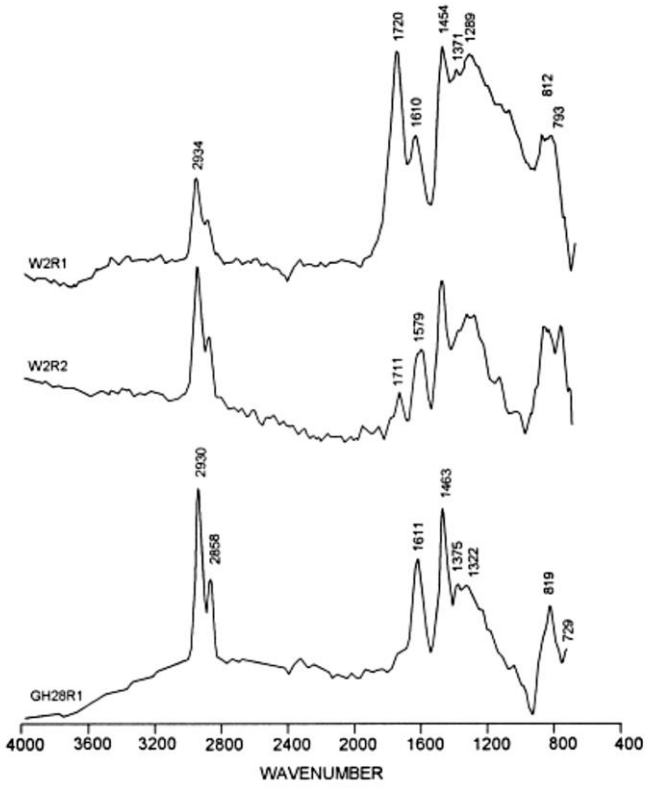

Figure 2.15 FTIR spectra of resinite from different coals (Guo and Bustin, 1998)

Resinite is mainly derived from resin content and is quite crucial in Oltu-stone. Resinite is a maceral belonging to the liptinite group. Several researchers have thoroughly examined the IR spectra of resinite (Lin and Patrick Ritz, 1993; McFarlane et al., 1993; Murchison, 1966). Guo & Bustin (1998) analyzed the resinite

from different coal, as illustrated in Figure 2.15. The main features of the resinite micro-FTIR spectra are the high aliphatic absorption at 3000–2800 cm^{-1} and 1460–1450 cm^{-1} and the strong aromatic ring intensity at 1610 cm^{-1}, and the aromatic CH out-of-plane deformation at medium to moderate intensities at 900–700 cm^{-1}. Some resinites exhibit absorption at 690 cm^{-1} due to five neighboring H-atom deformations comparable to sporinite. At 970 and 910 cm^{-1}, the aliphatic CH deformation in olefin occurs. Long-chain alkanes produce a peak at 720 cm^{-1}, although it is weaker than alginite, and it does not appear in resinite spectra, which have a peak at 690 cm^{-1}. In resinite, the degree of C=O group (1740-1690 cm^{-1}) absorption is inversely related to aliphatic CH absorption.

2.5 Agglomeration

Agglomeration is defined as forming large entities from solids particles by utilizing the material's property or binders. Agglomerate components are usually different, except the binder matrix or shrinkage due to the sintering process. The different particle combinations form a cluster through mechanical process technology is shown in Figure 2.16 (Pietsch, 2005).

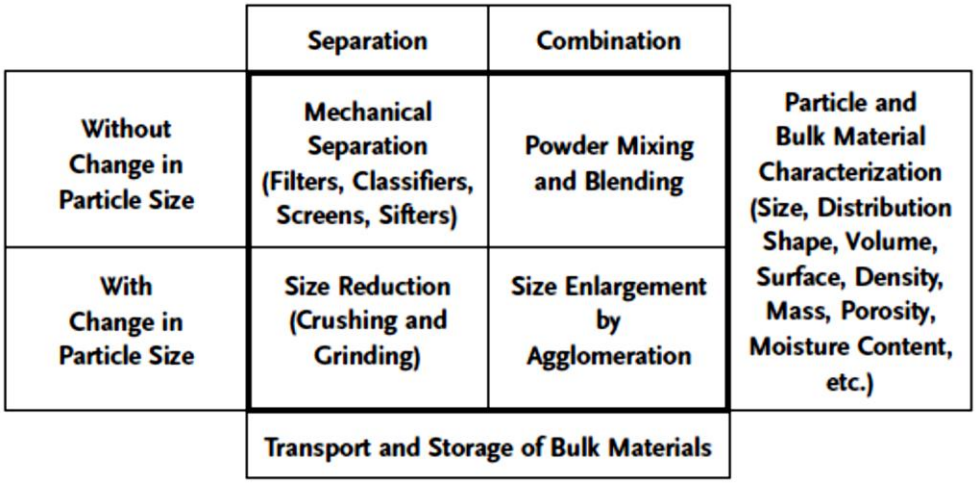

Figure 2.16 Agglomeration by mechanical process technology (Pietsch, 2005)

2.5.1 Agglomeration Theories and Techniques

There are three standard techniques adopted for agglomeration. (Pietsch, 2005);

1. Agglomeration by tumble or growth process (e.g., pelletizing).
2. Agglomeration by compaction or pressure (briquetting, compacting, tableting, extrusion).
3. Agglomeration by heat treatment (sintering, nodulizing, powder metal sintering).

Larger entities are produced by applying external forces to particles in closed dies that define the geometry of the agglomerated product. In pressure agglomeration, the amount of force exerted during densification and shaping is the most important distinguishing element. As a result, the technology was separated into three categories: low, medium, and high-pressure technology. According to the mechanisms involved, the process can be further categorized as those using binders and those without binders (Pietsch, 2005). Most coal wastes are agglomerated through pressure agglomeration, which includes the application of high pressure by pressing a machine. As illustrated in Figure 2.17, initially, pressure agglomeration creates a particle rearrangement that takes little force and does not modify particle form or size. Then there is a sudden increase in pressing force, causing brittle particles to break and malleable particles to deform. Brittleness and plasticity occur frequently or concurrently if brittle and malleable particles are present. The number of scientific works on fines agglomeration conducted. However, the iron ore fines pelletizing and coal briquetting are most renowned.

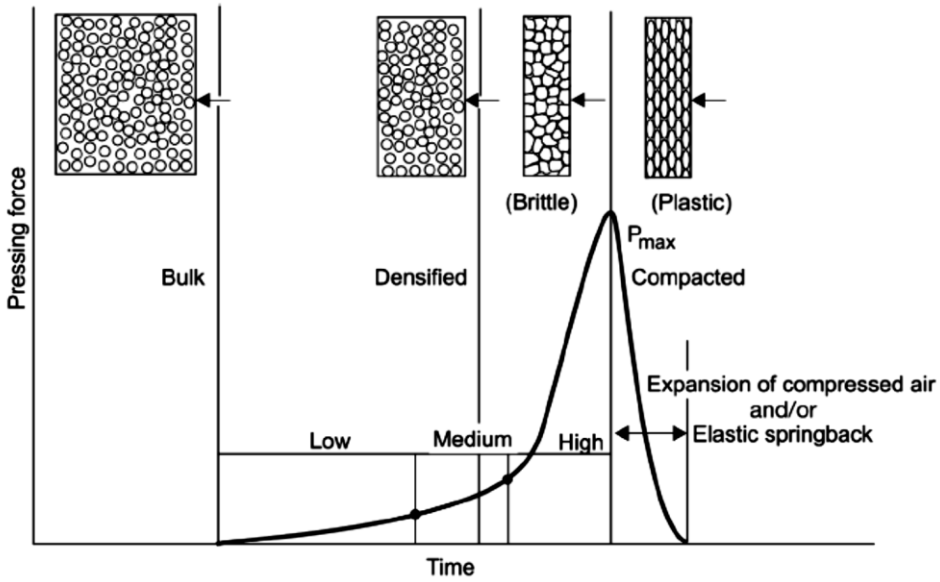

Figure 2.17 Mechanism of Pressure Agglomeration (Pietsch, 2005)

2.5.2 Agglomeration Mechanisms for Coal

For coal agglomeration, briquetting is a method of binding particles by applying pressure to the material. Briquettes can be made without binders if the coal allows it, such as a high vitrinite concentration and a caking tendency. Hot briquetting is another process that uses heat and pressure to create a binding. When briquetting coal particles that are difficult to briquette without additives, binders were used in case of coal fines. Biomass, organic binders, organic polymers, and phenolic resins are the many types of binders used for briquetting (Zhang et al., 2018).

There are numbers of variables to consider in the briquette production process. In general, two types of briquette forming mechanisms were proposed (Table 2.3) based on the research studies (Borowski and Hycnar, 2013; Zhang et al., 2018): binderless briquetting mechanism and cold-press briquetting mechanism with the binder. The binderless briquetting mechanism includes capillary theorem, adhesion between molecules, dense water, cation membrane theorem, and humic acid theorem (Olugbade and Ojo, 2021; Zhang et al., 2018). The binder briquetting mechanism includes the soaking and bridging, mechanical and chemical bonding force, and

bonding power due to contact angle (Zhang et al., 2018). Most of the binderless mechanism is based on water content, bituminite, and humic acid (Zhang et al., 2018). In coal briquetting, the compressive strength is responsible due to hydrogen bonding. Less moisture content makes less hydrogen bonding, but briquettes are still formed.

Table 2.3 Binding mechanism for coal (Zhang et al., 2018)

Mechanism		**Coal type**	**Conditions**
binderless	Capillary theorem	Lignite	Water present in capillary (under pressure)
	Molecule Adhesion	All coals	Water (under Pressure)
	Bituminous and humic acid theorem	Young lignite	Asphaltene (softening temperature 70-90˚C)
	Dense water and cation membrane	Wet coal particles	Water and cations (calcium and sodium ions)
	Colloid particle formation	Lignite	Granular humic acid (under pressure)
Binder	Soaking and bridging	All coals	Solid/liquid bridges between coal and binder
	Mechanical/chemical bonding force	All coals	Chemical functional groups or hydrogen bonding.
	Bonding power with less contact angle	All coals	Wettability (coal and binder)

Like minerals in the rock structure, macerals are building components of coal. Based on their chemical features, macerals are classed as reactive or inert. Vitrinite/huminite and liptinites are raw materials for liquefaction and gasification operations, while inertinite is required to produce activated carbon and graphite. The

enriched vitrinite macerals can mix with coal and increase the coke quality in the coke manufacturing process (Nag et al., 2018). Apart from the previously described binderless mechanism, the bonding process in binderless briquetting can be aided by the presence of high reactive macerals such as liptinite (especially resinite content) and vitrinite/huminite (Mangena and du Cann, 2007; Olugbade and Ojo, 2021). Their reactivity depends on the heating and its environment. Table 2.4 shows the thermal decomposition based on coal rank., including the point at which devolatilization begins and ignition temperature.

Table 2.4 Devolatilization and ignition temperature of different coals

Coal type	**Volatile Matter (˚C)**	**Ignition Temperature (˚C)**
Lignite	130-170	250-450
Bituminous	200-300	400-500
Anthracite	380-400	700-800

Mangena & du Cann (2007) studied the binderless briquetting characteristics of different coal, with reactive macerals around 55% in them. These briquettes yielded higher compressive strength and showed increasing strength properties with increasing vitrinite content because vitrinite content can deform and create stronger bonds.

Coal has several mineral impurities such as quartz, clay, pyrite, calcite, and siderite. Clay minerals increase the compressive strength with specific moisture amounts, mainly due to kaolinite. It enhanced the plasticity of briquettes obtained from it—however, other clays like illite harm strength properties (Botha, 2019). Apart from mineral content, higher organic sulfur makes coal more thermoplastic (Given, 1984). It was reported that the high organic sulfur vitrinite is melting at a lower temperature than low sulfur vitrinite in the same coal (Dai et al., 2020).

The size of the coal particles also plays a significant function in briquette without binder. The agglomerates are expected to boost compressive strength with an increased proportion of fine sizes, i.e., the greater the fine particle content in the coal agglomerates, the stronger the compression strength (Sun et al., 2014). Based on literature (Liu et al., 2014), it is explained in two ways. (1) an increase in the proportion of small and fine particles fills the gap of larger particles, thus increasing the carbon's contact area, thereby increasing the activity of the bond, and therefore the compression force; (2) the small particle size reduces the particle distance and thus increases the interaction strength between these particles. As a result, the overall force chains lengthen, resulting in high compressive strength. The force chain, a function of particle size and contact area, grows as the proportion of fine particles increases, resulting in increased compressive strength of lignite briquettes (Akinnuli and Olugbade, 2014). More fine particle concentrations increase the surface area between particles, likewise, increases the hydroxyl group percentage (such as COOH–COOH, OH–N, Cyclic, OH–ether, OH–OH, and OH–π), so more significant levels of hydrogen bonding occur (Miura et al. 2001). The greater the degree of hydrogen bonding, the greater the compression strength of the briquette (Olugbade and Ojo, 2021).

2.5.3 Amber Pressing

Oltu-stone is rich in liptinite, particularly resinite content, essential in Oltu-stone wastes agglomeration. Resinite macerals have similar petrographic characteristics to amber. Therefore, discussing the amber pressing mechanism is necessary to find the best way for Oltu-stone waste agglomeration. Since 1881 (pioneered by the Austria-Hungary company Stantien & Becker), small chips of Baltic amber that were too small for use in the jewelry trade have been softened (but not melted) to enable them to be pressed into larger blocks known as “Ambroid” (sometimes “Amberoid”).

According to scientific studies (Vikhareva et al., 2016), melting amber chips to generate a solid block with the same density as natural amber has been investigated.

Experiments with various pressures have reported that when the heat distortion temperature rises, the density of amber increases, but the color of the sample darkens. Natural amber has a density of 1.05-1.09 $g.cm^{-3}$ in most cases. In this reported work (Vikhareva et al., 2016), the researcher used polished and unpolished amber chips of various grain sizes. This method involves placing 1.7g of amber chips in the mold and heating it to 140-180 °C for 1 to 2 hours with pressures of 30-60 MPa using a mechanical screw press and a dynamometer to control the pressing force. Also, the three-point bending tests were determined On the GP 30 kN DLC test machine. The following Table 2.5 represents the results of pressed amber (Vikhareva et al., 2016).

Table 2.5 Dependence of density on the temperature at 31.8MPa and 63.7MPa (Vikhareva et al., 2016)

	Dist. temp.	Pressure MPa	Heating time	Bending strength, MPa	Density, g/cm^3
Polished	140	31.8	1 hour	5.90	1.03
			2 hours	4.32	1.02
	160	31.8	1 hour	5.16	1.08
			2 hours	5.08	1.05
	180	31.8	1 hour	9.99	1.08
			2 hours	9.19	1.06
Unpolished	140	31.8	1 hour	2.11	1.01
			2 hours	2.47	1.03
	160	31.8	1 hour	3.26	1.07
			2 hours	2.17	1.04
	180	31.8	1 hour	6.73	1.08
			2 hours	6.12	1.05
Polished	140	63.7	1 hour	3.72	1.04
			2 hours	3.93	1.03
	160	63.7	1 hour	4.71	1.04
			2 hours	6.09	1.06
	180	63.7	1 hour	7.73	1.06
			2 hours	6.82	1.06
Unpolished	140	63.7	1 hour	0.85	1.00
			2 hours	1.32	0.99
	160	63.7	1 hour	3.05	1.04
			2 hours	3.23	1.06
	180	63.7	1 hour	4.76	1.05
			2 hours	5.08	1.06

Various methods of natural succinite modification are utilized to advance or change the appearance of natural specimens. As modified Baltic amber, a gemstone has been treated to both heat and pressure treatment together. It alters physical properties such as transparency and color and qualities like hardness and solubility in organic solvents (Wagner-Wysiecka, 2018).

The heat-pressure treatment to amber fines and chips is one of the processing methods. This procedure takes place under controlled pressure and temperature

settings and allows for the creation of material from powder or small pieces of amber that can be utilized in jewelry and other techniques. Pressed succinite goods resemble products created from a single piece of succinite. Succinite modification can have significant environmental consequences (Wagner-Wysiecka, 2018). Examples of goods made from natural and modified Baltic amber are shown in Figure 2.18 and Figure 2.19.

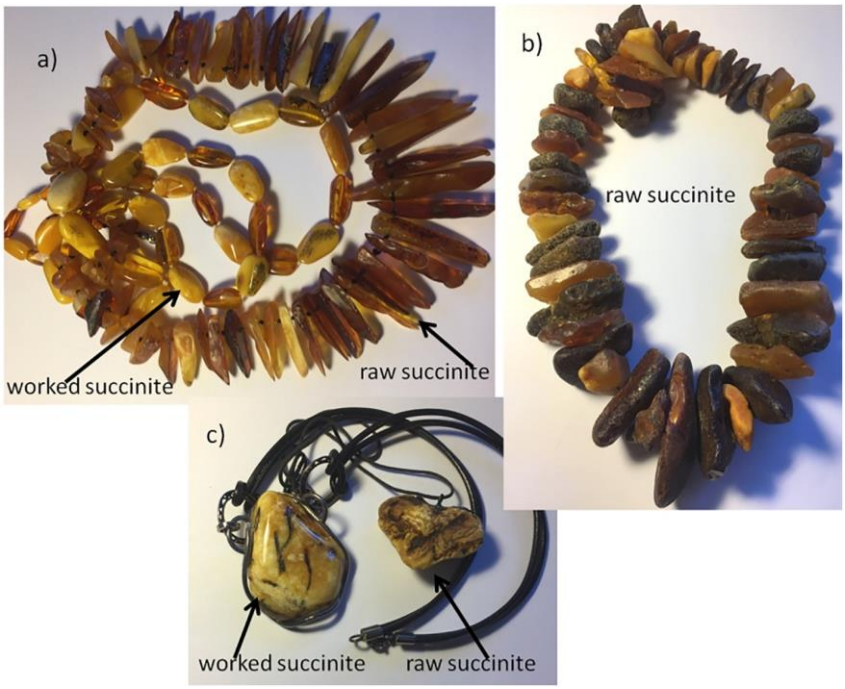

Figure 2.18 Examples of goods made from natural succinite (Wagner-Wysiecka, 2018).

Figure 2.19 Examples of modified Baltic amber - succinite (Wagner-Wysiecka, 2018).

2.5.4 Variety of binder used in the agglomeration

Briquetting and pressing amber/fossil resins are very similar processes. Briquette binder is split into three types based on material composition: organic binder, an inorganic binder, and compound binder. The strength of the inorganic links is only a few benefits of solid adhesive, cost, and high hydrophilicity. Inorganic briquette binders include clay, lime, plaster, cement, sodium silicate, and sodium silicate. Industrial briquette binder, civilian briquette binder, and environmental protection briquette binder are the different categories of inorganic binders (Zhang et al., 2018).

Organic binder not only has an excellent bonding performance, but it also has a high crush strength and drops test strength in briquettes. However, because the organic binder is easily decomposed at high temperatures, the mechanical strength and thermal stability of briquettes made with it are poor. Biomass binder, tar pitch and

petroleum bitumen binder, lingo-sulphonate binder, and polymer binder are the four forms of organic binders (Zhang et al., 2018).

2.5.5 Mechanical Properties of agglomerates

Oltu-stone is coal by origin but has characteristics like amber due to resinite macerals. One of the features of Oltu-stone is the polymeric chemical structure generated from the initial plant secretions that create macromolecular connections that are resistant to various environmental factors. The polymerization process imparts the feature of greater sensitivity to mechanical machining, increasing the utility of jewelers.

Jewelry producers can employ microhardness for practical purposes to check the physical characteristics of fossil resin or coal. Some specimens are either too brittle or soft to be mechanically treated (polishing, cutting). A decrease in hardness at a particular testing site indicates internal tension, breaking a large amber specimen into little pieces while cutting or polishing. As a result, the value of fossil resin is significantly reduced. Hardness measurement can also show whether amber or coal has been modified by heat treatment in an autoclave or furnaces, revealing if the physical appearance is natural or manufactured (Drzewicz et al., 2016).

Micro-hardness is simpler to evaluate in fossil resins, but coal characterization is complex since it comprises various organic entities termed macerals and specific inorganic components, internal pores, and fissures. Even though the micro-hardness of vitrinite and inertinite macerals are reliably assessed, the liptinite group micro-hardness cannot be determined due to the tiny size of the maceral inclusions. (Epshtein et al., 2015). Therefore, the Nano-indentation technique was recommended in the literature for mechanical properties. Nano-indentation is a sophisticated method where an indenter tip was used to touch the surface of the test sample in a specified manner. The material around the indenter was first deformed elastically by pressing the diamond indenter tip under specified loading

circumstances. As the stress is raised, the sample surface distorts or even shatter. The elastic deformation returned when the indenter load was lowered to zero, but the plastic deformation generated indentation fractures (Figure 2.20).

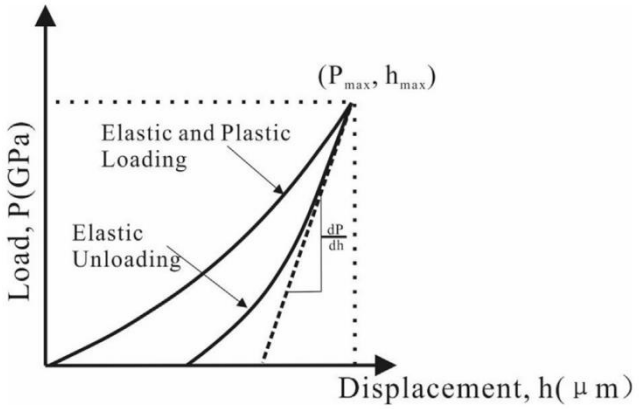

Figure 2.20 Nano-indentation curve for loading and unloading stage (Yu et al., 2018).

Many studies on nano hardness characterization of coal (Epshtein et al., 2015; Hou et al., 2020; Kossovich et al., 2016; Manjunath and Jha, 2019; Yu et al., 2018; Yihuai Zhang et al., 2020) show the effect of coal fracture, micropore, and mineral impurities (Figure 2.21 and Figure 2.22) on nano-indentation behavior, indicating the complexity of coal. However, the observation is mainly based on a 10mN load with the Oliver-Pharr method. It was revealed that the average values of hardness for liptinite maceral and vitrinite maceral groups were 408±24MPa and 538±61MPa, respectively, the contact modulus for the same groups was 4.57±0.02 GPa and 5.5±0.3 GPa (Epshtein et al., 2015).

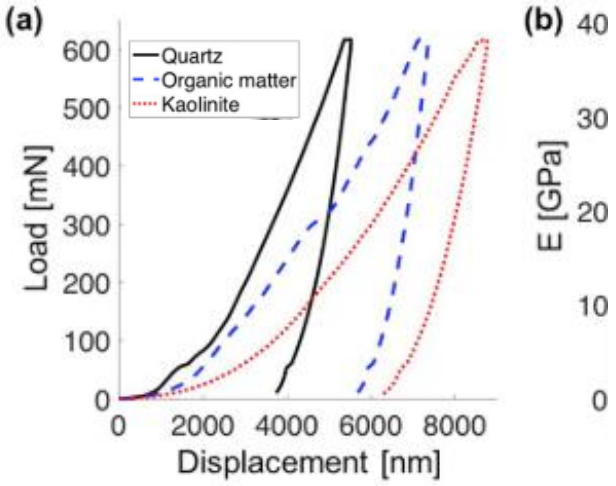

Figure 2.21 Loading and unloading curve of coal indentation (Manjunath and Jha, 2019)

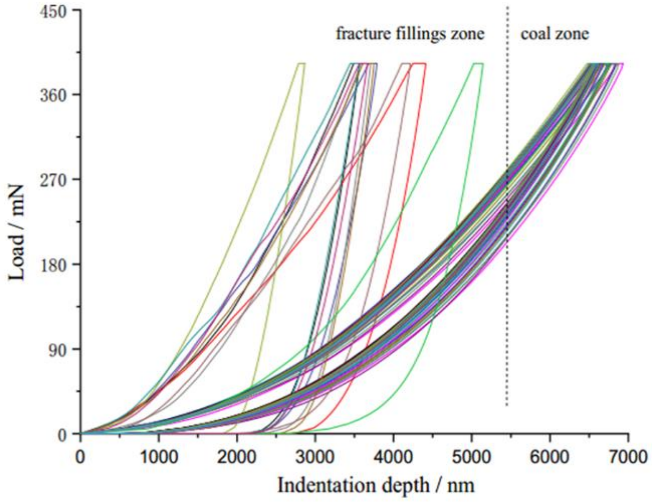

Figure 2.22 Coal phase under nano-indentation (Si et al., 2020)

CHAPTER 3

MATERIAL AND METHODS

3.1 Materials

The wastes are coming either from mines or ateliers after finishing the stone. Three types of waste are generated from mining to final polishing.

1. *Rock wastes:* Sandstone and claystone fragments are the primary rocks of the formation where Oltu Stone is extracted. Surfaces where the wall rocks touch with Oltu Stone lenses and fragments of Oltu Stone. During the extraction of Oltu-stone large blocks, the rock wastes are generated inside the mines (Figure 3.1A). This waste is termed rock wastes.
2. *Oltu-stone wastes (during hand sorting):* After extraction of Oltu-stone from mines, the large blocks are transported to the surface. The hammer is used to break those blocks (Figure 3.1B), and hand sorting is done to get a standard Oltu-stone (Figure 3.1C). This breaking generates lots of elongated chips containing minerals and an underdeveloped Oltu-stone. Some chips exhibit good quality stone but are not used due to size limitation (< 3cm) and discarded as waste. This waste combines standard Oltu-stone (<3mm), and Oltu-stone contains mineral impurities. In this study, this type was termed Oltu-stone wastes (OW).
3. *Oltu-stone wastes (during final processing):* After hand sorting of standard Oltu-stone, it was processed at Oltu ateliers, including cutting, crushing, grinding, and polishing. This process generates powder wastes in a small amount (Figure 3.1D).

The Oltu-stone wastes produced during hand sorting comprise 90-95% of extracted material based on ateliers data. For that reason, it was used in this study.

Figure 3.1 Types of Oltu-stone wastes. A) Rock wastes at galleries. B) Breaking of mined Oltu-stone. C) Hand sorting for standard Oltu-stone (>3mm). D) Oltu-stone powder wastes generated during grinding of standard Oltu-stone. E and F) Collection of Oltu-stone wastes samples, discarded after hand sorting.

3.2 Experimental Methodology

The experimental methodology of this work is shown in Figure 3.2. All the steps are discussed in detail in the next section.

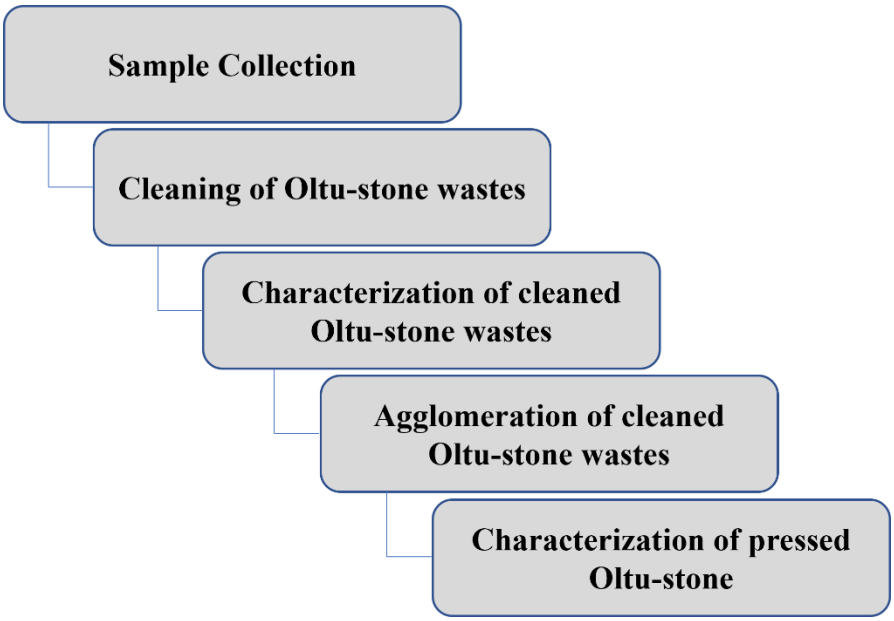

Figure 3.2 Experimental methodology of this work

3.2.1 Sample Collection

The Oltu-stone wastes produced during hand sorting comprises standard Oltu-stone (<3cm) and Oltu-stone containing mineral impurities. After hand sorting, the samples were collected from the vicinity of mines at Dutlu mountains (Figure 3.1E). The collected samples were brought to the mineral processing laboratory for examination.

3.2.2 Cleaning of Oltu-stone wastes

Oltu-stone wastes contain mineral impurities; therefore, a preconcentration is required before agglomeration, as shown in Figure 3.3. The air-dried collected samples were subjected to sieve analysis, resulting in different size fractions such as +20mm, -20+15mm, -15+10mm, -10+5mm, and -5mm. Due to the high amount, -10+5mm fraction was selected as a representative sample for cleaning and agglomeration. Then, the representative samples were crushed down to 1mm to liberate the mineral impurities.

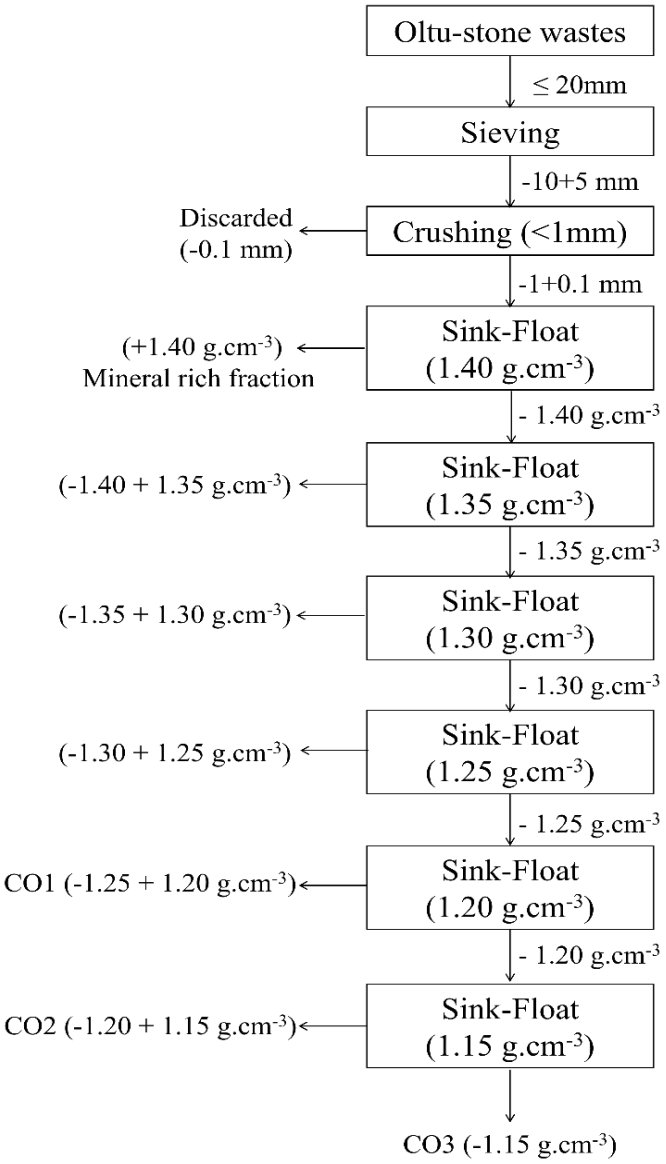

Figure 3.3 Flowsheet for Oltu-stone wastes cleaning

In contrast, the fines (below 100 µm) were discarded to avoid any coagulation during separation. The crushed sample (-1+0.1mm) was subjected to dense medium separation using $ZnCl_2$ solution of different densities gradients such as 1.15, 1.20, 1.25, 1.30, 1.35, 1.40 g.cm^{-3}. After that, the Ash was determined by ASTM D1374 standard method. Since the Oltu-stone is liptinite-rich coal, liptinite macerals have a density below 1.25 g.cm^{-3} (Stankiewicz et al., 1996; Yan et al., 2021). Therefore, the three float fractions i.e., CO1(-1.25+1.20 g.cm^{-3}), CO2 (-1.20+1.15 g.cm^{-3}), and CO3

(-1.15 g.cm^{-3}), were selected for characterization before agglomeration, and the rest i.e., -1.30+1.25 g.cm^{-3}, -1.35+1.30 g.cm^{-3}, -1.40+1.35 g.cm^{-3}, +1.40 g.cm^{-3} were excluded.

3.2.3 High-Pressure Agglomeration

Agglomeration is one of the known technologies for fine coal processing. The coal processing method is known as briquetting, which can be carried out with or without a binder. In binderless coal briquetting, the recommended temperature is 150˚C to achieve optimal compressive strength (Olugbade and Ojo, 2021).

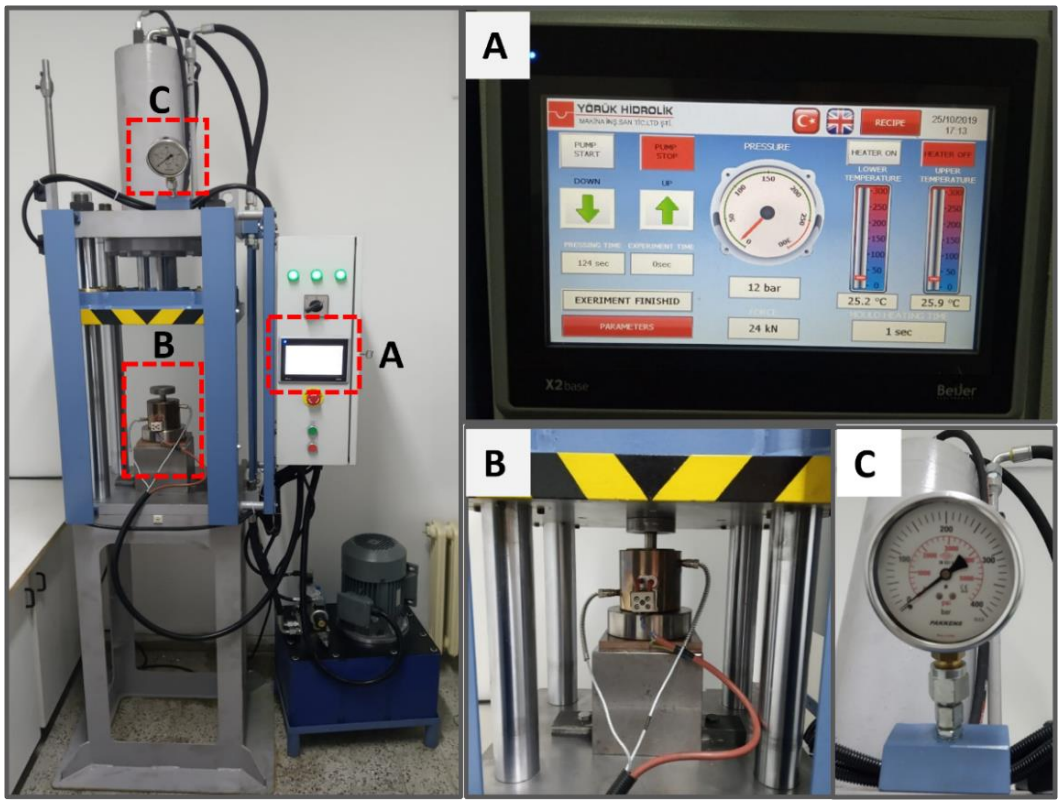

Figure 3.4 Hydraulic press used for agglomeration a). Digital meter shows the treatment parameters b). Mold under hydraulic press with controlled heating c). Pressure gauge indicating the capacity of the machine.

However, this study focused on binderless agglomeration of cleaned Oltu-stone waste to achieve similar physical and chemical characteristics as standard Oltu-stone

(SO). Therefore, the temperature was extended to 200˚C with different pressure using hydraulic pressure with a capacity of 1000 MPa, as shown in Figure 3.4. This machine was designed and manufactured by Yörük Makina, Ankara.

3.2.3.1 Sample Preparation

In order to optimize the particle size for agglomeration, the two types of samples were prepared from cleaned Oltu-stone wastes, i.e., below 100 µm and 30 µm. The cleaned Oltu-stone wastes obtained at 1.25 $g.cm^{-3}$ were subjected to grinding using a disc grinder, available at the Mineral processing laboratory, Mining Department, METU. Initially, it was ground for 10 seconds and yielded a particle size below 100 µm. Later, the grinding time was extended to one minute to get particles below 30 µm.

3.2.3.2 Agglomeration Methods

2g of powder sample were placed in a mold with a hole diameter of 20 mm and 100 mm length (Figure 3.4b). After that, it was pressed under heat and pressure treatment by using a hydraulic press (Figure 3.4). There are following methods were adopted to optimize the agglomeration conditions.

1. Method-A (MA)
    - A sample of less than 100µm size was put into an airtight mold, then fitted with a heater.
    - Preheating of sample till 100˚C from room temperature, which took 10 minutes.
    - After preheating, it was pressed under high pressure for 2 hours.
2. Method-B (MB)
    - A sample of less than 30µm size was put in an airtight mold, then fitted with a heater.
    - Two stages sample preheating.

a. Preheating at 100˚C for 30 minutes
b. Preheating at 200˚C for 30 minutes

- After preheating, it was pressed under high pressure for 60 minutes.

3. Method-C (MC)
   - This method is the same as B. Only addition of one more step, i.e., cooling.
   - After pressing, the treated sample remains under pressure till it cools down to 100˚C.
   - Different pressure and pressing time were used in this method.

3.2.4 Physical, Mechanical, and Chemical Properties Analysis

The following methods were used in this study to determine the different properties of cleaned Oltu-stone wastes before and after agglomeration. The agglomerates produced from cleaned Oltu-stone wastes were called “pressed Oltu-stone”.

3.2.4.1 Bulk Density

The density of pressed Oltu-stone was determined by direct measurement of length and diameter using a vernier caliper (±0.02mm). Disc surfaces were leveled by sandpaper. Electronic balance laboratory scales determined the mass of the individual disc. Determination of density was done 7 days after pressing. The following formula calculated bulk density:

$$\rho = \frac{4m}{\pi d^2 h}$$

Where ρ = Bulk density ($g.cm^{-3}$)

m = mass of cylindrical disc (g)

d = diameter of cylindrical disc (cm)

h = thickness of cylindrical disc (cm)

3.2.4.2 Nanoindentation Hardness

The CSM nanoindentation equipment available at METU central laboratory was used to determine the hardness (Hv) and elastic modulus (E). The main principle of Nanoindentation hardness is thoroughly described in reported studies (Fischer-Cripps, 2011; Hou et al., 2020; Yu et al., 2018). A flat and smooth surface is required for nanoindentation investigation. For a reason, polished sections from cleaned Oltu-stone grains and pressed Oltu-stone under various conditions were used. The 20mN load was applied by Berkovich indenter features a three-sided symmetric form, like a pyramid. Analysis was carried out under a load-controlled test in which the externally supplied load rises linearly with time during the loading stage, remains constant for 10 seconds during the holding stage, and drops linearly during the unloading stage. A series of 12 measurements were used on specifically chosen locations to note the spatial variability. The load and displacement at the tip-specimen contact surface are measured across three stages–loading, holding, and unloading. Then, data were analyzed by the Oliver-Pharr method to determine hardness (Hv) and elastic modulus (E).

3.2.4.3 Indirect Tensile Strength

After agglomeration, the pressed Oltu-stone were produced in a cylindrical-shaped disc with approximately 20mm diameter and 5 mm thickness. There is no equipment design for such kind of small sample. Therefore, the Load control testing equipment for laboratory scale was used in this work, which is manufactured by KONTROL-TEST equipment, Ankara. This machine is usually used to produce coal briquettes by applying a variable load. This machine has the capacity of applying a 50 KN load maximum with a variable loading rate. In this study, the disc specimen (pressed Oltu-stone) was loaded radially at a 1mm/min rate during indirect strength testing. The

maximum load at fracture was measured. The indirect tensile strength was calculated by following the formula.

$$\delta t = \frac{2P}{\pi \mathrm{DT}}$$

Where δt = Indirect tensile strength (MPa)

P = Failure load (N)

D = Diameter of cylindrical disc (mm),

T = Thickness (mm)

3.2.4.4 Petrographic Investigation

For petrographic investigation, polished sections were prepared from cleaned Oltu-stone waste fractions (CO1, CO2, CO3) and pressed Oltu-stone using METKON hot mounting resin. The maceral analysis was carried out by counting approximately 500 points using the point-counting method, and the random reflectance was measured on polished sections under reflected white and blue light excitation with 50x oil-immersion objectives coupled to a Leica DM4000M microscope. It is necessary to use immersion oil with a refractive index of 1.518 and a sapphire glass standard with a reflectance value of 0.589% to perform reflectance measurements. To investigate the fluorescence characteristics of liptinite macerals, TIDAS CCD UV–NIR was used.

3.2.4.5 SEM-EDS Analysis

SEM-EDS analyses were carried out to examine the morphology and mineral content on two machines. (i) JEOL instrument couples with EDS, at METU central laboratory, and (ii) inspect 50 (FEI company), coupled with an EDAX OCTANE (AMETEK Inc.), at General Directorate of Mineral and Exploration, Ankara (MTA).

It is challenging to identify organic species such as coal macerals. Mineral content looks lighter gray to white in BSE (backscattered electron) mode due to the atomic number contrast, while organic matter appears dark gray. Magnification and contrast of the image are critical for distinguishing maceral types under SEM. The grain samples were used for morphology and mineral content, whereas polished sections were used to analyze macerals. The grains samples belong to cleaned Oltu-stone wastes, and polished sections were from both cleaned Oltu-stone wastes and pressed Oltu-stone. The low voltage (10-20 KV) with high vacuum was used to differentiate macerals. Simultaneously, the EDS was used for semi-quantitative elemental analysis. Pressed Oltu-stone focused on EDS mapping to learn about the distribution of inorganic components around the surface.

3.2.4.6 XRD analysis

Based on the literature, the Oltu-stone is organic and has very low ash forming minerals, i.e., 2.5%. However, some studies revealed that Oltu-stone has crystalline carbon or turbostratic carbon. For that reason, the cleaned Oltu-stone wastes fractions (CO1, CO2, and CO3), Oltu-stone wastes, and standard Oltu-stone were used to analyze the carbon form and the mineral content. In this research, Rigaku ultima-IV powder XRDL was used to obtain an x-ray diffractogram, with 2θ (5˚-70˚) and a scan speed of 1˚/min.

3.2.4.7 Thermal Analysis

The thermal analyses include proximate and elemental analyses. For proximate analysis, Perkin Elmer STA6000 was used. This equipment is micro-TGA and requires a small sample of 15-20 mg. Czajka (2018) studied the coMParative study between mico-TGA and macro-TGA (ASTM standard) for coal and proposed a methodology (Figure 3.5) that is adopted in this work. LECO TruSpec micro CHNS

analyzer was used for elemental composition, using three different standards. A powder sample of less than 250 µm was used in both analyses.

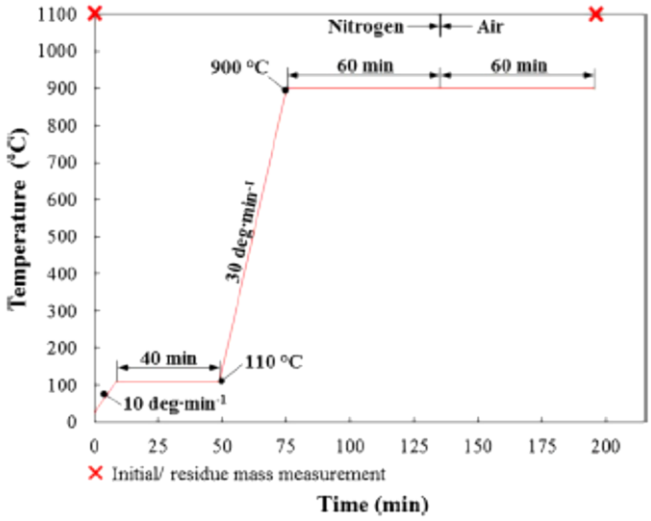

Figure 3.5 Micro-TGA steps for proximate analysis of coal (Czajka, 2018)

3.2.4.8 Chemical structure analysis by standard FTIR

Drift spectroscopy was performed on an FTIR spectrometer (spectrum-II, PerkinElmer) for functional group analysis. The scanning region ranged from 4000 cm^{-1} to 450 cm^{-1} (Mid-infrared region), with 32 scans at 4.0 cm^{-1} resolution. A powder sample (below 20 µm) was used to get FTIR spectra. Specific regions were then evaluated by a curve-fitting tool using peak-fit software for low absorption bands and overlapping bands. Peak positions were determined by the second derivative of the experimental curve, and the shape of the fitted peak was produced using a Gaussian method.

3.2.4.9 Chemical structure analysis by Nano-FTIR

In this work, Nano-FTIR (NeaSNOM, Neaspec GmbH) experiments were performed at Ankara University, TARLA. The polished sections from cleaned Oltu-stone wastes and pressed Oltu-stone were analyzed. Initially, the samples were observed under an optical microscope coupled with nano-FTIR. After that, the selected region was observed under AFM. A Pt coated Neaspec tip with resonance frequency 250-270 kHz and DFG broadband laser was used in measurements. The reference spectra were recorded on a silicon wafer. Spectra were collected with 16 cm^{-1} spectral resolution from selected points on the surface of samples. 30 spectra were collected (integration time was 10 ms/spectrum) to create the average spectrum.

CHAPTER 4

RESULTS AND DISCUSSION

4.1 Cleaning of Oltu-stone wastes

The cleaning of Oltu-stone wastes is a prerequisite before the agglomeration process. The cleaning process includes determining the particle size distribution of collected samples, crushing representative samples to liberate mineral impurities, and separating liptinite-rich content by dense medium separation. The particle size distribution of raw Oltu-stone wastes collected from the vicinity of Oltu-stone mines is illustrated in Figure 4.1. It shows that the wastes comprise particles between 3mm and 20mm, but a higher weighted fraction is –10+15 mm, approximately 50% of total waste. Therefore, it is considered the most representative sample of the waste. It yields an ash content between 13-18%, a higher amount than standard Oltu-stone, i.e., 2.33%. The -10+5 mm fraction was crushed down to 1mm to liberate the mineral content, and particle size distribution of crushed material is represented in Figure 4.2. It shows an abnormality jump in the curve within the size between 1mm and 0.5mm (Figure 4.2), which indicates liberation of most of the mineral impurities, consistent with the study of Wen et al. (1998). Therefore, the samples were prepared below 1mm and discarded below 0.1 mm to avoid fine clay and slimes. The washability curve of Oltu-stone wastes (Figure 4.3) shows the cleaned products obtained at different densities. The Oltu-stone is liptinite-rich coal, which has a density below 1.25 $g.cm^{-3}$ (Stankiewicz et al., 1996; Yan et al., 2021). Therefore, the three fractions were selected for characterization such as -1.15 $g.cm^{-3}$(CO3), -1.20+1.15 $g.cm^{-3}$ (CO2), -1.25+1.20 $g.cm^{-3}$ (CO1), respectively. CO3 has a very small yield, i.e., 4.5%, whereas CO1 and CO2 yield 50% and 80% of the cumulative float (Figure 4.3), which is considerable for waste utilization.

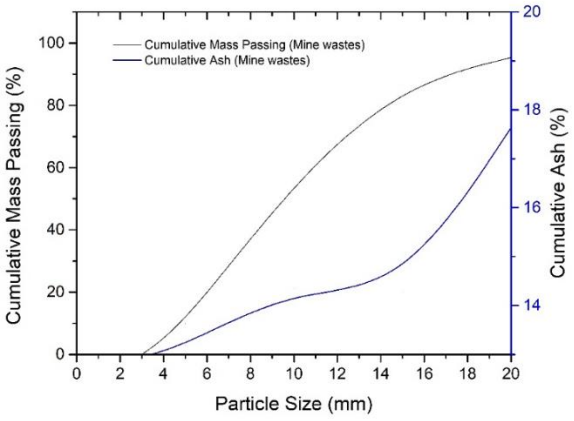

Figure 4.1 Particle size distribution of collected Oltu-stone wastes

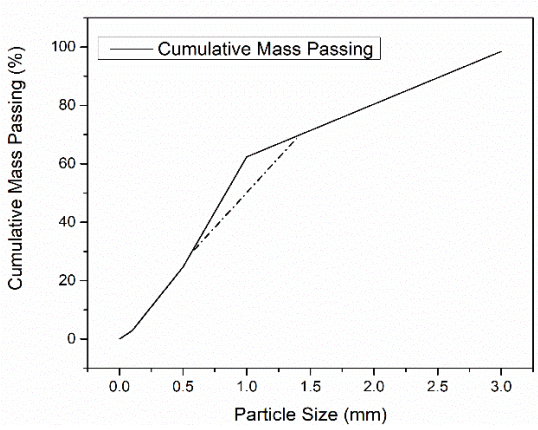

Figure 4.2 Particle Size distribution of crushed Oltu-stone wastes (-10+5mm)

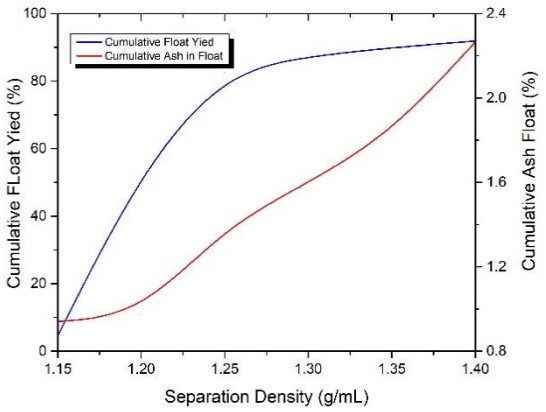

Figure 4.3 Washability curve of crushed Oltu-stone wastes

4.2 Characterization of cleaned Oltu-stone wastes

4.2.1 Optical microscopy

The float and sink fractions were observed under an optical microscope. The float fraction is mainly black due to Oltu-stone rich content (Figure 4.4a), whereas the sink fraction represents multi-colored mineral impurities (Figure 4.4b). In Figure 4.4c, some particles show the unliberated mineral traces on the surface. The dark brown resin content appears at the edges of the particles and is more visible as particle size reduces (Figure 4.4d). Resin appearance was improving with lower density fractions.

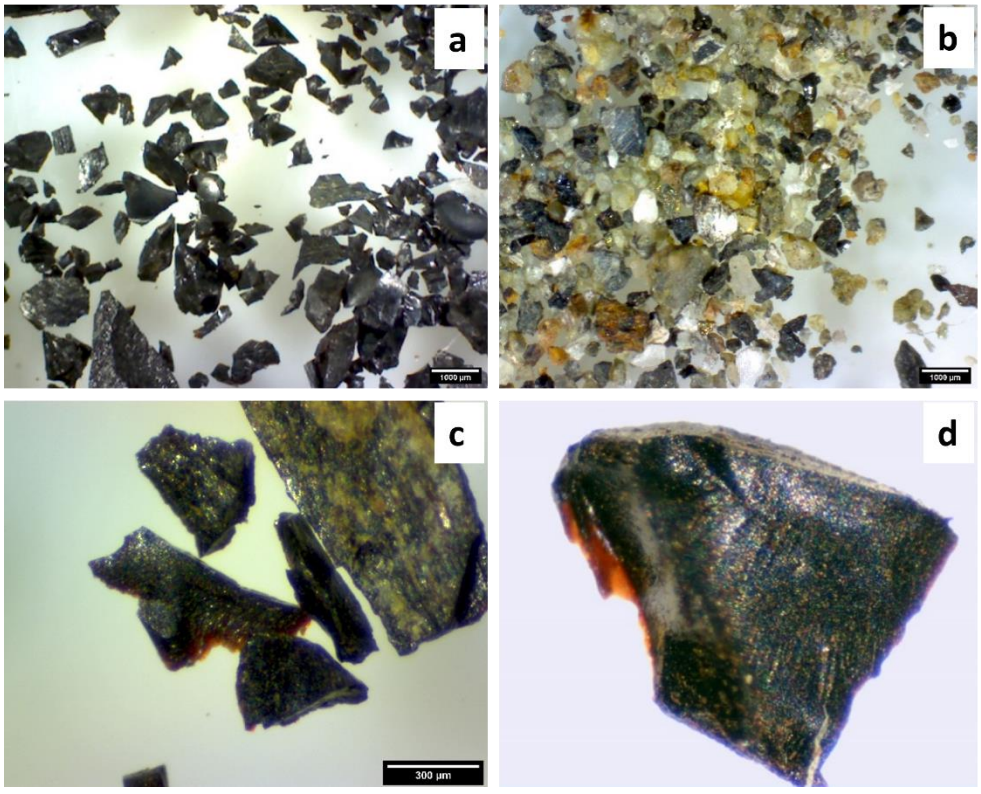

Figure 4.4 optical microscope images of CO1. a). Float fraction b). Sink fraction c). Particles showing minerals traces on the surface and resin orange color at the edges. d). Particles show the entrapment of resin.

4.2.2 Petrography microscopy

An optical microscope is good enough to see the picture of cleaning characteristics. However, finding resinite content (resin-rich maceral) evidence is not easy. Therefore, a petrographic microscopic analysis is required to analyze the maceral content and reflectance values. The petrographic investigation by the point-counting method is presented in Table 4.1. It revealed that the cleaned Oltu-stone wastes have 72-78%% of liptinite macerals and 19-23% huminite, and the rest are inorganics impurities. The liptinite content is observed to increase with a decrease in medium density. The reflectance values measured as R_{mean} are 0.39-0.40%. These values were taken mainly from huminite macerals which had embedded resinite content. The lower reflectance values indicate the presence of higher liptinite content (Petersen and Vosgerau, 1999).

Table 4.1 Maceral and Inorganic Percentages of the Oltu-stone and Its Reflection Values.

Samples	**Huminite (%)**	**Liptinite (%)**	**Inertinite (%)**	**Inorganics (%)**	**Pyrite (%)**	**Reflectance (Rmean%)**
CO1	23	72	0	2	3	0.40
CO2	19	77	0	2	2	0.39
CO3	20	78	0	-	2	0.39

Petrographic findings revealed altered suberinite cellular structure due to compaction by external forces (Figure 4.5a-b), which is different from the common rounded cellular structure reported by Toprak (2013). This alteration reduces the fluorescent character, probably due to an increase in coal rank. The spores are present in dark colors under white light (Figure 4.5c) and light colors under blue light excitation (Figure 4.5d). These spores (from sporinite) contain huminites in bright appearance (Figure 4.5c). In addition, the inorganics were evident within the cellular structure (Figure 4.5e), surrounded by huminite (light color) at their boundary. The low fluorescence properties of cell filling cavities indicate the presence of ultrafine inorganic impurities and some embedded resinite (Figure 4.5f).

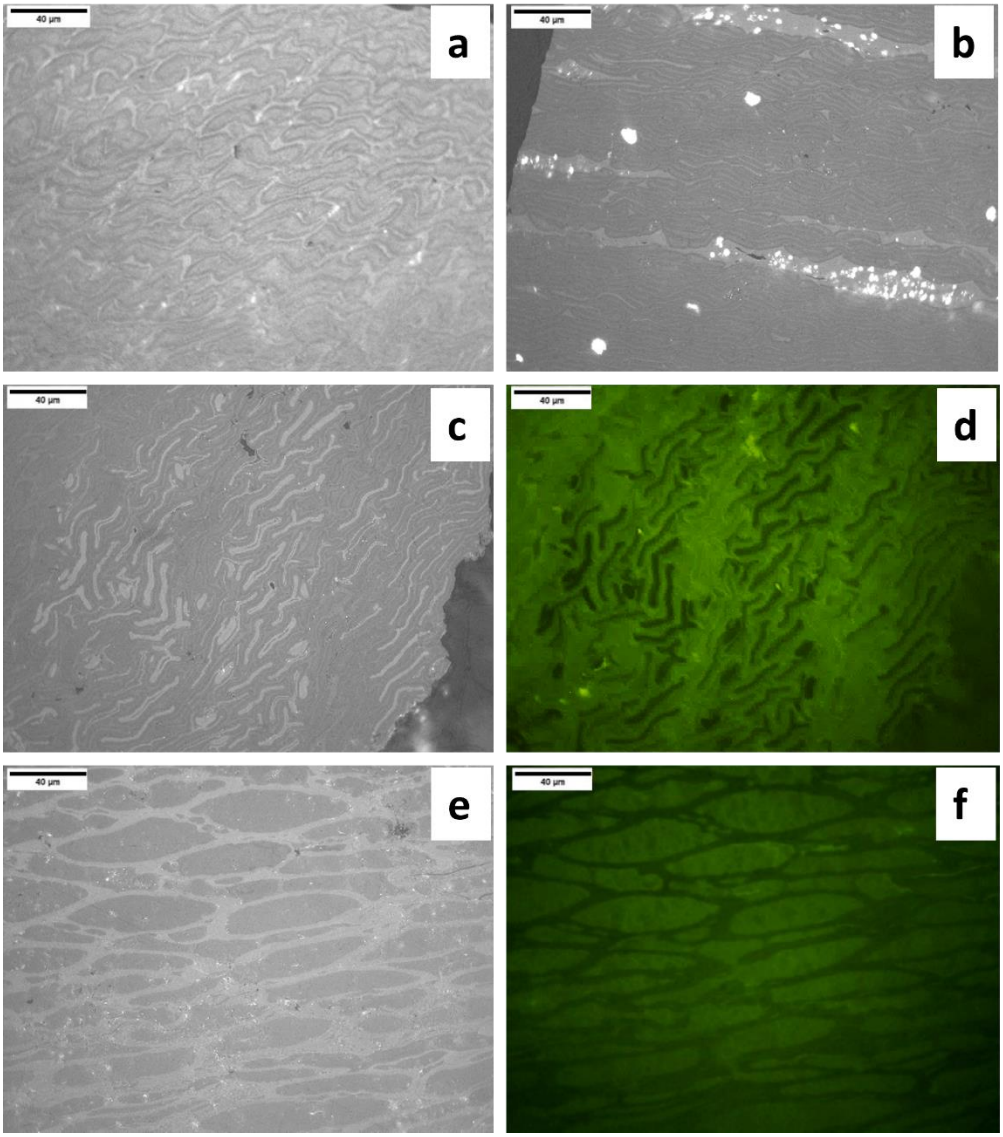

Figure 4.5 Photograph of cleaned Oltu-stone wastes a-b). Altered Suberinite cellular structure due to compaction. c) sporinite under white light. d) sporinite under blue light excitation e) Cell fillings with inorganics and resinite content, and cell boundary shows huminite. f) Panel-e under blue light excitation.

These variations occur because of deformation caused by various geological activities or other plant debris deposition. Apart from macerals, the inorganics were observed in cleaned Oltu-stone wastes such as pyrite and clay minerals. Most of the pyrites were encapsulated within the cellular structure, with a size range of 1-10µm. In dense medium separation, it is always challenging to deal with these fine inorganics widely distributed and enclosed in the macerals, resulting in their being

linked with the light density fractions (Huggins, 2002). In reflected white light, resinite macerals appeared in black-dark grey color, and in some cases, shows the lighter grey in low-rank coal (Pickel et al., 2017). Inorganics impurities like silicate minerals are identical to resinite under white light, but the blue light excitation can distinguish them. Resinite with varying characteristics can be found in the same coal (Hower et al., 2007). In cleaned Oltu-stone, two types of resinite are observed: primary cell filling resinite (Figure 4.6a) and secondary resinite (Figure 4.6c-f). The secondary is also exudatinite (Taylor et al., 1998). The globules resinite appeared in the huminite cell, showing greenish fluorescence color than secondary resinite with yellowish-greenish fluorescence color.

The fluorescence color variation in resinite content occurs due to resinite precursor, coalification history, and depositional conditions (Teerman et al., 1987). In Figure 4.6c, resinite is squeezed by the external forces, resulting in fluorescence color variation (Figure 4.6d). These color variations indicate resinite degradation or a gradual transition to huminite maceral (Suárez-Ruiz et al., 1994; Teerman et al., 1987). Apart from the varieties, some fine-sized resinite in dark grey color was observed under white light, but difficult to see under blue light excitation. It might be due to the presence of huminite and other liptinite macerals within the resinite content, as previously reported by Stankiewicz et al. (1996).

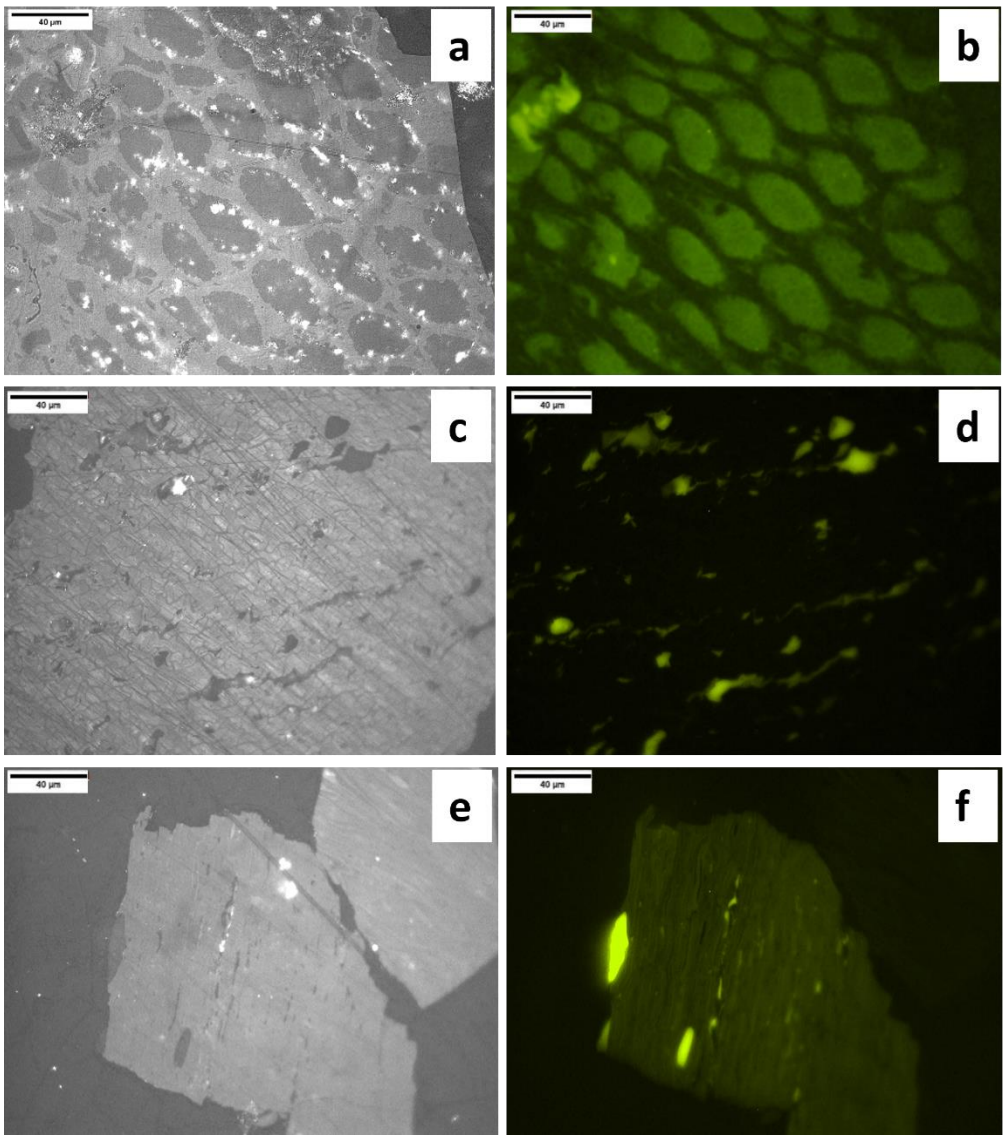

Figure 4.6 Different types of resinite in cleaned Oltu-stone wastes a). Primary cell filling resinite within huminite. b). Panel-a under blue light. c). Secondaryresinite showing transition due to compaction by external forces. d). Panel-c under blue light. e). Secondary resinite is referred to as exudatinite. f). Panel-e under blue light.

4.2.3 Thermal Analysis

The proximate analysis micro-TGA curves are shown in Figure 4.7, whereas proximate analysis and elemental composition numerical data are listed in Table 4.2. As discussed earlier (section 4.1), ash content was used to determine the cleaning

characteristics. Apart from ash, volatile matters are important due to the high proportion of liptinite content. The higher volatile amount indicates the presence of higher liptinite macerals (Potgieter-Vermaak et al., 2011). The volatile matter should increase by decreasing density (Stankiewicz et al., 1996). In this study, small changes indicate the uniform distribution of liptinite macerals among all cleaned Oltu-stone wastes (CO1, CO2, & CO3). In addition, some of the volatiles were lost (around 2-3%) upon grinding below 20 μm during FTIR sample preparation. It may occur due to escaping enclosed volatile matters during size reduction (Das et al., 2018).

Table 4.2 shows the elemental composition of Oltu-stone samples. Elements such as carbon, hydrogen, and sulfur decrease fractionally as density increases, whereas nitrogen increases as density decreases. Also, the H/C ratio implies a minor difference between the cleaned Oltu-stone wastes, Oltu-stone wastes, and standard Oltu-stone. In cleaned Oltu-stone wastes fractions, the increase in the H/C ratio with the decrease in density indicates increased liptinite content. According to the petrographic system (Kandiyoti et al., 2006) based on reflectance values (Table 4.1) and elemental carbon (Table 4.2), cleaned Oltu-stone waste can be marked as lignite to sub-bituminous coal.

The glass transition or softening temperature is critical for agglomeration. Figure 4.8 illustrates the DSC curves of cleaned Oltu-stone wastes at various heating rates. Each heating rate has a different reaction point, which may be attributed to a difference in the liptinite component in each analysis attempt. Only endothermic reactions were seen at 1˚C/min, whereas the others exhibited mainly exothermic reactions between 130 ˚C and 170 ˚C. Devolatilization in cleaned Oltu-stone wastes started at 250 ˚C (Figure 4.7), and it should be treated at or below this temperature for high-pressure agglomeration.

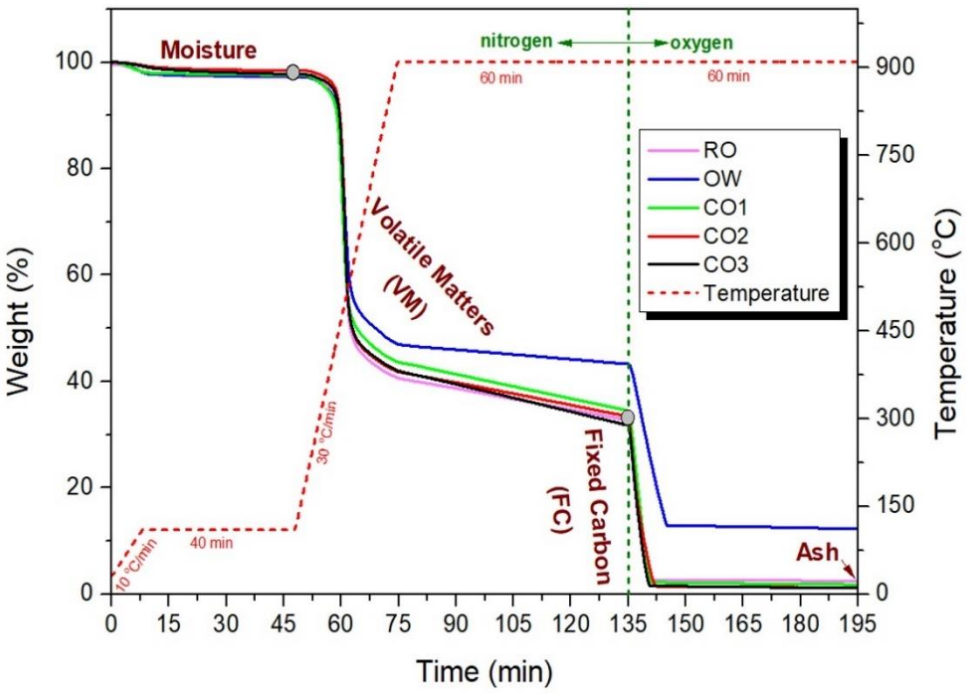

Figure 4.7 Proximate analysis curve of all Oltu-stones by the micro-TGA method.

Table 4.2 Proximate and Elemental analysis of all Oltu-stone samples

Sample	Proximate Analysis			Ultimate Analysis					
	VM	Ash	FC	C%	H%	N%	S%	O%*	H/C
OW	54.02	12.3	30.9	70.3	5.64	0.5	2.23	9.03	0.96
SO	64.5	2.5	30.2	77	6.33	0.41	1.99	11.77	0.99
CO1	63.03	1.78	32.79	76.9	6.12	0.44	1.98	12.78	0.96
CO2	64.9	1.22	32.28	75.3	6.08	0.48	0.41	16.51	0.97
CO3	65.94	1.1	30.7	74.1	6.06	0.52	0.6	17.62	0.98

O* = Calculated by difference method, H/C = H and C atomic ratio, VM = Volatile matters, FC = fixed carbon, C = carbon, H = hydrogen, N= nitrogen, S = total sulfur, O = oxygen

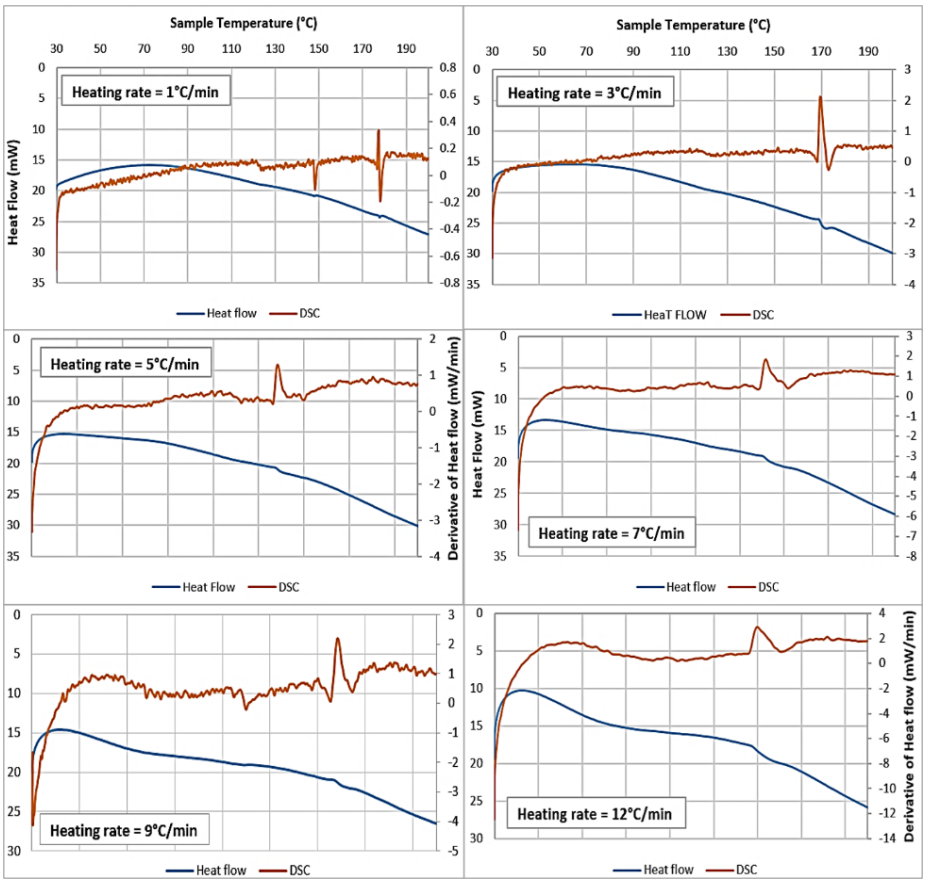

Figure 4.8 DSC curves of cleaned Oltu-stone wastes at different heating rates

4.2.4 SEM-EDS Analysis

Scanning electron microscope (SEM) equipped energy dispersive x-ray (EDS) SEM to observe morphology and mineral content in cleaned Oltu-stone waste. However, it was challenging to identify organic species such as coal macerals. Mineral matter looks lighter gray to white in BSE mode based on atomic number contrast, while organic matter appears dark gray. Image magnification and contrast are critical in distinguishing maceral types using SEM. Under SEM-EDS, the cleaned Oltu-stone wastes appeared as bark-like texture (Figure 4.9a), and the oblique section presented slices (Figure 4.9b). It is considered as a primary texture of Oltu-stone. Apart from texture, the inorganic impurities are also present in cleaned Oltu-stone wastes, such as framboidal pyrite, quartz, and clay mineral (particularly kaolinite), confirmed by

their morphology and elemental composition, as shown in Figure 4.10. The mineral impurities, mainly pyrite, increase the matt appearance of Oltu-stone and reduce its polishing characteristics, as reported by Toprak (2013). But resinite content improves its polishing characteristics and makes it unique.

The primary cell filling resinite (Figure 4.11) has some cracks and cavities, indicating the presence of gas bubbles (Pickel et al., 2017), which begin to escape during degradation and leave cavities behind. Chemically, the huminite has more oxygen than resinite (Figure 4.11), indicating more oxygen-containing species. Based on the study conducted by Balaeva et al. (2017), the oxygen contributed to moisture-holding capacity, and the more oxygen is, the more is holding capacity. Therefore, the softness of Oltu-stone during polishing when in contact with water is contributed by oxygen content, cell cavities, and clay. In general, resinite is hydrogen-rich compared to huminite. Nevertheless, it is worth noting that the elemental composition of huminite and resinite are determined in the absence of hydrogen because EDS is commonly not configured to detect hydrogen.

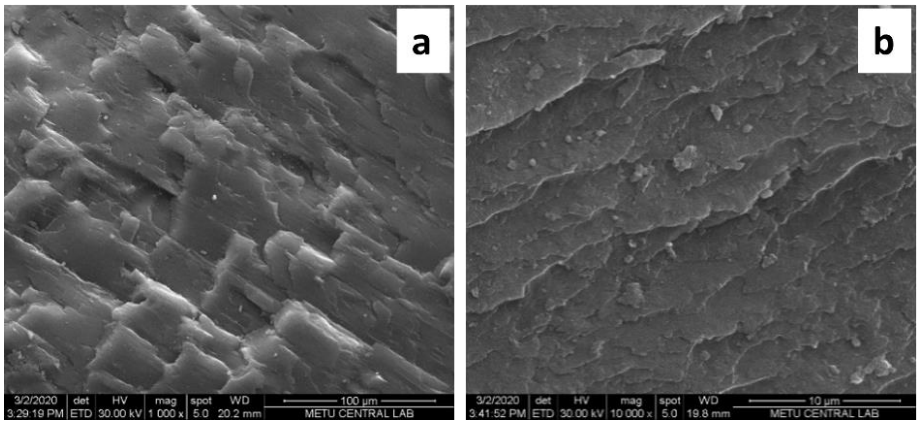

Figure 4.9 Cleaned Oltu-stone wastes surface morphology under SEM. a). Bark like texture b). Oblique section indicating slices

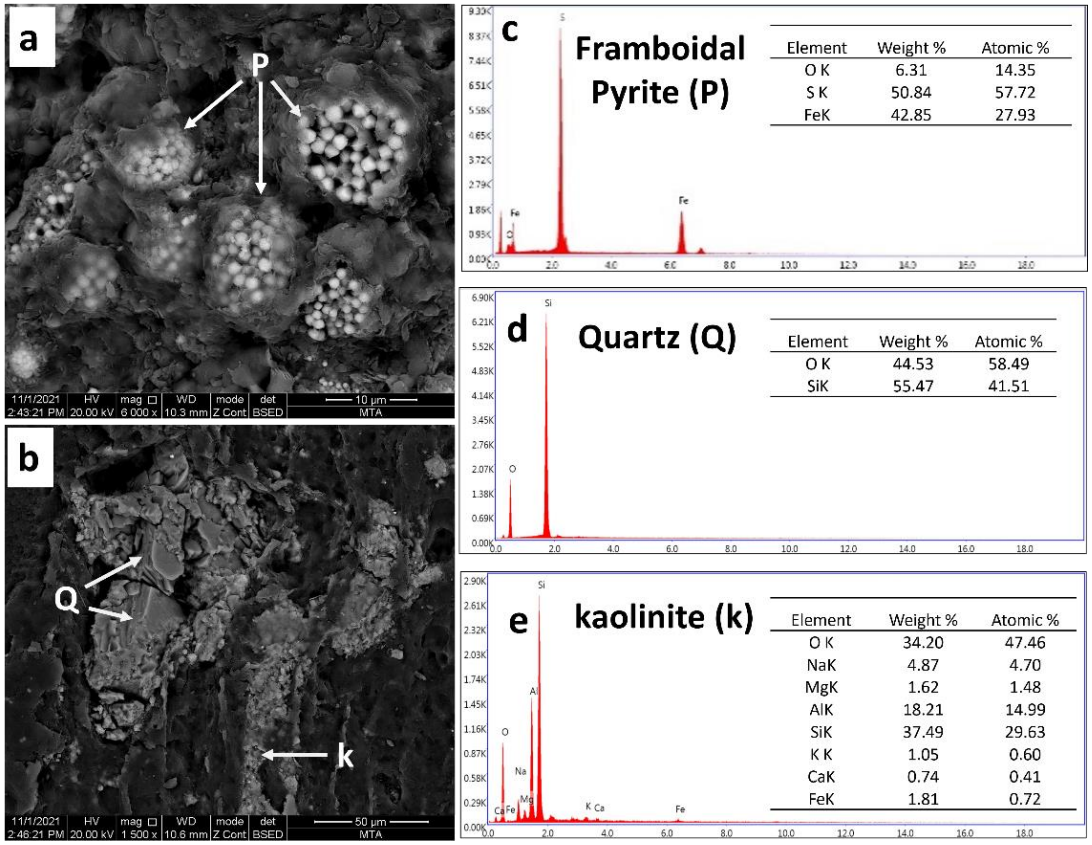

Figure 4.10 SEM-EDS analysis of mineral content present in cleaned Oltu-stone wastes. a). SEM image of framboidal pyrite. b). SEM image of quartz and kaolinite c). EDS spectrum of framboidal pyrite. d). EDS spectrum of quartz. e). EDS spectrum of kaolinite

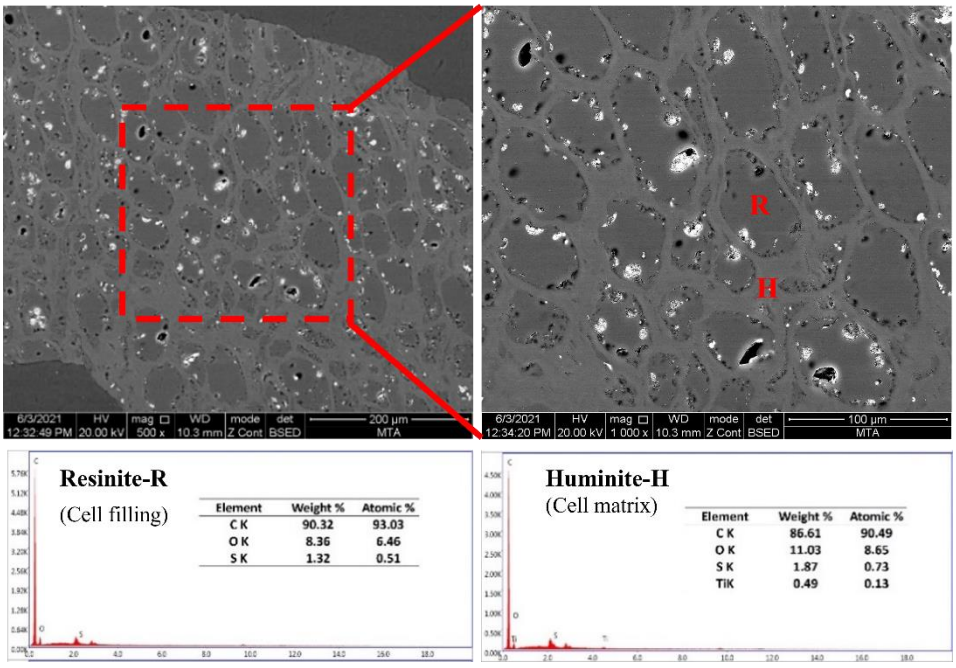

Figure 4.11 SEM-EDS results of Cleaned Oltu-stone wastes, showing primary cell resinite within huminite and their elemental composition.

4.2.5 XRD analysis

The mineral impurities and carbon phase in cleaned Oltu-stone wastes, Oltu-stone wastes, and standard Oltu-stone were analyzed by XRD, and their x-ray diffractograms are presented in Figure 4.12. The Oltu-stone wastes revealed the presence of various minerals, such as, as quartz (Q), pyrite (P), calcite (C), and Clay mineral (probably kaolinite-K) as in Figure 4.12. In CO1, the quartz is greatly reduced, but the pyrite peak is less affected during dense medium separation. Pyrite remains due to encapsulation within the cells in fine sizes, as seen under SEM images. The reduction in minerals continues with the transition from high (CO1) to low-density (CO3) fractions. From the x-ray diffractogram, it is noticed that cleaned Oltu-stone wastes are rich in amorphous carbon. Chen et al. (2021) explain the types of carbon structure by using XRD, i.e., aliphatic carbon atom (C_{al}) and aromatic carbon atom (C_{ar}). The peak of the aliphatic hydrocarbon branch chain may be found at the 20° band and includes different functional groups and alicyclic hydrocarbons

linked to aromatic rings. Microcrystals in aromatic rings and stacking between aromatic rings are correlated with C_{ar} spectra at 26° band. In this study, the aromatic carbon atom bands at 26.6˚ overlapped with quartz bands; therefore, it is difficult to distinguish one from another. Consequently, the presence of quartz is confirmed by XRD and SEM results. As a result, cleaned Oltu-stone has a more aliphatic carbon structure than micro-crystals in aromatic rings and mineral impurities such as pyrite and quartz. Moreover, the pyrite was challenging to liberate due to being enclosed within the cell structure in fine sizes.

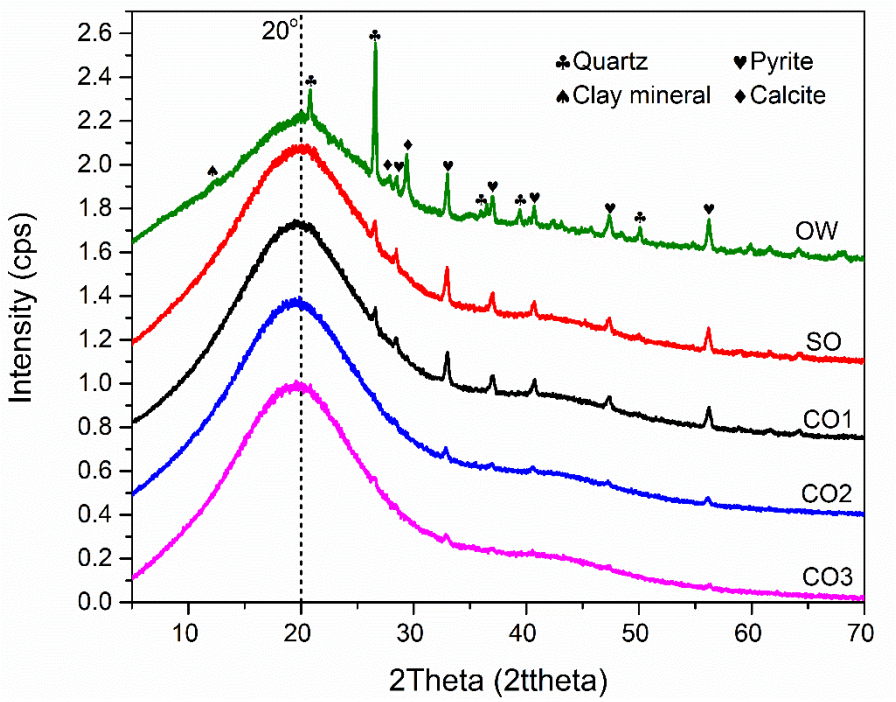

Figure 4.12 X-ray diffractograms of Oltu-stone samples

4.2.6 FTIR analysis

As shown in Figure 4.13, the FTIR spectra of SO, OW, and CO show similar absorption bands and peaks, except Si-O absorption (3700, 1103, 1035, and 520 cm^{-1}), which is removed after washing inorganic impurities such as clay and silicate particles (Liu et al., 2018; Manoj, 2016; Orrego-Ruiz et al., 2011). Curve fitting

analysis of different regions was used to assess weak absorption signals and find overlap peaks (Figure 4.14). Aromatic nuclei, aliphatic side chains, and certain oxygen-containing groups are all visible in the FTIR spectra. Aliphatic CH stretching is predominant at 2800-3000 cm^{-1}, such as 2956 cm^{-1}(CH_3 asymmetrical stretch), 2921 cm^{-1}(CH_2 asymmetrical stretch), 2885 cm^{-1}(CH_3 symmetrical stretch), and 2853 cm^{-1}(CH_2 symmetrical stretch) as shown in Figure 4.14b (Yao et al., 2011). At 1443 cm^{-1}, 1370 cm^{-1}, and 1325 cm^{-1}, there is aliphatic deformation and rocking vibrations. C=C stretching occurs at 1500 cm^{-1} and 1610 cm^{-1} in the aromatic ring and aromatic nucleus, respectively. The peak at 900-700 cm^{-1} is caused by C-H out-of-plane vibration in aromatic rings, while the peak at 3020 cm^{-1} is caused by the C-H aromatic ring nucleus stretching (Wang et al., 2017; Yao et al., 2011). Exocyclic methylene groups (3050, 1660, 898 cm^{-1}) are also present but have weak absorption, likely due to resinite content (Vassallo et al., 1991), as illustrated in Figure 4.14.

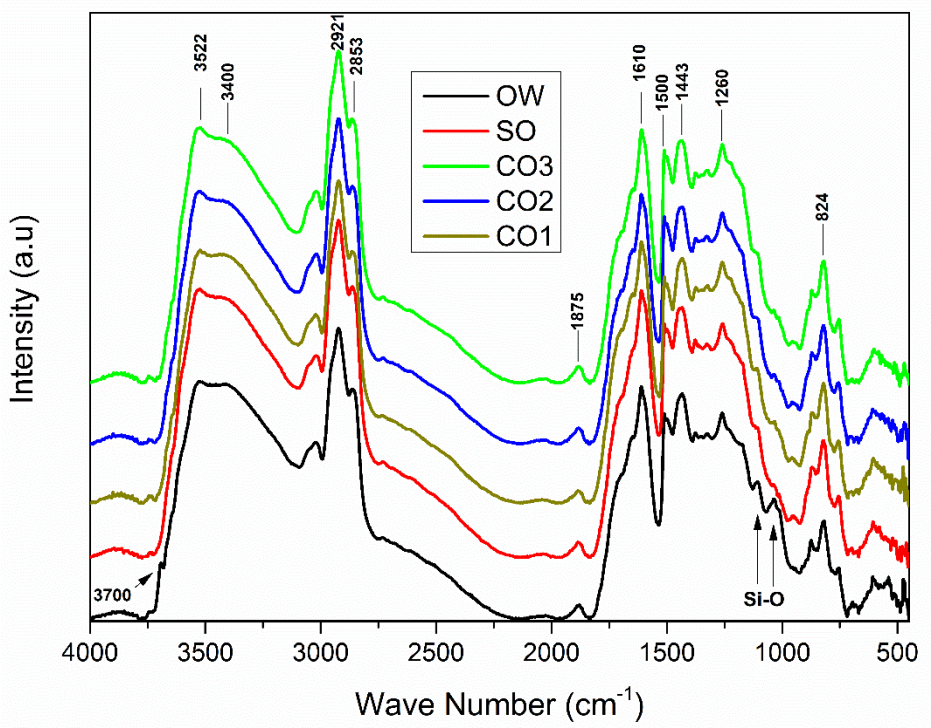

Figure 4.13 FTIR spectrum of Oltu-stone samples

Figure 4.14c, Oxygen-containing functional groups at 1740-1690 cm^{-1}, are mostly aliphatic ester at 1740-1730cm^{-1} and aromatic carbonyl or carboxylic (C=O) groups at around 1710-1690 cm^{-1} (Sun, 2005). Also, the 1875 cm^{-1} band was observed, likely due to carboxylic/carbonyl groups (Pagacz et al., 2020; Wang et al., 2010). At 1660 cm^{-1}, the bands belong to exocyclic double bonds and indicate immaturity in liptinite macerals, particularly resinite (Poulin and Helwig, 2012). These two regions (1740-1690cm^{-1} and 1660-1650 cm^{-1}) appear as the shoulder with an aromatic ring stretching (C=C) at 1610cm^{-1}. The intense band at 1610 cm^{-1} demonstrates phenolic groups or association of aromatic entities by methylene and possibly ether bridges (Painter et al., 1981). The broad zone 1300-1100cm^{-1} is due to C-O stretching vibrations in carboxylic acid, phenols, alcohol, and ether with an intense absorption peak at 1260 cm^{-1} (Chen et al., 2015; Song et al., 2017; W. Zhang et al., 2015). Furthermore, the OH groups appear at 3600-3100cm^{-1}, possibly due to different hydrogen bonds. In Figure 4.14a, five types of hydrogen bonds formed by OH groups in cleaned Oltu-stone wastes: OH-N (3195 cm^{-1}), tightly bound cyclic OH tetramers (3265 cm^{-1}); OH-O, ether (3330 and 3396 cm^{-1}); self-associated n-mers, i.e., OH-OH (3462 cm^{-1}); and OH-π hydrogen bonds (3532 cm^{-1}), respectively (Chen et al., 1998; Song et al., 2017; Yu. Zhang et al., 2020).

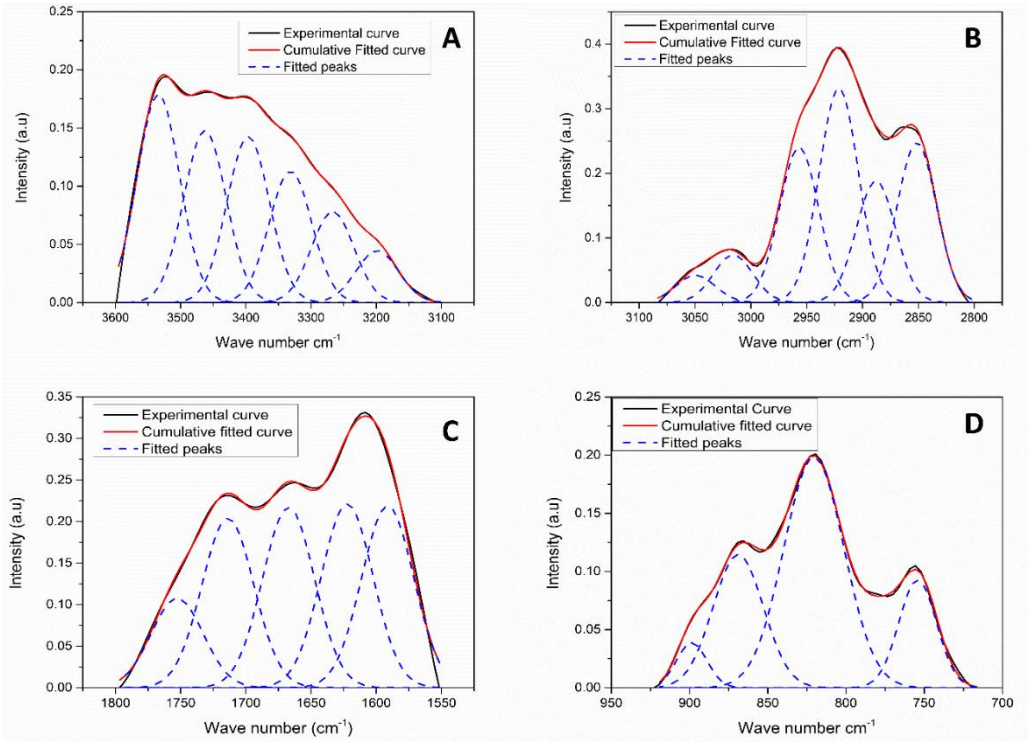

Figure 4.14 FTIR curve fitting analysis of CO1.

Due to less intense peaks at 3020 cm^{-1}, aromatic changes in C-H stretching were discussed in detail from the absorption bands between 900 and 700 cm^{-1} (Figure 4.14d). The peak at 824 cm^{-1} is the most prominent in this region, with the other two peaks (867 cm^{-1} and 754 cm^{-1}) appearing as weak shoulders. Based on the evidence presented in this paper, aromatic hydrogen is most abundant in compounds containing two/three adjacent C-H bonds (754 cm^{-1}), as well as Penta and ortho-substituted aromatic rings (867 cm^{-1}), respectively (Suárez-Ruiz et al., 1994). The lower intensity at 3020 cm^{-1}, evident that the aromatic ring is highly substituted and condensed (Li et al., 2007).

As a result, cleaned Oltu-stone waste is rich in CH_2 structure (2921 and 2863 cm^{-1}) and poor in C=O groups, indicating the longer and least branched aliphatic chain sides, which testified to the highest hydrocarbon generating potential (Guo et al., 1996; Guo and Bustin, 1998; Rojas et al., 2020). Aliphatic hydrocarbon and exocyclic methylene groups mainly belong to liptinite macerals (suberinite, resinite, and sporinite), whereas different phenols and alkylbenzenes result from huminite

(Stankiewicz et al., 1996). It is worth noting that phenols could also be derived from resinous materials (Crelling et al., 1991), supporting the petrographic evidence for resinite transition. The carboxyl/carbonyl groups are formed due to the oxidation of aliphatic components (Bai et al., 2019; Chen et al., 2012; Mastalerz et al., 2015). The Oltu-stone exhibits exceptionally high HI and low OI values, indicating that it has been protected from oxidation (Kara-Gülbay et al., 2018). These data indicate that Oltu-stone has numerous aliphatic compounds and low carboxylic groups linked with an aromatic structure.

4.2.7 Nano FTIR

Nano-FTIR is different than the conventional FTIR used commonly. But it can help to relate the results between them by analyzing the substrate at a nano-scale. Following the petrographic results, the study area was selected using an Optical microscope attached with Nano-FTIR. The most common appearance in the sample was studied initially (Figure 4.15) and then investigated the embedded resinite was (Figure 4.16). It was challenging to find resinite due to a similar appearance under Nano-FTIR coupled microscope. The shape of the bands under Nano-FTIR is different from the FTIR spectra discussed earlier. It might be due to different modes of measurement used in this analysis. In Figure 4.15, ultra-fines are embedded on the surface, either naturally or accumulated due to polishing. All the selected points of the FTIR spectrum indicate the presence of a more complex structure with variable intensities. The most common functional groups are carboxylic acid (1710-1690 cm^{-1}) and some aliphatic ester (1750-1730 cm^{-1}), appearing as a shoulder with an aromatic carbon nucleus at 1600 cm^{-1}. The embedded resinite (Figure 4.16, Point-1) has the aliphatic ester (1730 cm^{-1}) and carboxylic acid (1690 cm^{-1}). The presence of unsaturated double bonds (1645 cm^{-1}) in the shoulder with aromatic carbon (C=C, at 1600 cm^{-1}) indicated the exocyclic structure. The outer rim (huminite) revealed a similar shape for 1750-1550cm^{-1}, as illustrated in Figure 4.16.

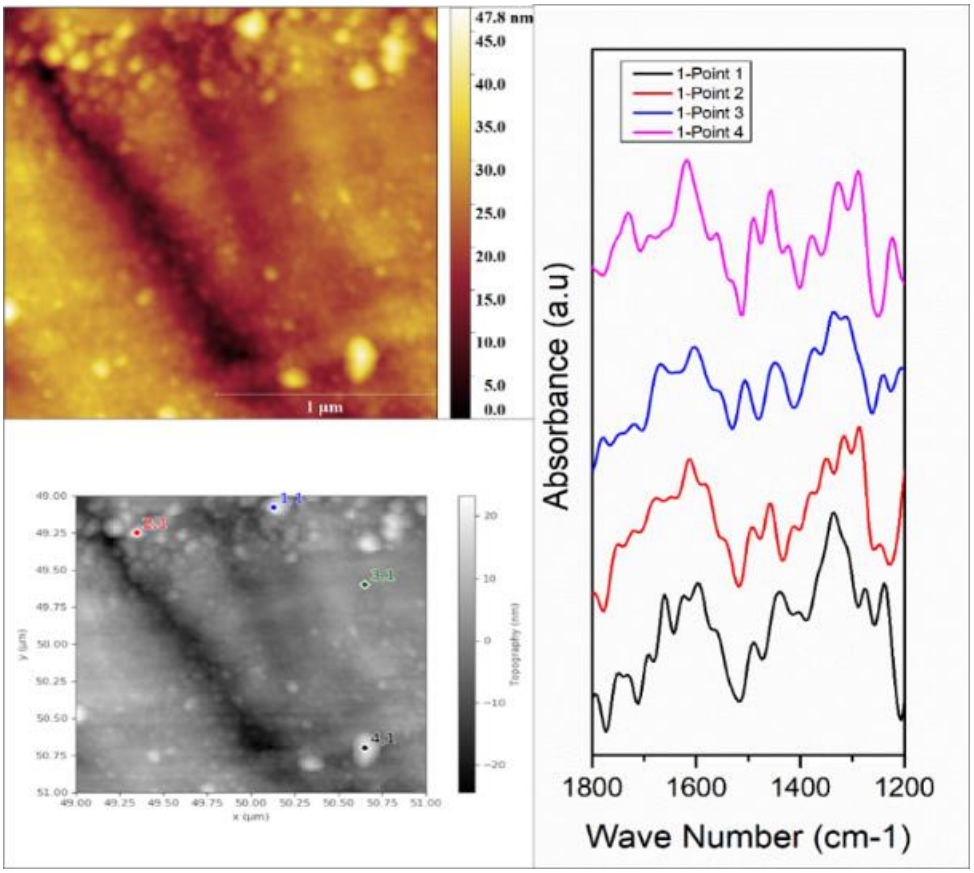

Figure 4.15 Nano-FTIR spectra (channel-A) of commonly observed surface in cleaned Oltu-stone.

Therefore, it was clear that huminite contains an aromatic carboxylic structure. In addition, the results of channel B are presented in Figure 4.17. The region between 1400-1000 cm-1 did not show any significant differences in cell filling and cell-matrix. Therefore, it was assumed, the results of FTIR were conclusive with the support of Nano-FTIR.

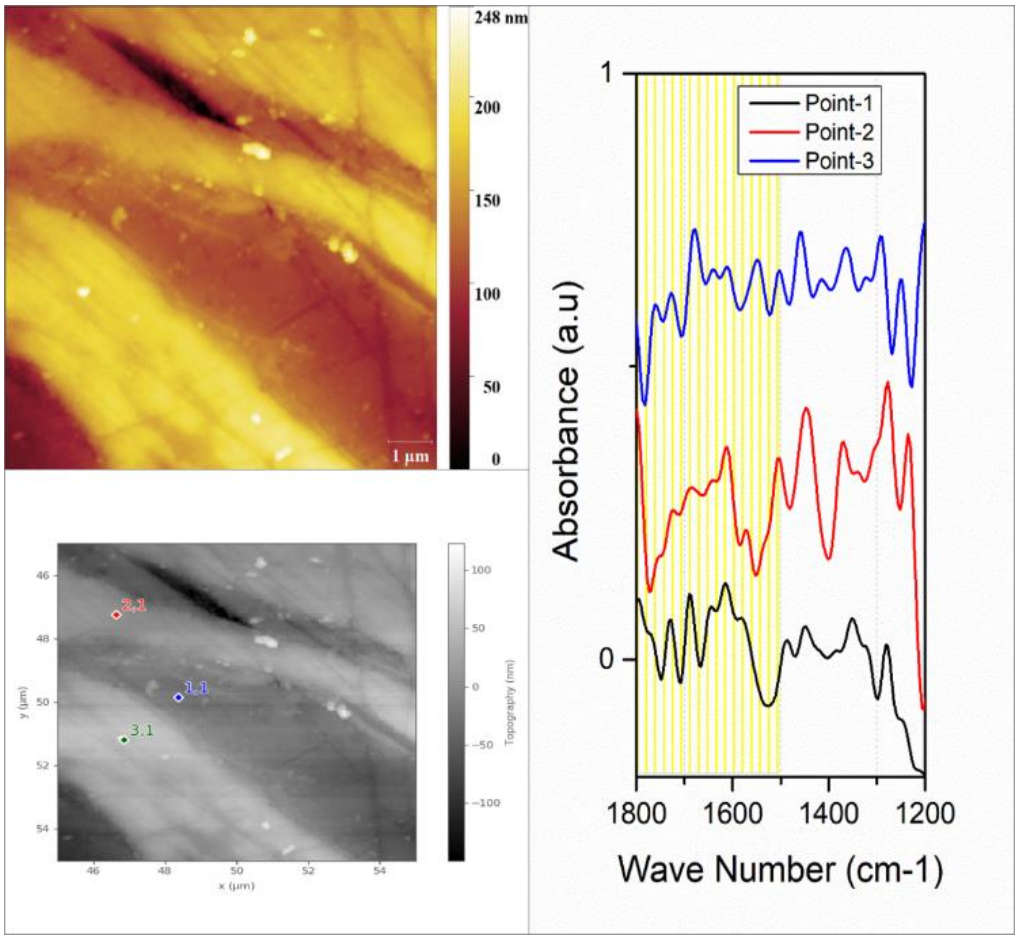

Figure 4.16 Nano-FTIR spectra (channel-A) of cell filling and cell-matrix surface in Cleaned Oltu-stone wastes.

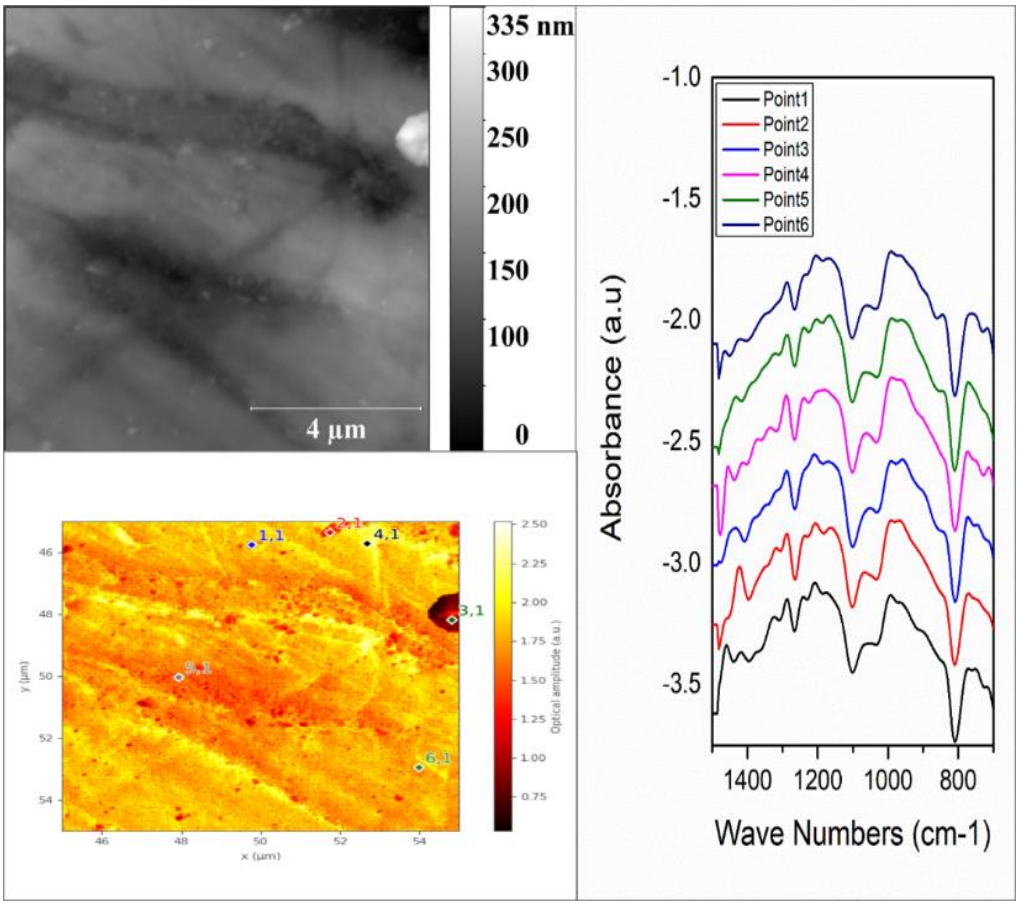

Figure 4.17 Nano-FTIR spectra (channel-B) of cell filling and cell-matrix surface in Cleaned Oltu-stone wastes.

4.3 Agglomeration of cleaned Oltu-stone wastes

After characterization of cleaned Oltu-stone wastes, it was revealed that the cleaned Oltu-stone wastes obtained at below 1.25 g.cm^{-3} (including CO1, CO2, and CO3) had similar characteristics compared to standard Oltu-stone. Therefore, the Oltu-stone wastes were cleaned below 1.25 g.cm^{-3} and used for agglomeration. Han et al. (2013) stated that the conditions such as pressure, temperature, and pressing time are essential variables to consider in the binderless agglomeration of coal. This section includes evaluating the best possible conditions for agglomeration of cleaned Oltu-stone wastes. These conditions were drawn in the form of three different methods (in section 3.2.3), i.e., method-A(MA), method-B(MB), and method-C (MC).

According to the DSC results (in section 4.2.3), the softening and glass transition temperatures of cleaned Oltu-stone wastes were between 130 ˚C and 180 ˚C. Therefore, the samples were heated to between 150 ˚C and 200 ˚C, higher than softening temperature. As per preliminary results, when heated to 200 ˚C during pressing, the samples were adequately pressed (Figure 4.18). As a reason, 200 ˚C temperature stays constant in all of the three methods used for agglomeration studies. After that, some characteristics, such as bulk density, indirect tensile strength, and microscopic analysis, were examined to optimize the best possible conditions for cleaned Oltu-stone wastes agglomeration.

Figure 4.18 Pressed Oltu-stone obtained from cleaned Oltu-stone wastes

The bulk densities of pressed Oltu-stone obtained from different methods are presented in Figure 4.19. Based on the results of different methods adopted, the bulk density of pressed Oltu-stone may range from 0.9 to 1.26 $g.cm^{-3}$ (Figure 4.19). MC was found to be the most effective compaction, resulting in higher bulk densities, i.e., 1.23-1.26 $g.cm^{-3}$. The change in bulk densities follows the trend: MA>MB>MC.

The bulk densities in MA were very low, ranging from 0.9 to 1.15 g.cm^{-3}. Later, in MB, it increased to 1.20 g.cm^{-3}. At last, MC showed the greatest bulk densities, i.e.,1.22-1.26 g.cm^{-3}. Large and irregularly shaped particles generate gaps and spaces that increase bulk volume, particularly in MA. On the other hand, the small particle size reduces the impact seen within MA. As a result, MC revealed a higher density than the other two methods.

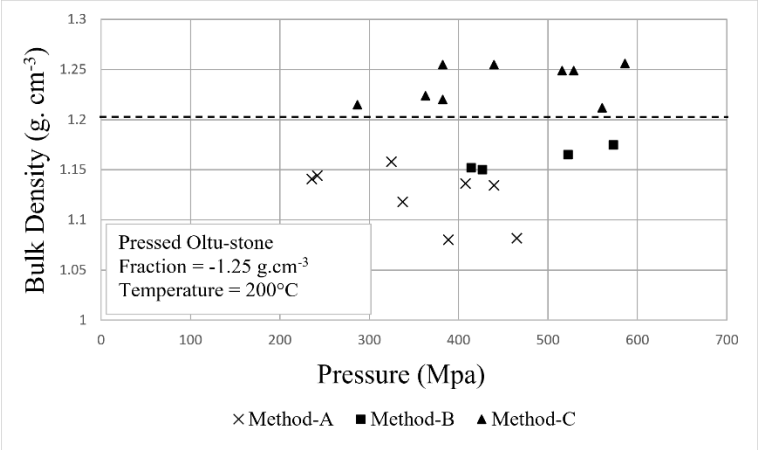

Figure 4.19 Bulk density of the agglomerates produced from cleaned Oltu-stone using a different methodology.

Apart from the particle size, cooling under pressure affects bulk density and density distribution. When the pressure was released after the experiment, it was mainly seen that the gases, which were most likely low-boiling volatiles (Olugbade and Ojo, 2021), were escaping. These volatile were isolated inside the matrix and might exert pressure on the particles and flow resinite, preventing them from adhering to one another (particularly in MB). Later, this impact was reduced by the curing effect (in the case of cooling under pressure in MC). As a result, MC was regarded as the most effective method of pressing the cleaned Oltu-stone wastes, leading to an increased density of 1.20-1.25 g.cm^{-3}, comparable to the bulk density of standard Oltu-stone. Therefore, it is revealed that pressure did not affect bulk density regardless of the technique used, but the particle size, preheating time, and cool under pressure create a difference.

Indirect tensile strength values are similar to bulk density when determined using various methods, as shown in Figure 4.20. Indirect tensile strength changed when particle size, gas bubbles, and curing effect interacted. MA failed because of the lack of contact between the particles due to coarse particle sizes. The indirect tensile strength of standard Oltu-stone, i.e., 7.39 MPa, was calculated to set the critical values. The findings show that strength obtained from MC is comparable to or higher than those obtained by using standard Oltu-stone. It is due to enough chemical reaction inside the matrix and between the particle edges to make strong bonding. The particle size utilized in this research was less than 30 µm for MB and MC, as provided in Appendix A. Based on particle size distribution, the powder used for pressing comprises 50% particles below 15 µm. Therefore, the particles below 15 µm were fine, and the rest (15-35 µm) were considered coarse particles. Fine particles were locked between coarse particles, reducing the distance between particles to interact.

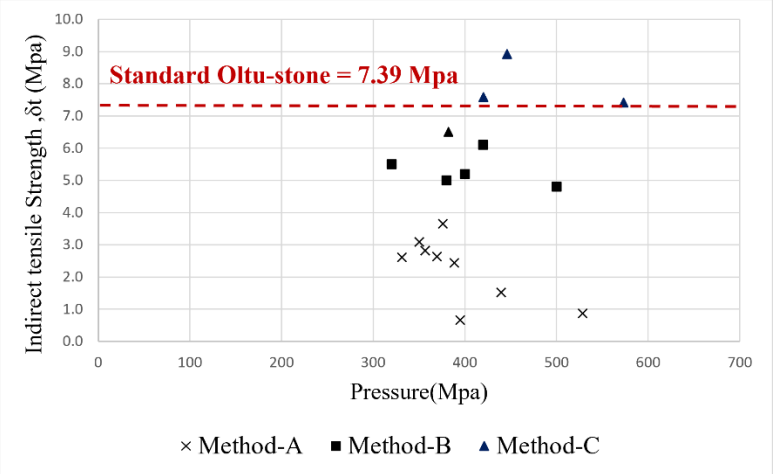

Figure 4.20 Indirect Tensile strength of Oltu-stone agglomerates produced by different methodologies.

Olugbade and Ojo (2021) discussed the significance of particle size in coal agglomeration. The strength of coal agglomerates increases with decreasing particle

size. It was described in two ways; (1) Increasing the proportion of small and fine particles increases the contact points. It allows forming stronger bonds, which enhances the strength. (2) Small particle size also increases the length of the force chain. This approach would extend the force chain, and great strength could be produced. As a reason, the force chain is dependent on particle size and contact area.

The pressed Oltu-stones were brought under an optical microscope to see the surface appearances. In MA (Figure 4.21), the binderless agglomeration may result in insufficient coal particle interaction and reduced strength due to large voids between particles. Consequently, these voids reduce the agglomerate overall strength. Such voids are reduced in the case of MB and MC due to small particle sizes. It is also possible to enhance the formation of mechanical interlocking between the particles in MB or MC (Figure 4.22) by increasing pressure. Pressed Oltu-stone strength was expected to improve as the fraction of small particles increases, i.e., the higher the concentration of small particles, the greater the strength, as stated by Sun et al. (2014).

Furthermore, the bonding of binderless pressed Oltu-stone could be enhanced by high reactive macerals such as liptinite (very reactive, containing resinite content) and huminite (partially reactive), both of which exist by origin in Oltu-stone. Coal oxidation and weathering can affect the bonding process adversely, but Oltu-stone has been protected from this effect, as previously reported (Kara-Gülbay et al., 2018). A chemical reaction between the particles is promoted in MC by cooling them under pressure. It resulted in significant chemical and physical bonding between the particles. This hardening effect was lacking in MB, resulting in less bonded than MC.

The binderless pressed Oltu-stone represented the standard Oltu-stone with nearly similar properties. Oltu-stone contains resinite by origin, which serves as a binder in binderless agglomeration, and produces the undiluted agglomerates. As a reason, the study was focused on binderless agglomeration.

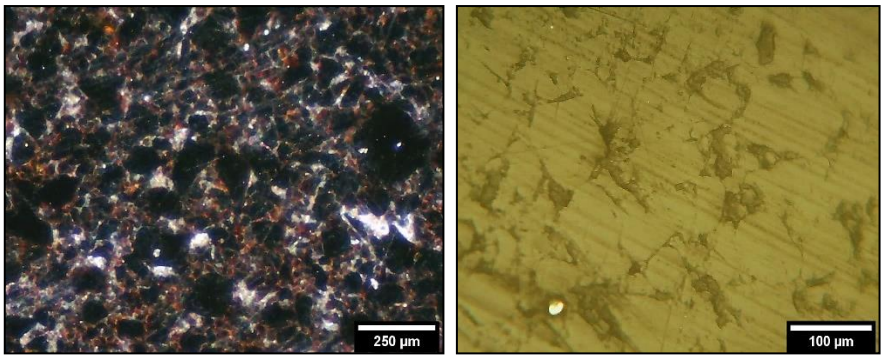

Figure 4.21 Optical microscope image of binderless agglomerates produced from cleaned Oltu-stone waste (Method-A).

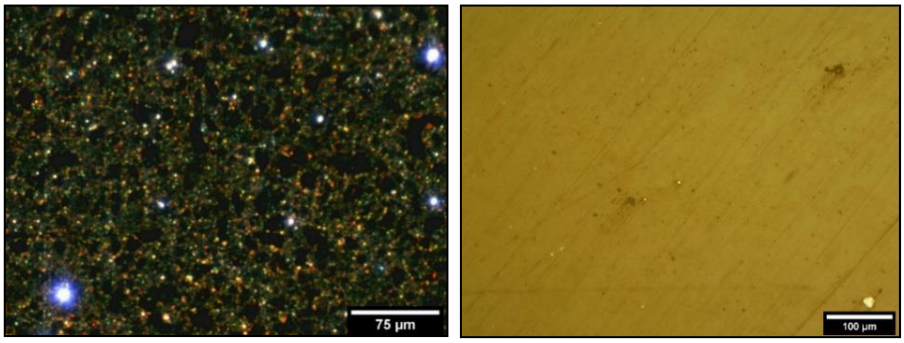

Figure 4.22 Optical microscope image of binderless agglomerates produced from cleaned Oltu-stone waste (Method-C).

4.1 Characterization of pressed Oltu-stone

After optimizing agglomeration parameters and conditions, the agglomerates obtained from Method-C were characterized and regarded as **"Pressed Oltu-stone (PO)**." This term was used throughout the characterization studies of agglomerates in this section. For that purpose, the cleaned Oltu-stone wastes were pressed under different pressure and pressing times to evaluate the best possible product compared to standard Oltu-stone.

4.1.1 Bulk Density

Regardless of different pressure and pressing times, the bulk density remains between 1.22-1.26 g.cm^{-3}. The increase in pressing time and pressure results in variation in bulk density, likely due to the readjustment of the particles or variation in liptinite content (which has low density). These differences are approximate 2-3%, which is come under error deviation. Therefore, it is assumed that the change in pressing time (Figure 4.23) and pressure (Figure 4.24) has little or no effect on bulk density.

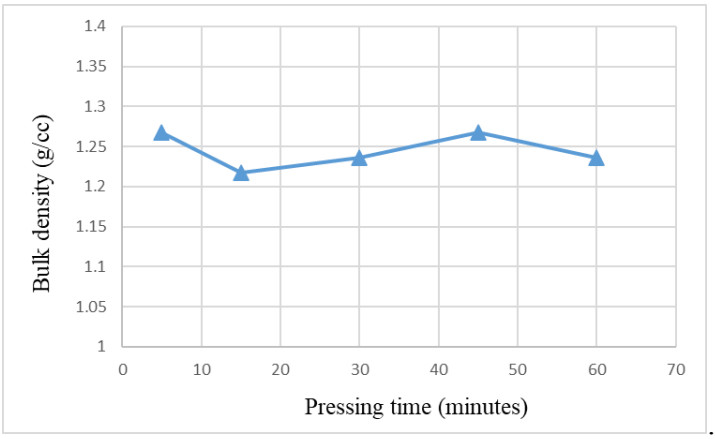

Figure 4.23 Bulk density of pressed Oltu-stone at a different pressing time at 450 MPa pressure

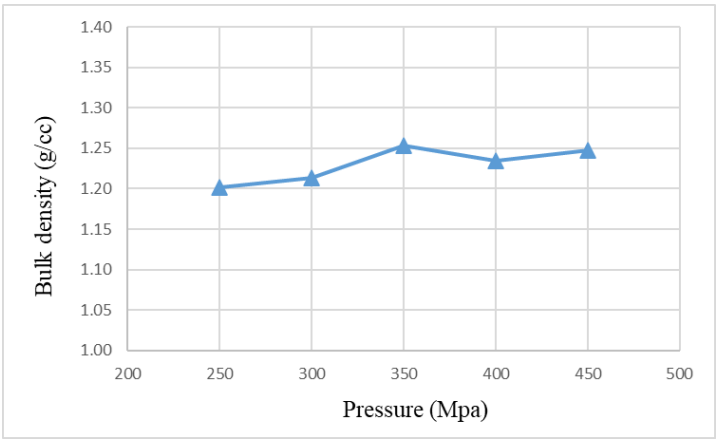

Figure 4.24 Bulk density of pressed Oltu-stone at different pressure with a constant time of one hour.

4.1.2 Indirect Tensile strength

In indirect tensile strength, three distinct behaviors were observed at different pressures with constant time. Compaction, breaking, and re-compaction were among the behaviors observed (Figure 4.25). The fine reactive particles (<15 μm) are pushed closer together and react with one another and the edges of coarse particles when the pressure is at 250 bar. Compared to standard Oltu-stone, it has a higher indirect tensile strength of 8 MPa, which is good enough. The space between coal particles reduces when pressure rises to 300 MPa, increasing contact forces such as capillary forces, van der Waal forces, and chemical bridges between reactive macerals (Olugbade and Ojo, 2021), increasing strength to 9.5 MPa. At 350 MPa, a significant decrease in strength was observed due to excessive pressure, suggesting bond breaking and elongated particle fragmentation, causing fractures inside the agglomerates. Meanwhile, the liptinite content (particularly resinite) inside the coarse particles (15-35 μm) softens but cannot move towards pores, fractures, or fissures due to a lack of pressure. In the following processing stages, the 400-450 MPa pressure mobilized the softened liptinite content towards fractures produced at 350 MPa pressure, filled the gap, and chemically bound them together, resulting in increased indirect tensile strength.

Change in time at a constant temperature, on the other hand, has little effect on the strength values (Figure 4.26), but it does cause some disagreement in the nano-hardness findings as to the length of time increases (in section 1.4.3). After 5 minutes of treatment, several pores were seen on the microscopic images (Appendix C) due to the evaporation of volatiles within the matrix. The high indirect tensile strength results show that this impact is limited to the disc surface or area studied, not the complete sample.

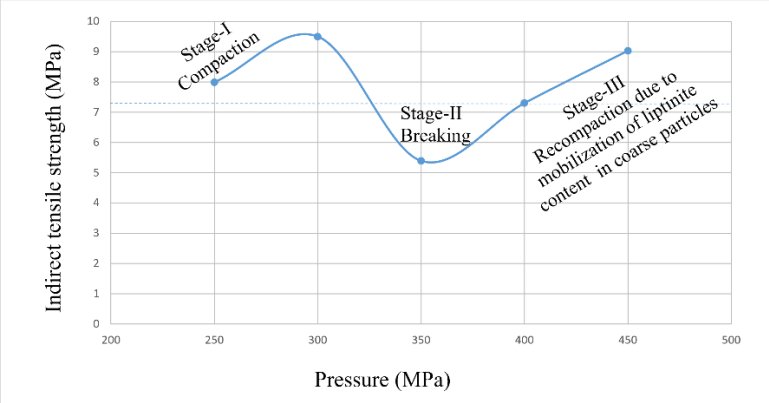

Figure 4.25 Indirect tensile strength of pressed Oltu-stone at different pressure (MPa), with constant pressing time (60 minutes)

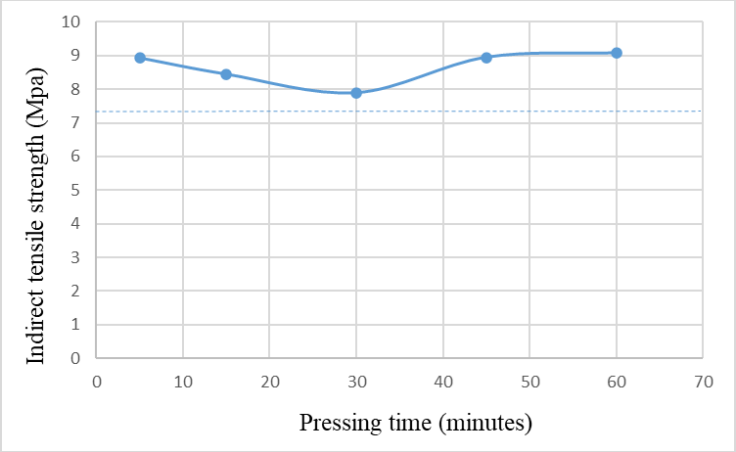

Figure 4.26 Indirect tensile strength of pressed Oltu-stone at pressing time (minute), with constant pressure (450MPa)

4.1.3 Nano Hardness

Nanoindentation is a multiphysics process that includes elastoplastic deformation, brittle failure, and elastic deformation. The properties of the material influence the transition from one phase to another. In metals and ceramics, the hardness is directly proportional to the elastic modulus values, while in organic matter, the relationship is weaker because of heterogeneity (Manjunath and Jha, 2019). The bright bluish colors in Figure 4.27 represent huminite or the transformation of liptinite to huminite upon heating, while the dark bluish colors represent the concentration of liptinite in

the sample. Under the specified conditions, a total of 12 distinct points were tested in a series (Figure 4.27a).

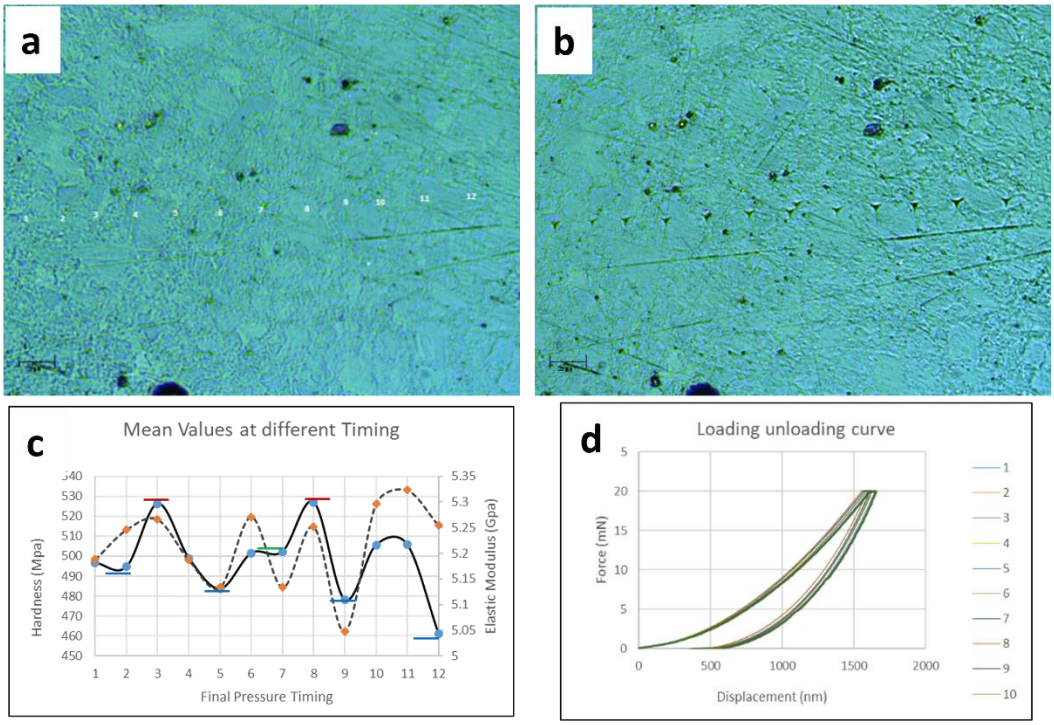

Figure 4.27 a). The appearance of pressed Oltu-stone under optical microscope attached with Nano-hardness testing equipment b). After indentation analysis. c). Hardness and elastic modulus values w.r.t positions. d). Loading and unloading w.r.t positions. (Pressing time = 45 minutes and pressure = 450 MPa)

The values of hardness (Hv) and elastic modulus (E) are changing with certain positions (Figure 4.27c). The lower values correspond to the matrix, which is most likely filled with resinite content or other liptinite macerals, while the higher values correspond to huminite particles or liptinite macerals that have degraded due to heating. The mean hardness value was 469.424 MPa, with a standard deviation of 22.192%. In addition, the elastic modulus produces mean values of 5.038 GPa with a standard variation of 0.088%. These nano hardness and elastic modulus values are slightly more significant than those published for liptinite maceral in the literature (Borodich et al., 2015; Epshtein et al., 2015), a positive indication. These variations occur due to the presence of huminite macerals in the cleansed Oltu-stone wastes and the heating action, which results in a decrease in plasticity. Furthermore, the

indentations loading and unloading curve (Figure 4.27d) is consistent with the numerical data, suggesting that the pressed Oltu-stone is mainly plastic.

In addition, the effects of pressure and pressing time were studied. Figure 4.28 shows that the rise in pressure did not affect Hv and E until 300 MPa. However, the tensile strength suddenly dropped when the pressure reached 350 MPa, consistent with the indirect tensile strength results (Figure 4.25). The H and Ev decreased due to breaking in the matrix rather than material plasticity. In contrast, the pressing time made little impact on H and Ev. After preheating, the liptinite (especially the resinite component) was softened and then pressed for 05 minutes, yielding satisfactory and even more significant results than those obtained with standard Oltu-stone (Figure 4.29). Some volatiles escaped from the matrix and lowered the Hv and E values during this process. Also, it is assumed that this impact was limited to the top surface or a limited chosen region. This assumption directly conflicted with the overall indirect tensile strength findings, which were satisfactory for 5 minutes pressing time compared to standard Oltu-stone (section 1.4.2). The reactive macerals mobilized more inside the coarse particles (15-35 µm), affecting the overall plasticity. It was found that the hardness and elastic modulus were similar for all pressing times but fluctuated with variable pressure.

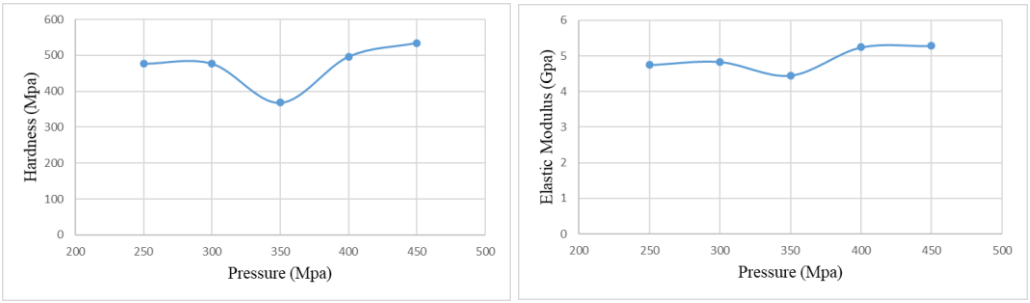

Figure 4.28 Effect of different pressure with constant pressing time (60 minutes) on hardness and elastic modulus.

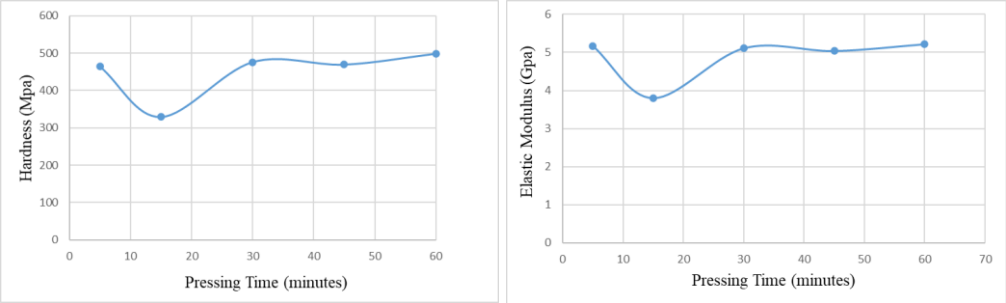

Figure 4.29 Effect of different pressing times with constant pressure (450 MPa) on hardness and elastic modulus.

4.1.4 Optical microscopic analysis

The pressed Oltu-stone shows more compressed and orange-reddish tints under halogen light, suggesting resinite content under an optical microscope (Figure 4.30a). Oltu-stone waste was cleaned and pressed, producing a disc about 2cm in diameter and 0.5cm thickness. The lateral disc area was shinier than the radial, indicating the resonate concentration (plastic material) in this area. As a reason, when resinite is subjected to high pressure, it gets softened and tends to flow towards the edges, resulting in more orange-reddish tints (Figure 4.30b). However, because of the compressed multilayers on top of each other, it was not easy to see the disc cross-section under the same conditions (Figure 4.30c). Internal reflection or oxidized surfaces may cause the orange-reddish to be misleading. Therefore, the optical microscope was sufficient to observe the pressed Oltu-stone matrix, but a petrographic microscope with white and blue light excitation was needed to establish the existence of liptinite content (particularly resinite).

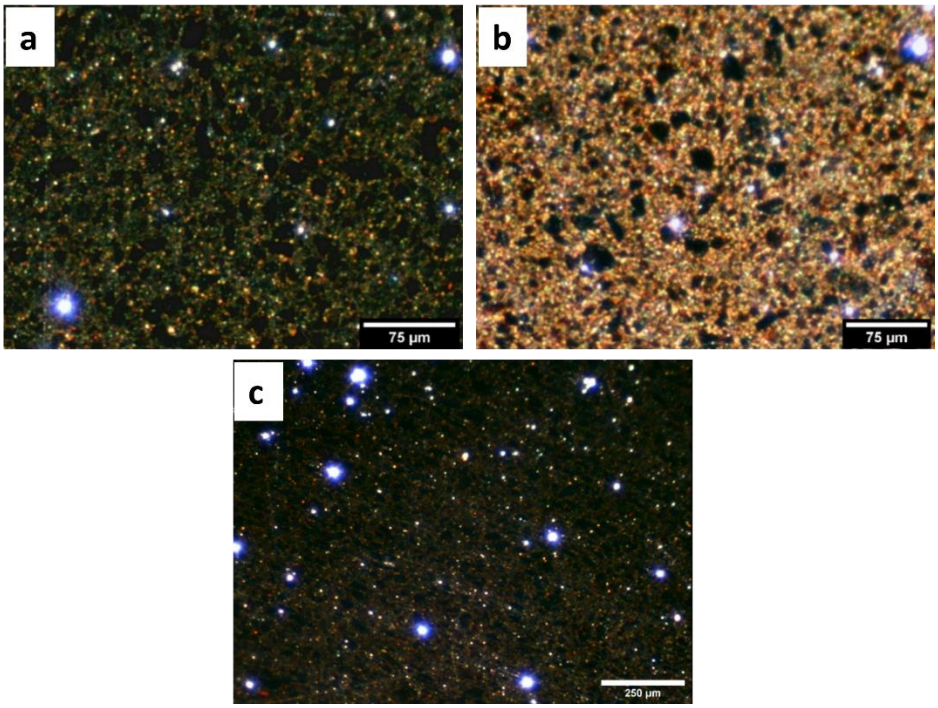

Figure 4.30 Optical microscopic images of pressed Oltu-stone obtained at 450 MPa pressure with 60 minutes pressing time, a). Disc top surface, b). The area near disc edges, c). The cross-section area of the disc.

In the petrographic microscopic investigation, the colors variation among the macerals was discussed in the characterization of cleaned Oltu-stone wastes. In Figure 4.31, It was difficult to see a macerals cellular structure in a petrographic microscope due to heat-pressure treatment. Four different observations were made under a petrographic microscope, as shown in Figure 4.31; (1) mobilization (Mob) of liptinite content within the coarse particles (15-35 µm), (2) matrix fillings comprised by both macerals groups, including liptinite (dark color) and huminite (light), (3) homogenous distribution of pyrite among the surface and (4) flow resinite content in the fractures or gaps between the coarse particles. The contribution of liptinite and huminite within the matrix was responsible for the binding of coarse particles. The liptinite macerals are highly reactive, softened upon heating, and rehardened upon cooling, especially resinite. Besides that, the huminite content also plays a role in binding due to organic sulfur content. As discussed earlier (in section 4.2.4), the huminite has more organic sulfur.

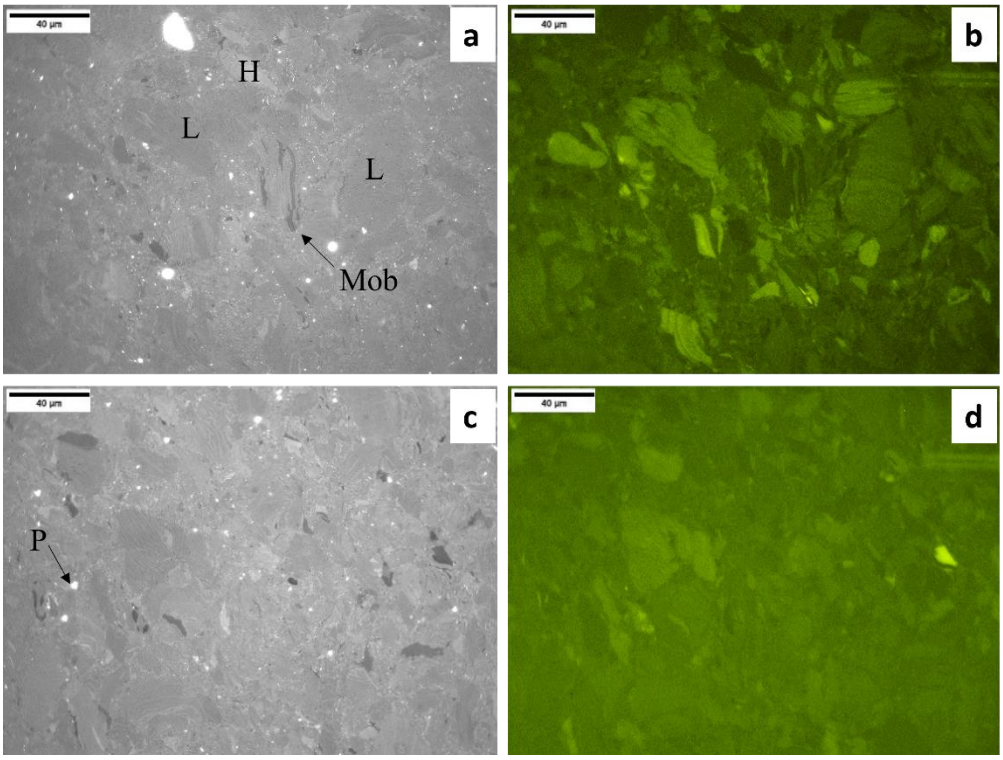

Figure 4.31 Pressed Oltu-stone a). radial surface showing mobilization (Mob) of liptinite content in coarse particles due to heat-pressure treatment. b). Panel-a under blue light excitation. c). cross-section part showing the homogenous distribution of macerals. d). Panel-c under blue light excitation. (L=liptinite, H=huminite, P=pyrite)

Based on a previous study by Dai et al. (2020), the coal containing organic sulfur tends to be more thermoplastic. This organic sulfur-containing huminite melt at a lower temperature in the same coal. Jiménez et al. (1998) define the pre-hydrous behavior of huminite, which is occurring due to resinization. This behavior of prehydrous provided the thermoplastic behavior upon heat-pressure treatment. Due to plastic behavior, huminite deformed during compaction, thereby assisting with the chemical bonding during binderless agglomeration. This huminite also contributed to its role in coal agglomeration due their reactivity and plasticity (Mangena and du Cann, 2007). However, only huminite was insufficient to provide a true strength as standard Oltu-stone. When treated under high pressure and temperature, the liptinite macerals (particularly the resinite content) increase strength. The comparison between the pressed Oltu-stone and standard Oltu-stone in terms of physical and mechanical properties, supporting these assumptions and hypotheses.

4.1.5 SEM-EDS results

The surface of pressed Oltu-stone shows very small pores and cavities (Figure 4.32a), but the cross-sectional part shows an intact structure (Figure 4.32b). The area was observed at high magnification, revealing the nanopore (Figure 4.32c), mesopores (Figure 4.32d), and macropores (Figure 4.32e). Due to the chemical changes upon heat treatment, it was challenging to distinguish macerals. However, a brighter area is huminite or degraded liptinite, and a dark area shows the concentration of unaffected/ less affected liptinite content. The transition of liptinite macerals towards huminite owing to agglomeration can be seen in a change in color from darker to lighter (Figure 4.32b). It may increase the rank of coal (Han et al., 2013). Apart from macerals, the framboidal pyrites were filled with liptinite mobilized material (Figure 4.32f), and the plasticity is linked to this mobile phase (Jiménez et al., 1998).

Furthermore, the EDS mapping of the selected surface of pressed Oltu-stone was analyzed, as shown in Figure 4.33. The majority of the surface area contained carbon, including the S, Fe, Na, Mg, Si, Al, P, Cl, K, Ca, and Ti. The oxygen content is less due to preservation from oxidation, as reported in the literature (Kara-Gülbay et al., 2018). The fingerprint mark of carbon indicates its association with other elements, whereas bright color represents carbon alone. In minerals impurities, the bright white spots are likely clay or quartz and pyrite. Iron (Fe) distribution mainly represented the pyrite, but S distribution represented both inorganic sulfur (pyrite) and organic sulfur. The numerical data of elemental is provided in Appendix B.

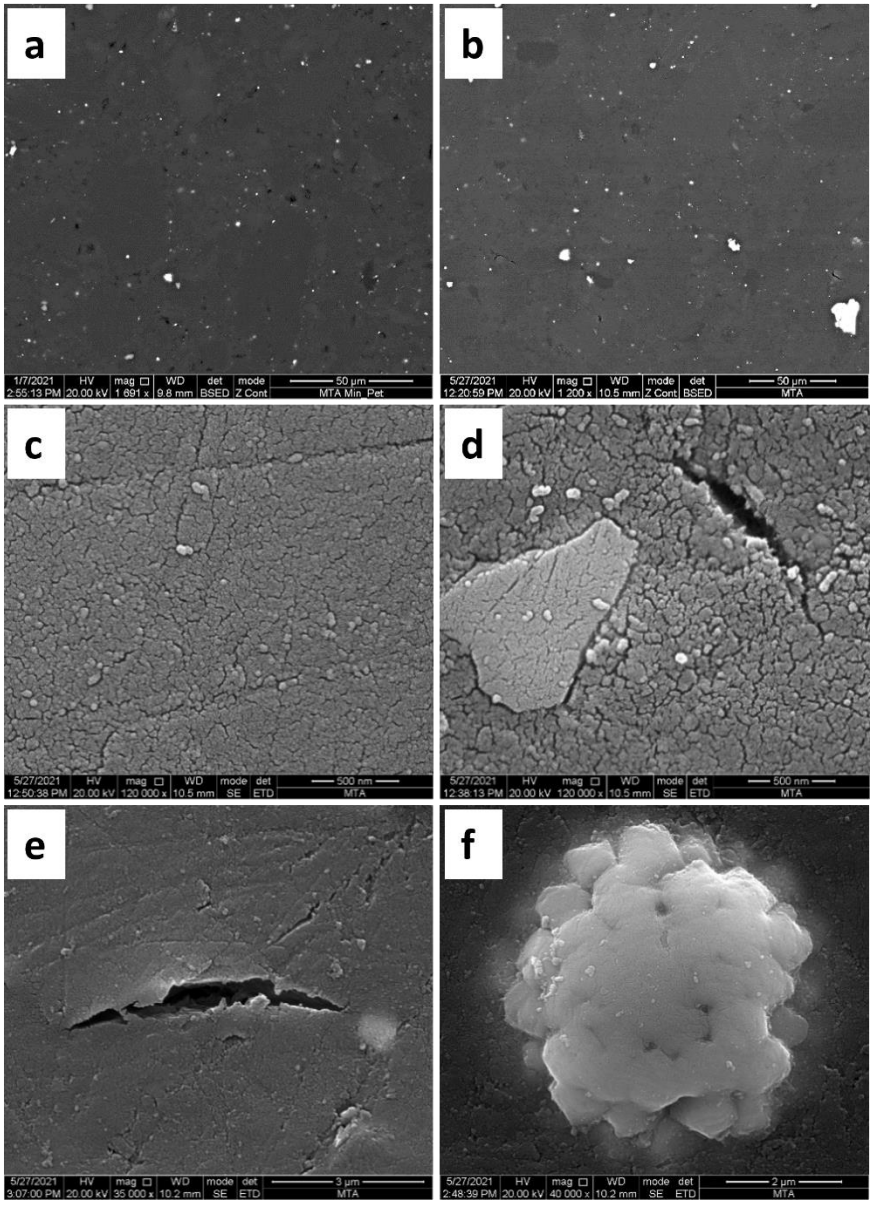

Figure 4.32 SEM images of pressed Oltu-stone, a). Top surface b). Cross-sectional surface c). Nano pores d). Meso and macropores e). Macro pores. f). Framboidal pyrite filled with mobilized liptinite content.

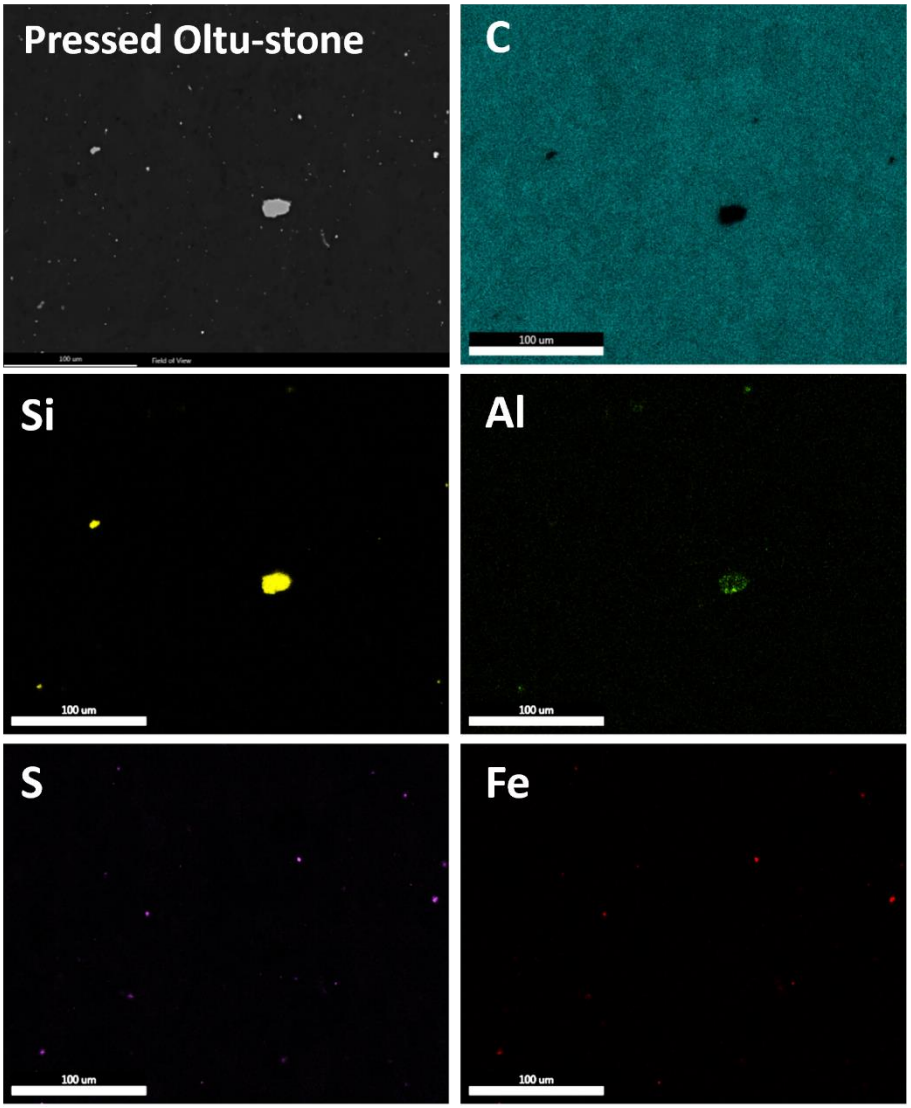

Figure 4.33 Elemental mapping of cross-sectional part of pressed Oltu-stone obtained at high pressure (450 MPa) and maximum pressing time (60 minutes)

4.1.6 Thermal analysis

As previously stated, because of the liptinite content, especially the resin-rich component, which is primarily volatile, and volatile matters are necessary for Oltu-stone. Heating has a more significant impact on such macerals than pressure. As a result, the pressed Oltu-stone was examined at both the lowest and maximum heating time under pressure. After cleaning, the quantity of volatile matter was 63.5%, which

was decreased to 60 % after the grinding of cleaned Oltu-stone wastes. This decrease was caused by escaping volatile substances trapped within the holes or pores. However, the decrease continues after agglomeration by 1-3%. The pressed Oltu-stone obtained at 5 minutes showed a 1.5% decrease in volatile content, while the pressed Oltu-stone obtained at 60 minutes indicated a 2-3% reduction in volatile matters (Table 4.3). The longer the heating time under pressure, the lower the volatile content, resulting in increased maturity.

Table 4.3 Volatile matters of pressed Oltu-stone compared to cleaned Oltu-stone

Sr	Sample	Nature	Volatile Matters (%)
1	CO1	Grain sample (-1+0.1mm)	63.5
2	CO1	Powder samples (-30 μm)	60
3	Pressed Oltu-stone (05minutes)	Broken pressed sample	58.5
4	Pressed Oltu-stone (60 minutes)	Broken pressed sample	57.4

4.1.7 FTIR analysis

The FTIR spectra of pressed Oltu-stone obtained under different pressure and pressing time conditions are shown in Figure 4.34. According to previous sections characterization results, the change in pressure affects overall indirect tensile strength but reveals similar surface mechanical properties. At the same time, the change in pressing time did not overall indirect tensile strength but revealed the small changes in volatile amounts. The change in pressing time under controlled heating conditions, on the other hand, affected chemical characteristics. As a result, the sample with the shortest pressing time (5 minutes) and the longest pressing time (60 minutes) was discussed for FTIR investigation. Except for the unsaturated double bonds or conjugated carbonyl at 1660 cm^{-1}, the agglomeration of cleaned Oltu-stone

wastes did not affect on chemical structure (Figure 4.34). The aliphatic area has not altered much, suggesting that the liptinite maceral structure (mainly the resinite content) has been less impacted by agglomeration. The band at 1660 cm^{-1} began to decrease at 5 minutes and eventually disappeared when the time approached 60 minutes (Figure 4.34), and it is more evident in the fitted curve of the selected region (Figure 4.35). The heating action enhanced the carboxylic bands in low-rank coal (Mursito et al., 2018; Wang et al., 2010). The band between 3550 cm^{-1} and 3400 cm^{-1} became more pronounced, suggesting a rise in OH groups due to hydrogen bonding. According to a previous study (Han et al., 2013), acidic functional groups are essential in coal structures because they are the most reactive sites. Carboxylic groups (COOH) contributed to hydrogen bonds, resulting in high strength. According to Olugbade and Ojo (2021), the hydroxyl groups (3600-3100 cm^{-1}) include COOH–COOH; OH–N, Cyclic, OH–O, ether; OH–OH; and OH– linkages rise with the number of small particles. Consequently, the rate of hydrogen bond formation increased. The greater the degree of hydrogen bonding generated, the stronger the agglomeration. Furthermore, the different pressure conditions similarly affect conjugated carbonyl (Figure 4.36) as observed under different pressing times. Therefore, no effect was seen under different pressure and pressing conditions.

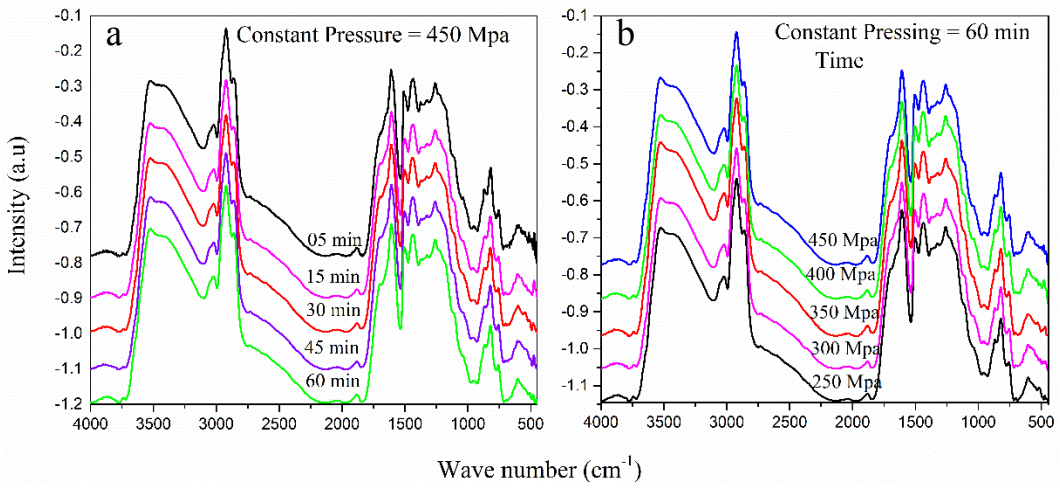

Figure 4.34 Drift-FTIR spectra pressed Oltu-stone at different a). pressing time and b). pressure

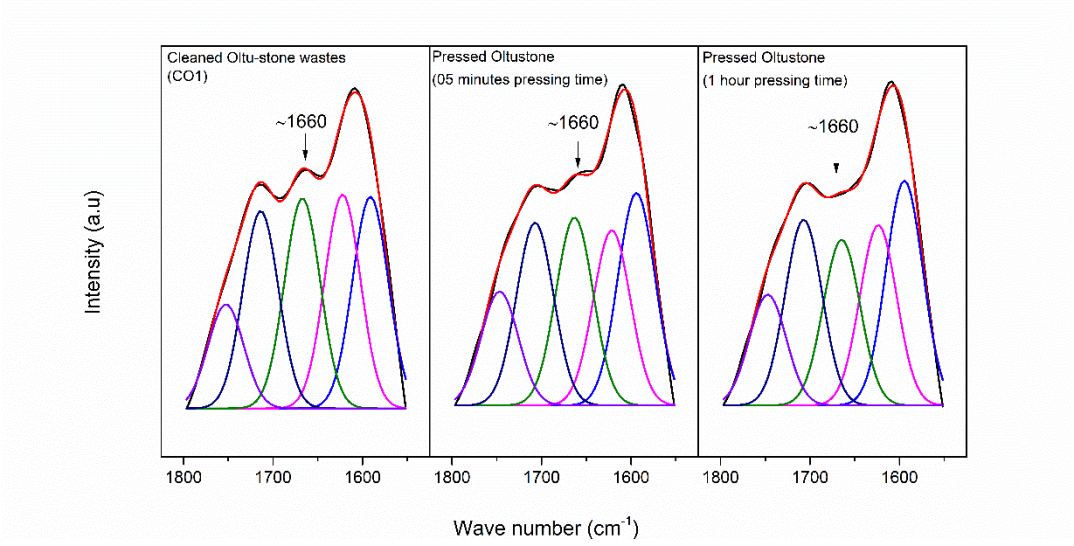

Figure 4.35 FTIR fitted curve of 1800-1550 cm^{-1}, showing an effect of pressing time on a conjugated carbonyl.

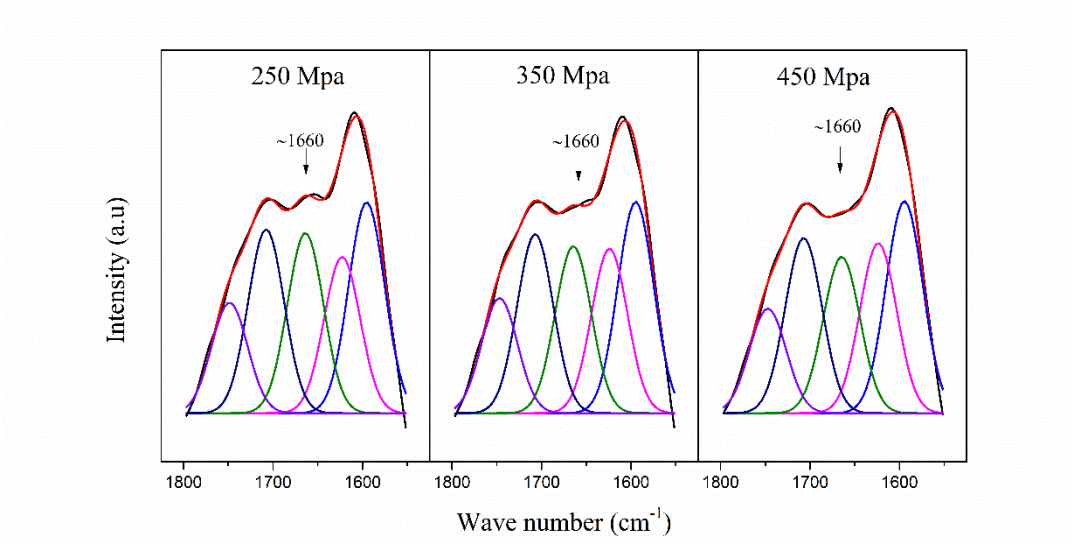

Figure 4.36 FTIR fitted curve of 1800-1550 cm^{-1}, showing an effect of pressure on a conjugated carbonyl.

The pressed Oltu-stone framework for bond formation is compatible with Ellison & Stanmore (1981). Acidic functional groups act as a base for bond formation, and both free carboxylic and phenolic groups contribute equally to this process. Condensation reactions between functional groups occur in covalent bonds between coal particles. A phenolic or other carboxylic group on one particle interacts with a carboxylic acid

group on a nearby particle. Therefore, the agglomeration process for pressed Oltu-stone is identical to how coalification happens and coal rank increases (Han et al., 2013).

4.1.8 Nano-FTIR

Except for some unsaturated double bond alterations at 1660 cm^{-1}, FTIR analysis of pressed Oltu-stone found a nearly similar structure to standard Oltu-stone. It was easy to understand more about the structure in detail using nano-FTIR. The surface investigation was divided into two selected regions; a coarse particle (15-35 μm, Figure 4.37) and a matrix phase (Figure 4.38). The matrix phase contains fine particles (15 μm) and mobilized liptinite macerals. Heat-pressure treatment activated the liptinite content (especially resinite) in coarse particles, resulting in a flow pattern under an AFM microscope (Figure 4.37). This surface contains carbonyl-carboxyl groups (1750-1690 cm^{-1}) as well as unsaturated bonds or conjugated carbonyl (1660 cm^{-1}) with the aromatic C=C shoulder (1620 cm^{-1}). These unsaturated bonds/conjugated carbonyls were still present in the pressed Oltu-stone, although in much lower concentrations (Figure 4.37, point-1). The flow pattern cavities/scratches (Figure 4.37, Point-2) showed aliphatic deformation between 1450-1300 cm^{-1} and alcohol, ester, and ether deformation between 1300-1100 cm^{-1}. These bands between 1300-1100 cm^{-1} have a similar shape to the shoulder peaks of baltic amber, as reported previously (Wagner-Wysiecka, 2018)—these observations are linked to the presence of resinite (resin-rich maceral), which remained unaffected.

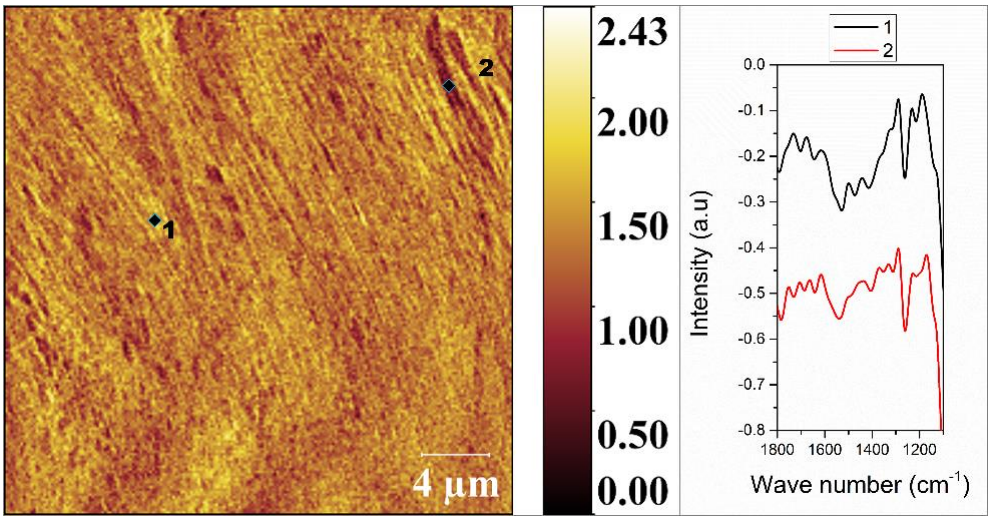

Figure 4.37 Nano-FTIR spectra of the selected region under coupled AFM microscope (Coarse particle in pressed Oltu-stone).

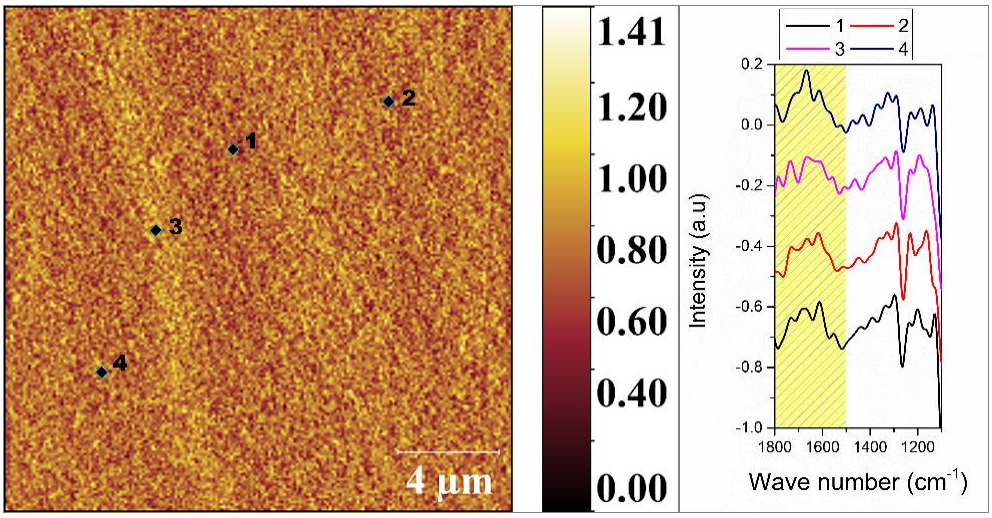

Figure 4.38 Nano-FTIR spectra of the selected region under coupled AFM microscope (matrix phase in pressed Oltu-stone).

The matrix in Figure 4.38 was mainly packed with fine particles that were more intact and chemically connected after heat-pressure treatment. All of the selected points exhibit comparable structural bands of varying intensities. The carbonyl/carboxyl bands (1750-1690 cm^{-1}) were present at all of the examined locations, which appeared as the shoulder with aromatic carbon (C=C, 1600 cm^{-1})

and unsaturated bonds/conjugated carbonyl (C=O, 1660 cm^{-1}) at some locations. In contrast, the presence of 1660 cm^{-1} bands indicated the presence of an exocyclic structure. The band shapes were almost similar at 1450-1300 cm^{-1}, implying that the aliphatic deformation was the same after treatment. There was a shift in alcohol, phenol, ester, and ether at 1300-1100 cm^{-1}. As a result, these findings backed with the FTIR findings, which showed that the agglomeration process less influenced the chemical structure of the pressed Oltu-stone.

4.1.9 Final Product

For preliminary evaluation of pressed Oltu-stone as an alternative market product, the pressed Oltu-stone was processed and made by the ateliers, as in Figure 4.39. Based on hardness and polishing characteristics, ateliers reported that the product made from pressed Oltu-stone has similar properties compared to standard Oltu-stone. Therefore, it can be used as an alternative product.

Figure 4.39: Prayers beads and locket made from pressed Oltu-stone

CHAPTER 5

CONCLUSION AND RECOMMENDATIONS

This work was based on the binderless agglomeration of Oltu-stone wastes. Many impurities (such as clay, quartz, and framboidal pyrite) are present in Oltu-stone wastes, making agglomeration extremely difficult. The Oltu-stone wastes must be cleaned using dense medium solutions at a 1.25 $g.cm^{-3}$ density before agglomeration. Compared to standard Oltu-stone, the cleaned Oltu-stone wastes had almost identical characteristics (petrographical, physical, chemical, and thermal). Cleaned Oltu-stone waste was classified as lignite to sub-bituminous coal using a petrographic method based on reflectance values and elemental composition. Cleaning reduced the mineral content and enriched the liptinite macerals (especially resinite), which is the main component of Oltu-stone. Liptinite macerals (including resinite) are highly reactive when heated and act as a natural binder in agglomeration. Based on the thermal investigation, the cleaned Oltu-stone must be treated below 250 ˚C.

Three different methods or conditions were adopted for binderless agglomeration, and method-C (MC) was the most effective method for agglomerating cleaned Oltu-stone wastes. The pressure and pressing time adjustment did not affect the bulk density and gave similar densities, i.e., 1.20-1.26 $g.cm^{-3}$. The product produced by using the shortest pressing time (05 minutes) with the highest pressure (450 MPa) had a sufficient indirect tensile strength (8.93 MPa) and nanoindentation hardness (Hv=464.6 MPa, E=5.2 GPa). That product was comparable to standard Oltu-stone and acceptable for ateliers. Despite the physical and strength characteristics, there was little effect on chemical structure and thermal properties. The quantity of volatile matter decreased by around 2-3%, increasing fixed carbon. Pressed Oltu-stone has a high concentration of aliphatic carbon, which has a polymeric and alicyclic structure less influenced by heating. However, conjugated carbonyl groups and exocyclic structure disappeared, whereas coal maturity and carboxylic structure increased.

Heating enhanced the carboxylic structure of low-rank coals to a considerable degree.

This research was carried out with a fixed dimension of pressed Oltu-stone, 20 mm diameter, and 5mm thickness. The effect of the size of the pressed Oltu-stone on their properties should be investigated. Also, the aging properties, including oxidation of studied pressed Oltu-stone, are not determined yet. It would help in determining the long-term effect on its polishing characteristics and human skin.

REFERENCES

Akinnuli, B.O., Olugbade, T., 2014. Development and Performance Evaluation of Piggery and Water Hyacinth Waste Digester for Biogas Production. nternational J. Eng. Innov. Technol. 3, 271–276.

Bai, F., Liang, H., Qu, H., 2019. Structural Evolution of Burmese Amber during Petrifaction Based on a Comparison of the Spectral Characteristics of Amber, Copal, and Rosin. J. Spectrosc. 2019. https://doi.org/10.1155/2019/6904541

Balaeva, Y.S., Miroshnichenko, D. V, Kaftan, Y.S., 2017. Moisture-holding capacity of coals. Solid Fuel Chem. 51, 337–348. https://doi.org/10.3103/S0361521917060027

Bilgin, Ö., Kalkan, E., Dilmaç, M., 2011. Equipments used for production and processing of Oltustone, in: The Proccedings of 3rd Mining Machinery Symosium, May 05-06,İzmir, Turkey (in Turkish).

Borowski, G., Hycnar, J.J., 2013. Utilization of fine coal waste as a fuel briquettes. Int. J. Coal Prep. Util. 33, 194–204. https://doi.org/10.1080/19392699.2013.787993

Botha, D.L., 2019. Evaluation of binders in briquetting of coal fines for application in combustion processes. Potchefstroom Campus of the North-West.

Chen, C., Gao, J., Yan, Y., 1998. Observation of the Type of Hydrogen Bonds in Coal by FTIR. Energy & Fuels 12, 446–449. https://doi.org/10.1021/ef970100z

Chen, T., Dai, R., Yellezuome, D., Zhang, K., Zhao, R., Liu, G., Wu, J., 2021. Effect of density on physicochemical and thermal conversion characteristic of Naomaohu coal. Fuel 284, 119045. https://doi.org/10.1016/j.fuel.2020.119045

Chen, Y., Mastalerz, M., Schimmelmann, A., 2012. Characterization of chemical functional groups in macerals across different coal ranks via micro-FTIR spectroscopy. Int. J. Coal Geol. 104, 22–33. https://doi.org/https://doi.org/10.1016/j.coal.2012.09.001

Chen, Y., Zou, C., Mastalerz, M., Hu, S., Gasaway, C., Tao, X., 2015. Applications of micro-fourier transform infrared spectroscopy (FTIR) in the geological sciences—A Review. Int. J. Mol. Sci. 16, 30223–30250. https://doi.org/10.3390/ijms161226227

Çiftçi, E., Coşkun, S., Yalçınalp, B., 2002. Oltu-stone-mineralogical and physical properties, in: 55th Geological Congress of Turkey. pp. 34–35.

Çiftçi, E., Yalçin, M., Yalçınalp, B., Kolaylı, H., 2004. Mineralogical and physical

characterization of the Oltustone, a gemstone occurring around Oltu (Erzurum-Eastern Turkey)., in: International Congress on Applied Mineralogy (ICAM), September 19-22, Brazil.

Crelling, J.C., Pugmire, R.J., Meuzelaar, H.L.C., McClennen, W.H., Huai, H., Karas, J., 1991. Chemical structure and petrology of resinite from the Hiawatha "B" coal seam. Energy & Fuels 5, 688–694. https://doi.org/10.1021/ef00029a010

Cruz-Ceballos, L.F., García-González, M., Cruz-Guevara, L.E., Avendaño-Sánchez, G.M., 2020. Geochemical Characterization and Thermal Maturation of Cerrejón Formation: Implications for the Petroleum System in the Ranchería Sub-Basin, Colombia. Geosci. . https://doi.org/10.3390/geosciences10070258

Czajka, K.M., 2018. Proximate analysis of coal by micro-TG method. J. Anal. Appl. Pyrolysis 133, 82–90. https://doi.org/10.1016/j.jaap.2018.04.017

Dai, S., Hower, J.C., Finkelman, R.B., Graham, I.T., French, D., Ward, C.R., Eskenazy, G., Wei, Q., Zhao, L., 2020. Organic associations of non-mineral elements in coal: A review. Int. J. Coal Geol. 218, 103347. https://doi.org/https://doi.org/10.1016/j.coal.2019.103347

Das, B., Nag, D., Dash, P.S., 2018. Effect of Grinding on Chemical and Coking Properties of a Highly Volatile Bituminous Coal and Its Size Fractions. Int. J. Coal Prep. Util. 38, 355–360. https://doi.org/10.1080/19392699.2016.1258403

Drzewicz, P., Natkaniec-Nowak, L., Czapla, D., 2016. Analytical approaches for studies of fossil resins. TrAC - Trends Anal. Chem. 85, 75–84. https://doi.org/10.1016/j.trac.2016.06.022

El Nady, M.M., Ramadan, F.S., Hammad, M.M., Lotfy, N.M., 2015. Evaluation of organic matters, hydrocarbon potential and thermal maturity of source rocks based on geochemical and statistical methods: Case study of source rocks in Ras Gharib oilfield, central Gulf of Suez, Egypt. Egypt. J. Pet. 24, 203–211. https://doi.org/https://doi.org/10.1016/j.ejpe.2015.05.012

Ellison, G., Stanmore, B.R., 1981. High strength binderless brown coal briquettes part I. Production and properties. Fuel Process. Technol. 4, 277–289.

Epshtein, S.A., Borodich, F.M., Bull, S.J., 2015. Evaluation of elastic modulus and hardness of highly inhomogeneous materials by nanoindentation. Appl. Phys. A Mater. Sci. Process. 119, 325–335. https://doi.org/10.1007/s00339-014-8971-5

Ethem, M.Y., 1990. Precious Stones and semi-precious Stones from A to Z., 2nd ed. Mars Production, Ankara (in Turkish).

Feist, M., Lamprecht, I., Müller, F., 2007. Thermal investigations of amber and copal. Thermochim. Acta 458, 162–170. https://doi.org/10.1016/j.tca.2007.01.029

Fischer-Cripps, A.C., 2011. Nanoindentation. Springer-Verlag New York. https://doi.org/10.1007/978-1-4757-5943-3

Given, P.H., 1984. An Essay on the Organic Geochemistry of Coal, in: GORBATY, M.L., LARSEN, J.W., WENDER, I.B.T.-C.S. (Eds.), . Academic Press, pp. 63–252. https://doi.org/https://doi.org/10.1016/B978-0-12-150703-9.50008-1

Göymen, G., 1976. About Oltu stone., in: Earth and Human. Turkish Geological Institute, Ankara, pp. 46-47 (in Turkish).

Greb, S.F., Eble, C.F., Hower, J.C., 2017. Coal, in: White, W.M. (Ed.), Encyclopedia of Geochemistry: A Comprehensive Reference Source on the Chemistry of the Earth. Springer International Publishing, Cham, pp. 1–16. https://doi.org/10.1007/978-3-319-39193-9_153-1

Guo, Y., Bustin, R.M., 1998. Micro-FTIR spectroscopy of liptinite macerals in coal. Int. J. Coal Geol. 36, 259–275. https://doi.org/10.1016/S0166-5162(97)00044-X

Guo, Y., Renton, J.J., Penn, J.H., 1996. FTIR microspectroscopy of particular liptinite- (lopinite-) rich, Late Permian coals from Southern China. Int. J. Coal Geol. 29, 187–197. https://doi.org/https://doi.org/10.1016/0166-5162(95)00024-0

Han, Y., Tahmasebi, A., Yu, J., Li, X., Meesri, C., 2013. An Experimental Study on Binderless Briquetting of Low-Rank Coals. Chem. Eng. Technol. https://doi.org/10.1002/ceat.201300067

Hatipoğlu, M., Ajò, D., Kibici, Y., Passeri, D., 2012. Natural carbon black (Oltu-stone) from Turkey: a micro-Raman study. Neues Jahrb. für Mineral. - Abhandlungen 189, 97–101. https://doi.org/10.1127/0077-7757/2012/0211

Hatipoğlu, M., Cesaro, S.N., Ajò, D., 2014. Comparative fourier transform infrared investigation of oltu-stone (Natural Carbon Black) and jet. Spectrosc. Lett. 47, 161–167. https://doi.org/10.1080/00387010.2013.785435

Hou, C., Jiang, B., Liu, H., Song, Y., Xu, S., 2020. The differences of nanoscale mechanical properties among coal maceral groups. J. Nat. Gas Sci. Eng. 80, 12. https://doi.org/10.1016/j.jngse.2020.103394

Hower, J.C., Suárez-Ruiz, I., Mastalerz, M., Cook, A.C., 2007. The investigation of chemical structure of coal macerals via transmitted-light FT-IR microscopy by

X. Sun. Spectrochim. Acta - Part A Mol. Biomol. Spectrosc. 67, 1433–1437. https://doi.org/10.1016/j.saa.2006.11.034

Huggins, F.E., 2002. Overview of analytical methods for inorganic constituents in coal. Int. J. Coal Geol. 50, 169–214. https://doi.org/https://doi.org/10.1016/S0166-5162(02)00118-0

Hunter, F.J., McDonnel, J.G., Pollard, A.M., Morris, C.R., Rowlands, C.C., 1993. The scientific identification of Archaeological Jet-like artefacts. Archaeometry 35, 69–89. https://doi.org/https://doi.org/10.1111/j.1475-4754.1993.tb01024.x

Jiménez, A., Iglesias, M.J., Laggoun-Défarge, F., Suárez-Ruiz, I., 1998. Study of physical and chemical properties of vitrinites. Inferences on depositional and coalification controls. Chem. Geol. 150, 197–221. https://doi.org/https://doi.org/10.1016/S0009-2541(98)00048-5

Kalkan, E., Bilici, Ö., Kolaylı, H., 2012. Evaluation of Turkish black amber : A case study of Oltu (Erzurum), NE Turkey. Int. J. Phys. Sci. 7, 2387–2397. https://doi.org/10.5897/IJPS12.092

Kandiyoti, R., Herod, A.A., Bartle, K.D., 2006. Fossil Fuels: Origins and Characterization Methods, in: Solid Fuels and Heavy Hydrocarbon Liquids. Elsevier Science Ltd, Oxford, pp. 13–35. https://doi.org/https://doi.org/10.1016/B978-008044486-4/50002-7

Kara-Gülbay, R., Korkmaz, S., Yaylalı-Abanuz, G., Erdoğan, M.S., 2018. Organic Geochemistry and Depositional Environment of the Oltu Gemstone (Coal) in the Erzurum Area, NE Anatolia, Turkey. Energy & Fuels 32, 1451–1463. https://doi.org/10.1021/acs.energyfuels.7b03486

Karayigit, A.I., 2007. Origin and properties of Oltu gemstone coal. Energy Sources, Part A Recover. Util. Environ. Eff. 29, 1279–1284. https://doi.org/10.1080/00908310500434549

Kinaci, E.H., 2013. Mineralogical and Gemmological Investigation and Genesis of Oltu Stone (carbon black). Dokuz Eylül University.

King, R., 2006. Minerals Explained 44: Amber (Part 1). Geol. Today 22, 232–237.

Kocaman, S., 2011. Turistik bir ürün olarak rus taşi (gürcistan siyah kehribari) ve erzurum oltu taşi sektörüne etkileri 115–135.

Kossovich, E.L., Dobryakova, N.N., Epshtein, S.A., Belov, D.S., 2016. Mechanical properties of coal microcomponents under continuous indentation. J. Min. Sci. 52, 906–912. https://doi.org/10.1134/S1062739116041382

Labus, M., Matyasik, I., 2019. Application of different thermal analysis techniques for the evaluation of petroleum source rocks. J. Therm. Anal. Calorim. 136, 1185–1194. https://doi.org/10.1007/s10973-018-7752-3

Lahn, E., 1939. Türkiye'deki Karakehribar Yatakları. rapor:690. Ankara (in Turkish).

Li, Z., Fredericks, P.M., Rintoul, L., Ward, C.R., 2007. Application of attenuated total reflectance micro-Fourier transform infrared (ATR-FTIR) spectroscopy to the study of coal macerals: Examples from the Bowen Basin, Australia. Int. J. Coal Geol. 70, 87–94. https://doi.org/https://doi.org/10.1016/j.coal.2006.01.006

Lin, R., Patrick Ritz, G., 1993. Studying individual macerals using i.r. microspectrometry, and implications on oil versus gas/condensate proneness and "low-rank" generation. Org. Geochem. 20, 695–706. https://doi.org/https://doi.org/10.1016/0146-6380(93)90055-G

Liu, L., Yuan, Y., Kumar, S., Wang, Z., He, Y., Lv, Y., Liu, J., Gul-e-Rana, J., Cen, K., 2018. Catalytic effect of metal chlorides on coal pyrolysis and gasification part II. Effects of acid washing on coal characteristics. Thermochim. Acta 666, 41–50. https://doi.org/10.1016/j.tca.2018.06.001

Liu, Z., Quek, A., Balasubramanian, R., 2014. Preparation and characterization of fuel pellets from woody biomass, agro-residues and their corresponding hydrochars. Appl. Energy 113, 1315–1322. https://doi.org/https://doi.org/10.1016/j.apenergy.2013.08.087

Machnikowska, H., Krztoń, A., Machnikowski, J., 2002. The characterization of coal macerals by diffuse reflectance infrared spectroscopy. Fuel 81, 245–252. https://doi.org/https://doi.org/10.1016/S0016-2361(01)00125-9

Mangena, S.J., du Cann, V.M., 2007. Binderless briquetting of some selected South African prime coking, blend coking and weathered bituminous coals and the effect of coal properties on binderless briquetting. Int. J. Coal Geol. 71, 303–312. https://doi.org/https://doi.org/10.1016/j.coal.2006.11.001

Manjunath, G.L., Jha, B., 2019. Nanoscale fracture mechanics of Gondwana coal. Int. J. Coal Geol. 204, 102–112. https://doi.org/10.1016/j.coal.2019.02.007

Manoj, B., 2016. A comprehensive analysis of various structural parameters of Indian coals with the aid of advanced analytical tools. Int. J. Coal Sci. Technol. 3, 123–132. https://doi.org/10.1007/s40789-016-0134-1

Mastalerz, M., Hower, J.C., Chen, Y., 2015. Microanalysis of barkinite from Chinese coals of high volatile bituminous rank. Int. J. Coal Geol. 141–142, 103–108. https://doi.org/https://doi.org/10.1016/j.coal.2015.03.004

McFarlane, R.A., Gentzis, T., Goodarzi, F., Hanna, J. V, Vassallo, A.M., 1993. Evolution of the chemical structure of Hat Creek resinite during oxidation: a combined FT-IR photoacoustic, NMR and optical microscopic study. Int. J. Coal Geol. 22, 119–147. https://doi.org/https://doi.org/10.1016/0166-5162(93)90021-2

Mills, J.S., White, R., Gough, L.J., 1984. The chemical composition of Baltic amber. Chem. Geol. 47, 15–39. https://doi.org/https://doi.org/10.1016/0009-2541(84)90097-4

Murchison, D.G., 1966. Properties of Coal Macerals, in: Coal Science, Advances in Chemistry. AMERICAN CHEMICAL SOCIETY, pp. 19–307. https://doi.org/doi:10.1021/ba-1966-0055.ch019

Mursito, A.T., Hirajima, T., Listiyowati, L.N., Sudarsono, S., 2018. Surface physicochemical properties of semi-anthracitic coal from Painan-Sumatra during air oxidation. Int. J. Coal Sci. Technol. 5, 156–166. https://doi.org/10.1007/s40789-018-0207-4

Nag, D., Kopparthi, P., Dash, P.S., Saxena, V.K., Chandra, S., 2018. Enrichment of reactive macerals in coal: its characterization and utilization in coke making. Rev. Metall. D Informations Tech. 115, 209.

Olugbade, T.O., Ojo, O.T., 2021. Binderless briquetting technology for lignite briquettes: a review. Energy, Ecol. Environ. 6, 69–79. https://doi.org/10.1007/s40974-020-00165-3

Orrego-Ruiz, J.A., Cabanzo, R., Mejía-Ospino, E., 2011. Study of Colombian coals using photoacoustic Fourier transform infrared spectroscopy. Int. J. Coal Geol. 85, 307–310. https://doi.org/10.1016/j.coal.2010.12.013

Ozen, T., Bilgin, O., Caglar, M., 2013. Chemical and mineralogical characterizations of the Oltustone (Turkish Black amber), in: 13th International Multidisciplinary Scientific GeoConference, SGEM. Albena, Bulgaria, pp. 559–565. https://doi.org/10.5593/sgem2013/ba1.v2/s04.004

Pagacz, J., Naglik, B., Stach, P., Drzewicz, P., Natkaniec-Nowak, L., 2020. Maturation process of natural resins recorded in their thermal properties. J. Mater. Sci. 55, 4504–4523. https://doi.org/10.1007/s10853-019-04302-0

Pagacz, J., Stach, P., Natkaniec-Nowak, L., Naglik, B., Drzewicz, P., 2019. Preliminary thermal characterization of natural resins from different botanical sources and geological environments. J. Therm. Anal. Calorim. 138, 4279–4288. https://doi.org/10.1007/s10973-019-08157-0

Painter, P.C., Snyder, R.W., Starsinic, M., Coleman, M.M., Kuehn, D.W., Davis, A., 1981. Concerning the Application of Ft-Ir To the Study of Coal: a Critical

Assessment of Band Assignments and the Application of Spectral Analysis Programs. Appl. Spectrosc. 35, 475–485. https://doi.org/10.1366/0003702814732256

Parlak, T., 2001. Oltu Stone and Jewelry Art in the Erzurum., Development of Oltu Stone Art, Protection of Artisans and Improvement Association Cheirmanship, Oltu-Erzurum, Turkey (in Turkish).

Parlak, T., 1989. The Gemstone from source to showcase, Erzurum Atatürk University Press. Erzurum.

Parlak T, 2001. Oltu Stone and Jewelry Art in the Erzurum. Dev. Oltu Stone Art, Prot. Artis. Improv. Assoc. Cheirmanship, Oltu-Erzurum, Turkey (in Turkish). 103.

Parlak, Y., 2018. Oltustone and a rosary master in Oltu. Ulakbilge J. Soc. Sci. 6, 179–191. https://doi.org/10.7816/ulakbilge-06-21-04 (in Turkish)

Pastorelli, G., 2009. Archaeologıcal Baltic amber: degradation mechanisms and conservation measures (PhD Thesis). University of Bologna. Italy.

Petersen, H.I., Vosgerau, H., 1999. Composition and organic maturity of Middle Jurassic coals, North-East Greenland: evidence for liptinite-induced suppression of huminite reflectance. Int. J. Coal Geol. 41, 257–274. https://doi.org/https://doi.org/10.1016/S0166-5162(99)00022-1

Pickel, W., Kus, J., Flores, D., Kalaitzidis, S., Christanis, K., Cardott, B.J., Misz-Kennan, M., Rodrigues, S., Hentschel, A., Hamor-Vido, M., Crosdale, P., Wagner, N., 2017. Classification of liptinite – ICCP System 1994. Int. J. Coal Geol. 169, 40–61. https://doi.org/https://doi.org/10.1016/j.coal.2016.11.004

Pietsch, W., 2005. Agglomeration in Industry Occurrence and Applications (Two Volumes). Wiley-VCH Verlag GmbH, Weinheim, 2005.

Potgieter-Vermaak, S., Maledi, N., Wagner, N., Van Heerden, J.H.P., Van Grieken, R., Potgieter, J.H., 2011. Raman spectroscopy for the analysis of coal: A review. J. Raman Spectrosc. 42, 123–129. https://doi.org/10.1002/jrs.2636

Poulin, J., Helwig, K., 2012. Class Id resinite from Canada: A new sub-class containing succinic acid. Org. Geochem. 44, 37–44. https://doi.org/https://doi.org/10.1016/j.orggeochem.2011.11.012

Rochdi, A., Landais, P., 1991. Transmission micro-infrared spectroscopy: An efficient tool for microscale characterization of coal. Fuel 70, 367–371. https://doi.org/https://doi.org/10.1016/0016-2361(91)90124-S

Rodgers, K.A., Currie, S., 1999. Thermal analytical study of some modern and

fossil resins from New Zealand. Thermochim. Acta 326, 143–149.

Rojas, G., Patricia, O., Blandón, A., Perea, C., Mastalerz, M., 2020. Petrographic characterization, variations in chemistry, and paleoenvironmental interpretation of Colombian coals. Int. J. Coal Geol. 227, 103516. https://doi.org/https://doi.org/10.1016/j.coal.2020.103516

Savkevich, S., 1981. Physical methods used to determine the geological origin of amber and other fossil resins: some critical remarks. Phys. Chem. Miner. 7, 1–4.

Si, L., Cao, Y., Fan, G., Wang, S., 2020. Study on fracture shape distribution characteristics and micromechanical properties of middling coal. AIP Adv. 10. https://doi.org/10.1063/5.0015946

Smith, A.H. V, 2005. Coal microscopy in the service of archaeology. Int. J. Coal Geol. 62, 49–59. https://doi.org/https://doi.org/10.1016/j.coal.2004.01.007

Song, H., Liu, G., Zhang, J., Wu, J., 2017. Pyrolysis characteristics and kinetics of low rank coals by TG-FTIR method. Fuel Process. Technol. 156, 454–460. https://doi.org/10.1016/j.fuproc.2016.10.008

Stankiewicz, B.A., Kruge, M.A., Mastalerz, M., 1996. A geochemical study of macerals from a Miocene lignite and an Eocene bituminous coal, Indonesia. Org. Geochem. 24, 531–545. https://doi.org/https://doi.org/10.1016/0146-6380(96)00038-1

Suárez-Ruiz, I., Jiménez, A., Iglesias, M.J., Laggoun-Defarge, F., Prado, J.G., 1994. Influence of Resinite on Huminite Properties. Energy and Fuels 8, 1417–1424. https://doi.org/10.1021/ef00048a033

Sun, B., Yu, J., Tahmasebi, A., Han, Y., 2014. An experimental study on binderless briquetting of Chinese lignite: Effects of briquetting conditions. Fuel Process. Technol. 124, 243–248. https://doi.org/https://doi.org/10.1016/j.fuproc.2014.03.013

Sun, X., 2005. The investigation of chemical structure of coal macerals via transmitted-light FT-IR microspectroscopy. Spectrochim. Acta - Part A Mol. Biomol. Spectrosc. 62, 557–564. https://doi.org/10.1016/j.saa.2005.01.020

Sutcu, E.C., Toprak, S., 2013. Petrographical, chemical and FT-IR properties of a suberinitic coal from Aydin–Germencik area, Western Turkey. Int. J. Coal Geol. 116–117, 36–45. https://doi.org/https://doi.org/10.1016/j.coal.2013.06.005

Taylor, G.H., Teichmüller, M., Davis, A., Diessel, C.F.K., Littke, R., Robert, P., 1998. Organic Petrology. Schweizerbart Science Publishers, Stuttgart,

Germany.

Teerman, S.C., Crelling, J.C., Glass, G.B., 1987. Fluorescence spectral analysis of resinite macerals from coals of the Hanna Formation, Wyoming, U.S.A. Int. J. Coal Geol. 7, 315–334.

Teichmüller, M., 1952. Vergleichende mikroskopische Untersuchungen versteinerter Torfe des Ruhrkarbons und der daraus entstandenen Steinkohlen. C.R. 3 ième Congrès Int. Strat. Géol. Carbonifère 2, 607–613.

Toprak, S., 2013. Petrographical properties of a semi-precious coaly stone, Oltu stone, from eastern Turkey. Int. J. Coal Geol. 120, 95–101. https://doi.org/10.1016/j.coal.2013.10.004

Tyson, R., 1995. Sedimentary Organic Matter: Organic facies and palynofacies, 1st ed. Springer Netherlands, Chapman and Hall, London. https://doi.org/10.1007/978-94-011-0739-6

Vassallo, A.M., Liu, Y.L., Pang, L.S.K., Wilson, M.A., 1991. Infrared spectroscopy of coal maceral concentrates at elevated temperatures. Fuel 70, 635–639. https://doi.org/https://doi.org/10.1016/0016-2361(91)90178-D

Vikhareva, A.S., Melnikov, A.G., Utyev, O.M., 2016. Technology for melting amber chips to produce a solid block. IOP Conf. Ser. Mater. Sci. Eng. 124. https://doi.org/10.1088/1757-899X/124/1/012147

Wagner-Wysiecka, E., 2018. Mid-infrared spectroscopy for characterization of Baltic amber (succinite). Spectrochim. Acta - Part A Mol. Biomol. Spectrosc. 196, 418–431. https://doi.org/10.1016/j.saa.2018.02.053

Wang, D., Zhong, X., Gu, J., Qi, X., 2010. Changes in active functional groups during low-temperature oxidation of coal. Min. Sci. Technol. 20, 35–40. https://doi.org/10.1016/S1674-5264(09)60157-5

Wang, S., Liu, S., Sun, Y., Jiang, D., Zhang, X., 2017. Investigation of coal components of Late Permian different ranks bark coal using AFM and Micro-FTIR. Fuel 187, 51–57. https://doi.org/10.1016/j.fuel.2016.09.049

Wen, S.B., Yang, C.S., Hsih, C.S., 1998. The abnormal size distribution of comminuted heterogeneous ores due to detachment of grain boundaries fracturing. Int. J. Miner. Process. 53, 183–200. https://doi.org/10.1016/S0301-7516(97)00080-X

White, D., 1933. Role of water conditions in the formation and differentiation of common (banded) coals. Econ. Geol. 28, 556–570. https://doi.org/10.2113/gsecongeo.28.6.556

Yan, Y., Qi, Y., Marshall, M., Jackson, W.R., Stanger, A., Tran, Q.A., Stanger, R., Chaffee, A.L., 2021. Characterisation of coal density fractions separated from Victorian brown coal by reflux classification. Fuel 292, 120385. https://doi.org/10.1016/j.fuel.2021.120385

Yao, S., Zhang, K., Jiao, K., Hu, W., 2011. Evolution of coal structures: FTIR analyses of experimental simulations and naturally matured coals in the Ordos Basin, China. Energy Explor. Exploit. 29, 1–19. https://doi.org/10.1260/0144-5987.29.1.1

Yu, H., Zhang, Y., Lebedev, M., Han, T., Verrall, M., Wang, Z., Al-Khdheeawi, E., Al-Yaseri, A., Iglauer, S., 2018. Nanoscale geomechanical properties of Western Australian coal. J. Pet. Sci. Eng. 162, 736–746. https://doi.org/10.1016/j.petrol.2017.11.001

Zhang, G., Sun, Y., Xu, Y., 2018. Review of briquette binders and briquetting mechanism. Renew. Sustain. Energy Rev. 82, 477–487. https://doi.org/10.1016/j.rser.2017.09.072

Zhang, W., Jiang, S., Wang, K., Wang, L., Xu, Y., Wu, Z., Shao, H., Wang, Y., Miao, M., 2015. Thermogravimetric dynamics and FTIR analysis on oxidation properties of low-rank coal at low and moderate temperatures. Int. J. Coal Prep. Util. 35, 39–50. https://doi.org/10.1080/19392699.2013.873421

Zhang, Yihuai, Lebedev, M., Smith, G., Jing, Y., Busch, A., Iglauer, S., 2020. Nano-mechanical Properties and Pore-Scale Characterization of Different Rank Coals. Nat. Resour. Res. 29, 1787–1800. https://doi.org/10.1007/s11053-019-09572-8

Zhang, Yu., Zhang, X., Hu, S., 2020. Structural Transformations of Coal at Low Temperature Oxidation via In-situ FTIR. Combust. Sci. Technol. 00, 1–18. https://doi.org/10.1080/00102202.2020.1716341

APPENDICES

A. Particle Size Distribution

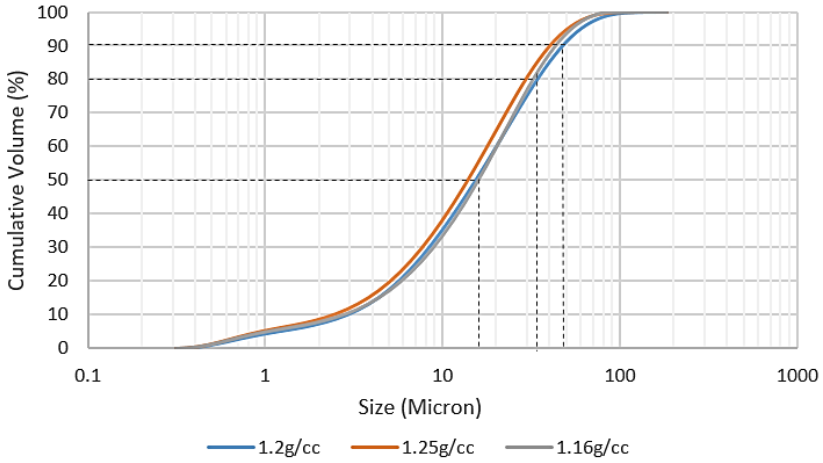

Figure A.1 Particle size distribution of grounded samples used in Method-B and Method-C

Table A.1 Critical particle size w.r.t cumulative mass passing, obtained from figure A.1

	-1.25+1.2g.cm-3	-1.2+1.15g.cm-3	-1.15g.cm-3
D_{50}	14.1µm	15.2 µm	15.9 µm
D_{80}	29.7 µm	34.1 µm	33.8 µm
D_{90}	40.1 µm	49.9 µm	44.8 µm
D_{95}	51.9 µm	60.1 µm	52.5 µm

B. SEM-EDS Analyses

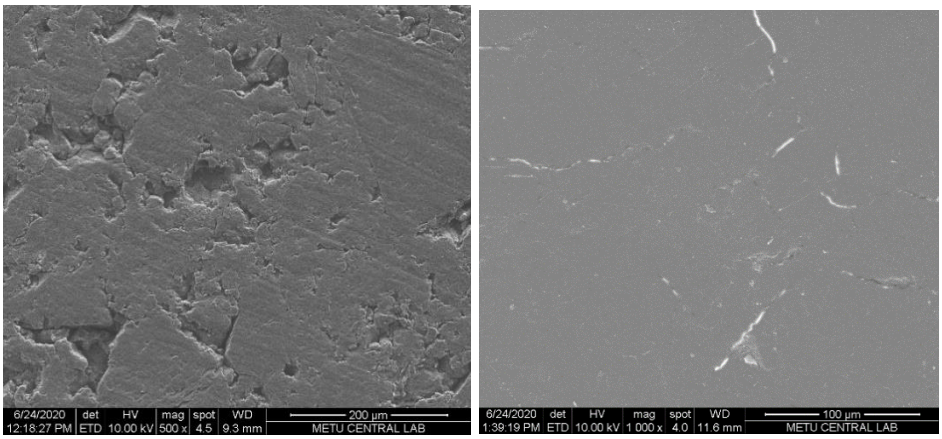

Figure B.1 Pressed Oltu-stone by a) Method-A (MA) b). Method-C (MC)

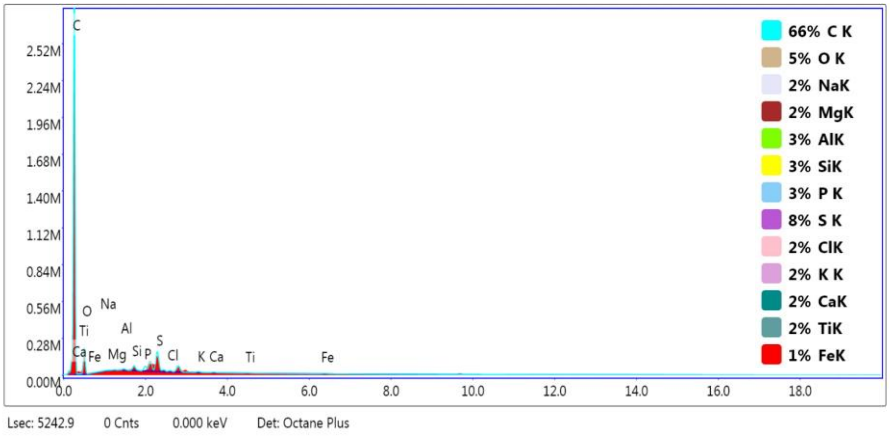

Figure B.2 EDS spectrum of pressed Oltu-stone elemental mapping

Table B.1 The semi-quantitative analysis extract from EDS spectrum in Figure B.2

Element	Weight %	Atomic %	Net Int.
C K	83.24	87.96	2687.80
O K	13.62	10.80	191.80
NaK	0.09	0.05	6.40
MgK	0.06	0.03	7.40
AlK	0.10	0.05	14.90
SiK	0.32	0.14	55.20
P K	0.38	0.15	55.70
S K	1.67	0.66	256.20
ClK	0.12	0.04	16.90
K K	0.12	0.04	14.10
CaK	0.10	0.03	9.60
TiK	0.05	0.01	4.60
FeK	0.15	0.03	7.90

C. Nano-indentation analysis

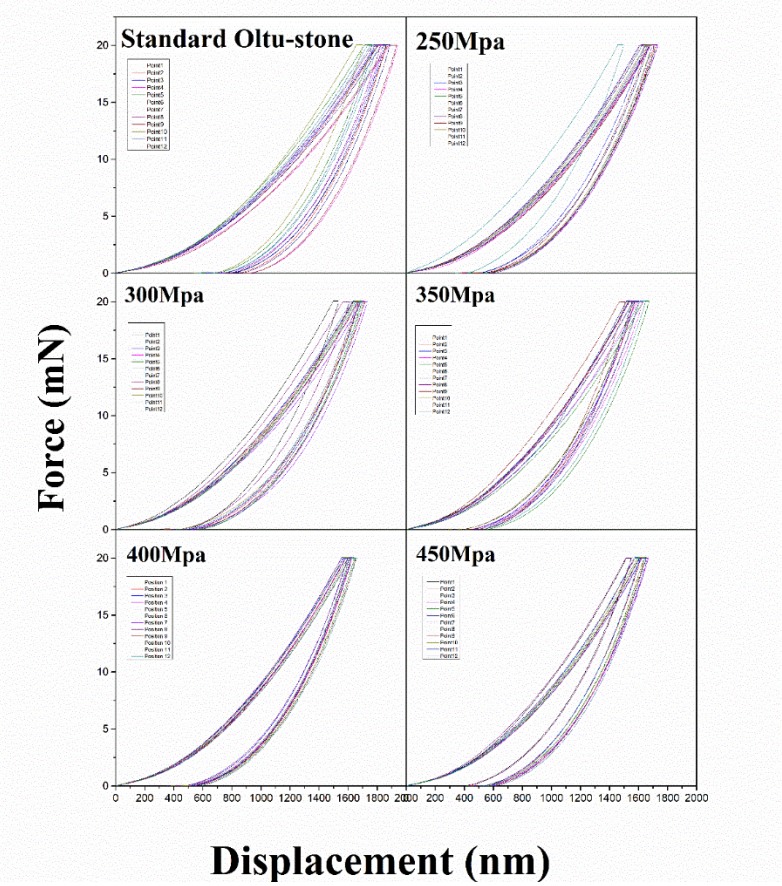

Figure C.1 Loading and unloading curves obtained from CSM for nanoindentation analysis at different pressure

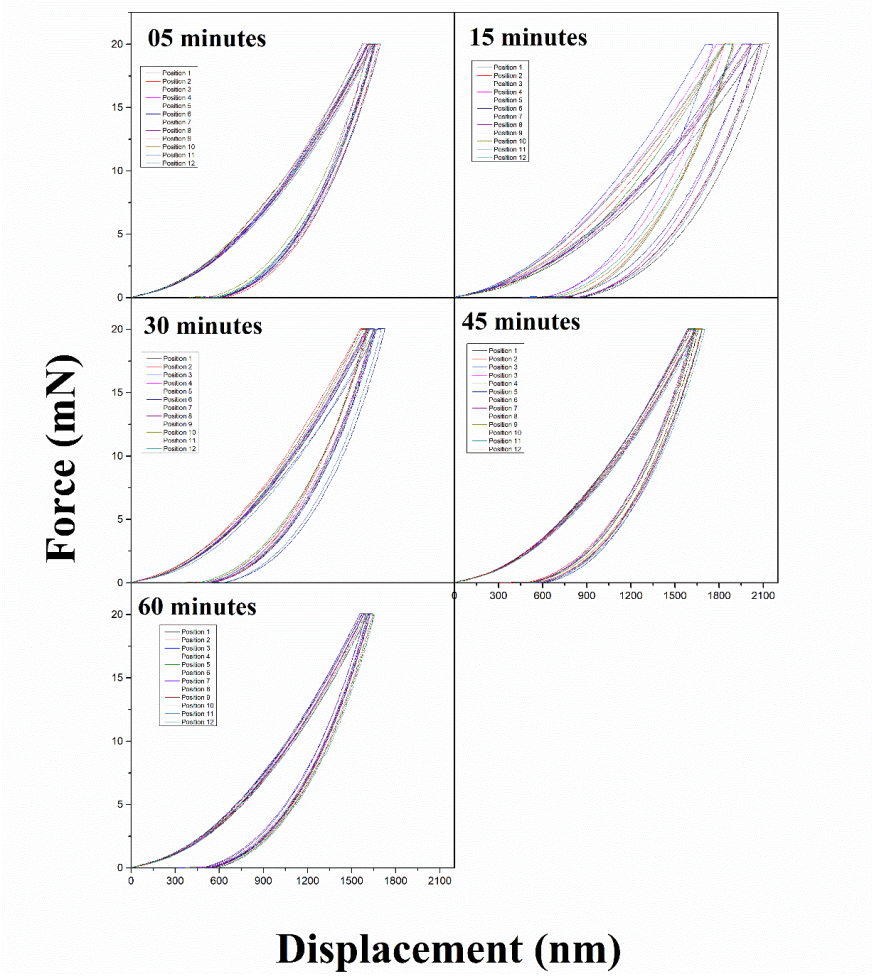

Figure C.2 Loading and unloading curves obtained from CSM for nanoindentation analysis at different pressing time

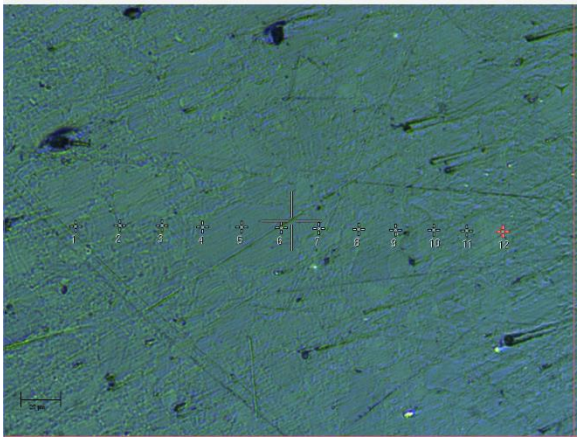

Figure C.3 The optical microscope image (attached with CSM) at 15 minute pressing time.